NOAA Technical Memorandum ERL PMEL-89

INSTRUMENTATION, FIELD OPERATIONS, AND DATA PROCESSING FOR PMEL DEEP OCEAN BOTTOM PRESSURE MEASUREMENTS

M. C. Eble
F. I. Gonzalez
D. M. Mattens
H. B. Milburn

Pacific Marine Environmental Laboratory
Seattle, Washington
August 1989

UNITED STATES DEPARTMENT OF COMMERCE

Robert A. Mosbacher
Secretary

NATIONAL OCEANIC AND ATMOSPHERIC ADMINISTRATION

John A. Knauss
Under Secretary for Oceans and Atmosphere/Administrator

Environmental Research Laboratories

Joseph O. Fletcher
Director

NOTICE

Mention of a commercial company or product does not constitute an endorsement by NOAA/ERL. Use of information from this publication concerning proprietary products or the tests of such products for publicity or advertising purposes is not authorized.

Contribution No. 1000 from NOAA/Pacific Marine Environmental Laboratory

For sale by the National Technical Information Service, 5285 Port Royal Road
Springfield, VA 22161

CONTENTS

LIST OF FIGURES

LIST OF TABLES

List of terms:

f	=	frequency of Paros pressure sensor
τ	=	period of Paros pressure sensor
$\bar{\tau}$	=	integration period
Θ	=	temperature
C, D, τ_0	=	temperature dependent calibration coefficients
N	=	number of cycles completed over one integration period
N_0	=	number of cycles completed at zero pressure and temperature
P	=	pressure (psia)
P_{msl}	=	mean sea level induced pressure
p	=	signal amplitude
σ	=	$2\pi/T$ = radial frequency of signal with period T
dH	=	equivalent least count change of sea water head
dH_0	=	static sensitivity at zero pressure
dH_{10K}	=	static sensitivity at 10,000 psia
$\psi(\omega)$	=	frequency response function
M	=	temperature counts
n_{ro}	=	24-bit or 16-bit register rollover
H_{ro}	=	24-bit rollover depths
P_{ro}	=	24-bit rollover pressures
A_j, Q_j	=	tidal constituent amplitude and phase
σ_j	=	tidal frequencies

Instrumentation, Field Operations, and Data Processing for PMEL Deep Ocean Bottom Pressure Measurements

M.C. Eble, F.I. Gonzalez, D.M. Mattens, and H.B. Milburn

ABSTRACT. The focus of this report is on the collection and processing of deep-ocean bottom pressure measurements made using the Paroscientific Model 410K-017 digiquartz pressure transducer. The observational program was initiated in 1986 for the purpose of collecting high quality data during the generation, propagation, and coastal runup stages of a tsunamigenic event. Because of its diversity and flexibility, the bottom pressure recorder (BPR) is also an important tool in many other areas of oceanic research, particularly when coupled with other instrumentation.

1. INTRODUCTION

High quality bottom pressure recorder (BPR) measurements in the deep ocean contribute to our understanding of important oceanographic processes over a wide range of time scales. These vary from relatively long period (months to hours) variations induced by planetary waves, oceanic tides and meteorological forcing events, to relatively shorter period (hours to seconds) phenomena such as tsunamis, long surface gravity waves, and microseisms.

1.1 Early Ocean Bottom Pressure Experiments

Eyries (1968), Snodgrass (1968), and Filloux (1969, 1970) are recognized as pioneers in the development and deployment of self-contained bottom recording pressure units (Warren and Wunsch, 1985). Measurements of pelagic and near-coastal tides were made using vibrating wires, strain gauges, and Bourdon-tube transducers, described in Section 2. Since these deployments, the use of BPRs in oceanic programs has been diverse.

Wunsch and Wimbush (1977) incorporated a Vibrotron and several strain gauge pressure transducers into a program designed to monitor the Florida Current in the Miami-Bimini region. Beardsley *et al.* (1977) deployed strain gauges, Vibrotrons and Filloux Bourdon-tube pressure transducers in the Middle Atlantic Bight to study both ocean tides and weather-induced bottom pressure fluctuations. Mofjeld and Wimbush (1977) deployed Filloux Bourdon-tube transducers in the Gulf of Mexico and the Caribbean to measure oceanic tides. Wyrtki (1979) deployed pressure transducers in the Equatorial Pacific to monitor currents via sea level variations. Wearn and Baker (1980) studied transport fluctuations of the Antarctic Circumpolar Current using quartz-resonator pressure transducers deployed in Drake Passage. Filloux (1982, 1983) recorded tides, seismic, and tsunami waves off the Gulf of California. Bernard and Milburn (1985) deployed quartz-resonator transducers in the equatorial Pacific as part of a long-wave observation program in which a small tsunami ($\approx$1 cm) was successfully detected in the open ocean, and storm-induced barotropic disturbances were identified.

1.2 PMEL Deep Ocean Bottom Pressure Observational Program

During the period 1982-1985, the Pacific Marine Environmental Laboratory (PMEL) of the National Oceanic and Atmospheric Administration (NOAA) engaged in the development of a reliable deep ocean BPR. During this time, six deployments were made in the equatorial Pacific with varying degrees of success of data recovery (Table 1). Bernard and Milburn (1985) used this first generation of BPR instrumentation for their work in the equatorial Pacific.

The need for high quality deep ocean tsunami data has long been recognized (Bernard and Goulet, 1981; Raichlen, 1985); indeed, the initial focus of this project was on the acquisition of such data (Gonzalez *et al.*, 1987). Since 1946, six tsunamis have inflicted 355 fatalities and 485 million dollars worth of property damage on the U.S. One half of these tsunamis were generated by earthquakes in the highly active Alaska-Aleutian Seismic Zone, and these caused 82% of all fatalities and 85% of the damage (Bernard and Goulet, 1981). One sub-region in this zone is the Shumagin Seismic Gap, long identified as having a high probability for the occurrence of a great ($M_s > 8$) tsunamigenic earthquake (Jacob, 1984). BPR site selection attempted to optimize the observation of any tsunamis generated in this region, and the network is configured to acquire such data in both the tsunami near-field and far-field (Fig. 1).

In the existing station configuration (Fig. 1c) a station is located on the landward slope of the Aleutian Trench in the Shumagin Seismic Gap itself. A triangular array is centered in deep water approximately 230 km seaward of the slope station, and the fifth site is a distance of approximately 2200 km from the Shumagin Seismic Gap, 450 km due west of the Columbia River entrance (specific deployment information is given in Table 1). This station is also near the great circle route which connects the Shumagin Seismic Gap region with Crescent City, California. This is of particular interest because Crescent City sustained fatalities and severe damage during the 1964 Alaskan earthquake tsunami (Spaeth and Berkman, 1967).

Predictably, the research objectives of the project have broadened to include other oceanographic phenomena which can be investigated through measurement of deep ocean bottom pressure. With this inevitable expansion of project goals in mind, the initial sites were chosen to supplement BPR time series with other sources of oceanographic and meteorological data. The west coast site and the triangular array are each situated in the vicinity of a permanently moored NOAA National Data Buoy Center (NDBC) environmental buoy, which routinely provides hourly observations of atmospheric pressure, surface wind speed and direction, air and sea surface temperature, and sea state. Also, each site is within a few kilometers of U.S. Navy GEOdetic SATellite (GEOSAT) ground tracks, along which altimeter-derived estimates of sea-level variations are obtained. Each apex of the triangular array is situated at the crossover point of the ground tracks of an ascending and descending orbital pair.

TABLE 1. BPR deployment and recovery information.

Identification Nos.			Position		Deployment			Recovery			Depth		
Depl.	Paros	SeaData	Lat (°N)	Long (°W)	GMT	JD	Year	GMT	JD	Year	(m)	Location	Comments
--	2592	--	3.0°S	95.0	--	98	1982	--	306	1982	3700		Memodyne/Bellows
--	15022	--	3.0°S	95.0	--	306	1982	--	93	1983	3700		Sea Data/Bellows
--	3605	--	3.0°S	95.0	--	93	1983	--	284	1983	3700		Sea Data/Bellows
--	17789	--	1.5	140.0	--	296	1983	(Not recovered)			4200		Sea Data/Bourdon
--	15022	--	0.0	140.0	--	291	1983	--	12	1984	4200		Sea Data/Bourdon
--	17787	--	1.5	140.0	--	300	1983	(Not recovered)			4200		Sea Data/Bourdon
--	2592	--	0.0	140.0	--	120	1984	--	325	1984	4200		Sea Data/Bellows
--	15022	--	0.0	140.0	--	325	1984	(Not recovered)			4200		Sea Data/Bourdon
--	21988	--	0.0	140.0	--	165	1985	--	188	1985	4200		Sea Data/Bourdon
AK1	24063	53	52.614	155.581	2355	225	1986	1238	224	1987	4523	AK array	
AK2	24064	54	52.099	155.697	1628	225	1986	0302	224	1987	4662	AK array	
AK3	24061	52	51.785	155.044	1548	226	1986	1400	223	1987	4692	AK array	
AK4	24026	55	51.907	156.485	0259	227	1986	2157	223	1987	4600	AK array	
WC5	21988	25	44.863	130.365	1235	292	1986	1935	113	1987	2402	Juan de Fuca Ridge	
AK6	21988	25	52.025	155.727	0730	224	1987	(Not recovered)			4684	AK array	
AK7	29103	155	52.733	155.003	1841	224	1987	0111	76	1988	4463	AK array	
AK8	26706	154	52.733	156.480	0116	225	1987	1430	75	1988	4535	AK array	
WC9	24061	52	45.979	129.990	0300	266	1987	1754	192	1988	1527	Axial Caldera	
AK10	24026	55	54.286	158.520	0514	299	1987	2122	208	1988	1656	Aleutian Trench slope	
AK11	24063	53	52.720	155.003	0128	76	1988	1829	257	1988	4440	AK array	
AK12	24064	54	52.723	156.471	1859	75	1988	2101	258	1988	4516	AK array	
AK13	29103	155	52.024	155.728	0133	208	1988	(Summer 1989)			4764	AK array	
AK14	26704	153	54.164	158.249	1844	208	1988	(Summer 1989)			4100	Aleutian Trench Slope	
WC15	24061	52	45.960	130.020	1649	249	1988	(Summer 1989)			1558	Axial Caldera	
AK16	24026	55	53.422	154.281	0140	258	1988	(Summer 1989)			4471	AK array	
AK17	26706	154	53.425	157.221	0540	259	1988	(Summer 1989)			4633	AK array	

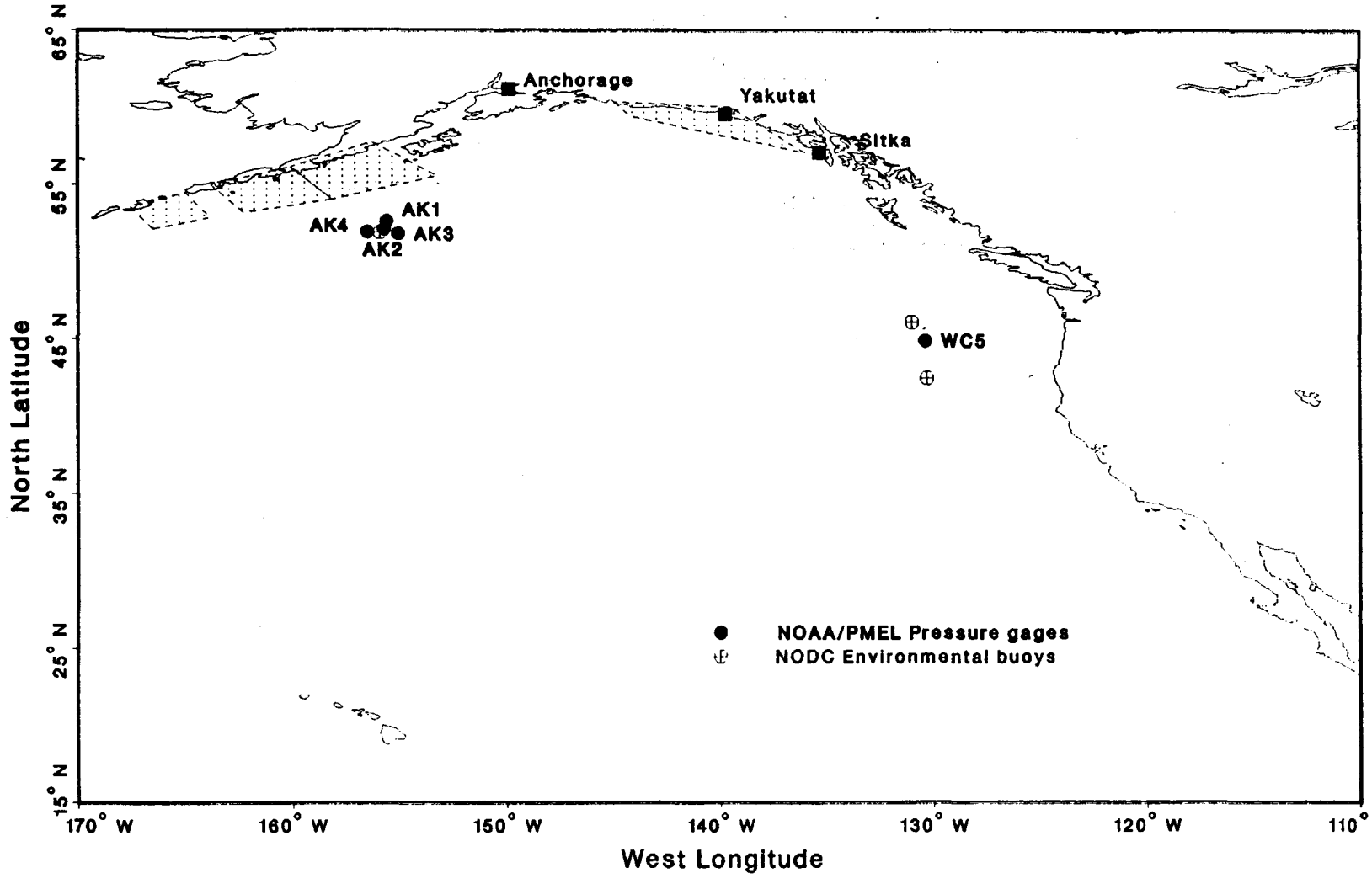

Figure 1a. Map of study area showing the 1986-1987 BPR Network. Hachured regions near Yakutat and along the Aleutian Islands are seismic gaps.

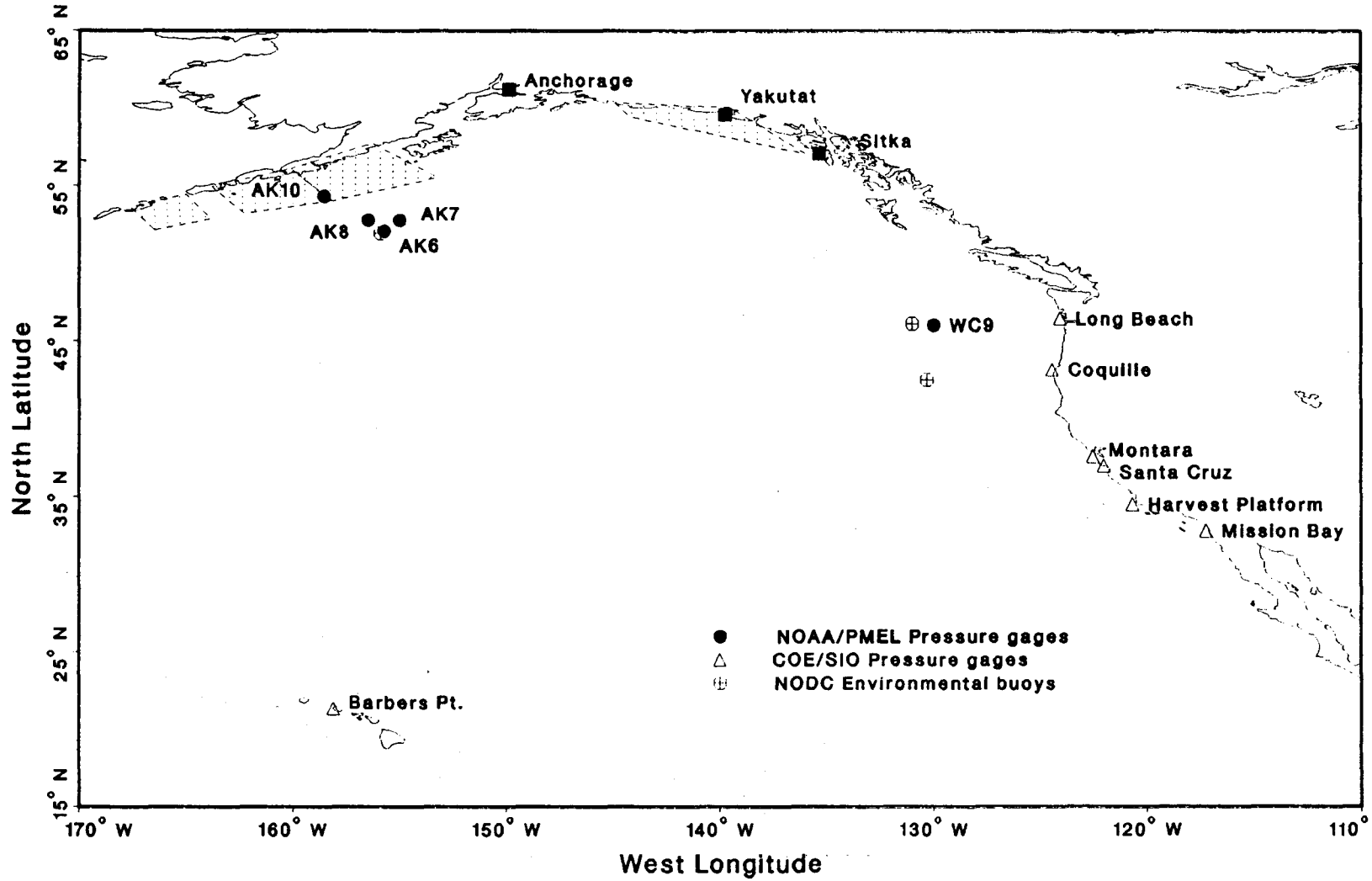

Figure 1b. Map of study area showing the 1987-1988 BPR Network. Hachured regions near Yakutat and along the Aleutian Islands are seismic gaps.

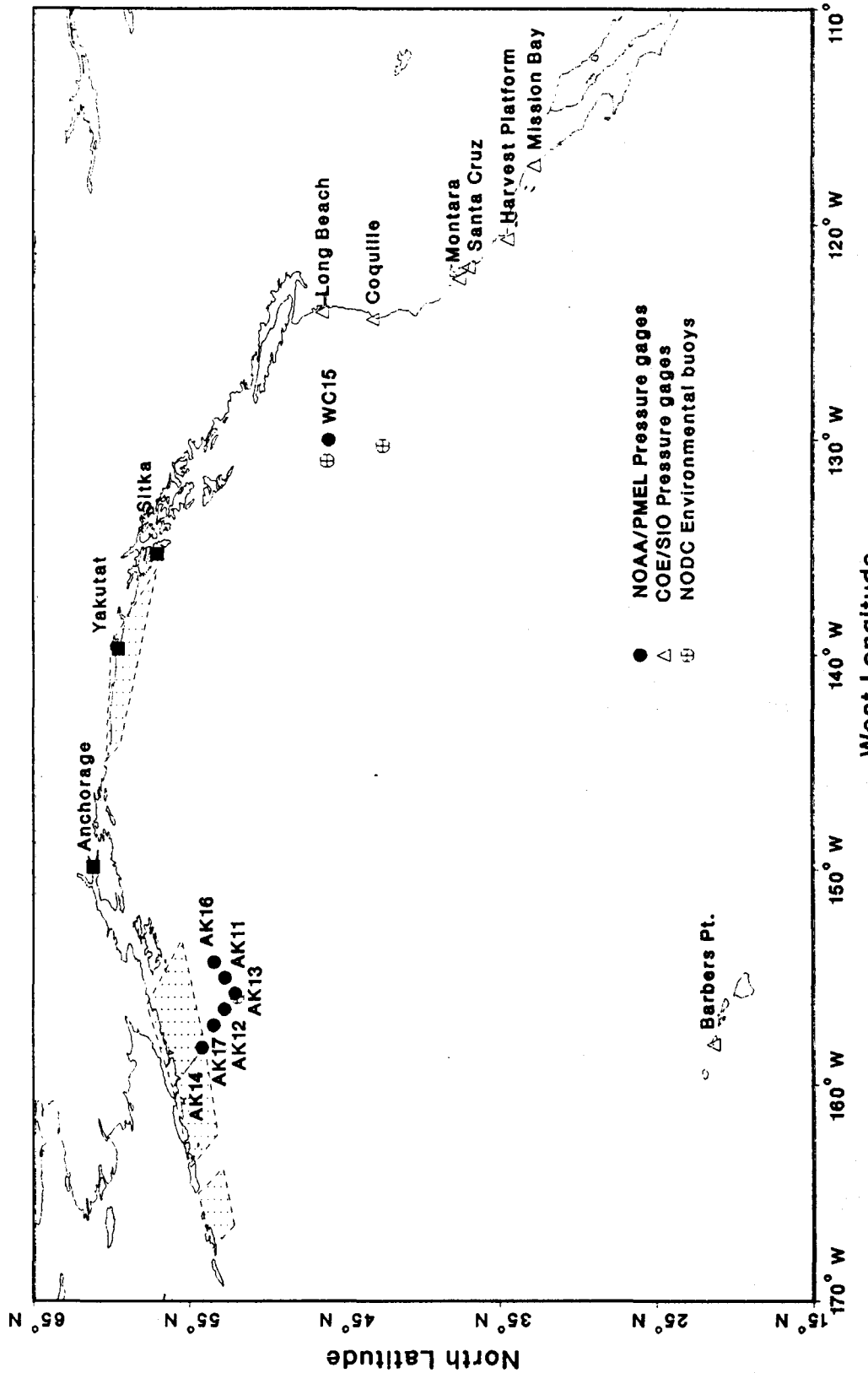

Figure 1c. Map of study area showing the 1988-1989 BPR Network. Hachured regions near Yakutat and along the Aleutian Islands are seismic gaps.

The focus of this report is on the technical and procedural aspects of data collection and processing. This report will not address the 1982-1985 early development period, and will instead focus on activities which began in 1986, when PMEL initiated a long-term deep ocean bottom pressure monitoring program with the deployment of five BPRs in the North Pacific. A total of 12 BPR deployments have been performed since 1986, and 11 of these units have been successfully recovered. Station information is presented in Table 1 and their locations are shown in Fig. 1. Specific experiment results are not discussed in this report, although much of the data obtained to date are presented in Appendices A and B.

2. INSTRUMENTATION

Several types of transducers have been incorporated into pressure sensor units designed for oceanic applications. The most common include vibrating wires, strain gauges, quartz-crystal resonators, Bourdon tubes, and various capacitance devices, each discussed below.

Vibrating wire designs typically utilize pressure-induced strain to vary the natural frequency of vibration of the wire. The Vibrotron, which was developed and patented in the 1940's by Rieber, represents one of the earliest designs (Lefcort, 1968). An alternating current in the presence of a magnetic field is passed through a tungsten wire attached to a diaphragm. Variations in external pressure vary the tautness, and thus the resonant frequency, of the wire. The Vibrotron was first used in the 1950's by the Byron-Jackson Pump Company to monitor oil wells, but it is no longer commercially manufactured (Wimbush, 1976).

Capacitance plate transducers, such as those described by Harris and Tucker (1963), incorporate parallel capacitance plates in which the inter-plate distance varies as a function of pressure applied to an attached diaphragm. Capacitance is inversely proportional to the plate gap and acts to tune an LC oscillator. This design represented an improvement over the Vibrotron with respect to accuracy, flexibility, and cost; however, the mechanical design of these transducers proved inherently unstable.

Strain gauge pressure sensors utilize the variation in the resistance of a conductor with mechanical deformation caused by pressure acting on a flexible element. Many designs have been used, most incorporating a Wheatstone Bridge to increase sensitivity and minimize temperature effects. Gwilliam and Collar (1974) and Collar and Cartwright (1972) report on successful uses of strain gauge sensors to measure tides. However, they are not well suited for long-term deep deployments where a large dynamic range, high sensitivity, and low drift are required.

Quartz-crystal resonator transducers measure pressure-induced changes in the vibrational frequency of a quartz beam. An early Hewlett-Packard sensor utilized a piezo-electric resonator. Characterized by increased pressure sensitivity and decreased temperature sensitivity, this design represented an improvement over the vibrating wire, capacitance plate, and strain gauge designs

(Gwilliam and Collar, 1974). More recent transducers, such as those currently marketed by Paroscientific, Inc., display somewhat improved long-term stability and significantly greater accuracy than their predecessors (Wearn, 1985a; Wearn, 1985b).

In 1973, a comparison of the performance of various pressure transducers was made in an experiment designed and conducted by the Scientific Committee on Oceanic Research (SCOR, 1975). In addition, mooring and recovery techniques were evaluated for the purpose of optimizing recovery rates and data quality. This study found that the most important deficiencies of various instruments included limited pressure sensitivity, large magnitude of temperature dependency, restricted frequency response, excessive power requirements, and long-term transducer instability. Based on these experimental results, the SCOR working group concluded that the quartz-crystal resonator transducer performed significantly better than all other transducers examined during the study. Consistent with these results, PMEL has chosen quartz-crystal transducers for use in its BPRs. Specifically, the Paroscientific Model 410K-017 Digiquartz Pressure Transducer, with a dynamic range of 0 to 10,000 psia is utilized.

The internal design and housing of the Paroscientific transducer is shown in Fig. 2. The design utilizes an oscillating quartz crystal beam which is piezoelectrically induced to vibrate in its lowest resonant flexural mode (Wearn and Larson, 1982). Changes in fluid pressure are converted into a change in the axial compressive load on the beam via a Bourdon tube and lever arm arrangement. In turn, the change in axial load alters the natural frequency of oscillation of the beam. Therefore, the output frequency of the associated oscillator circuit is a measure of the applied external pressure. The current design includes either a Yellow Springs International (YSI) Model 44032 thermistor, or a crystal temperature sensor installed alongside the pressure transducer cavity inside silicone rubber potting material. Accurate temperature measurements of the quartz crystal are critical since the frequency of oscillation of the sensor is a function of temperature as well as applied pressure, as discussed in Section 2.1.

During the first five deployments, the YSI thermistor was mounted to the electronics frame in close proximity to the pressure transducer, but still outside of the potted cavity. These earlier records are therefore characterized by a time difference between the ambient temperature of the transducer and that of the thermistor. The effect of this difference, however, is insignificant since typical temperature fluctuations in the deep ocean are of order hundredths of a degree.

The pressure and temperature signals are measured and recorded by a SeaData Model 635-7H Recorder. A quartz-crystal clock controls the averaging period of all measurements, and data are digitally recorded on cassette tape at selectable intervals ranging from 4 to 128 samples per hour. Data are typically acquired at 64 samples per hour, or every 56.25 seconds. Additional specifications are provided in Table 2.

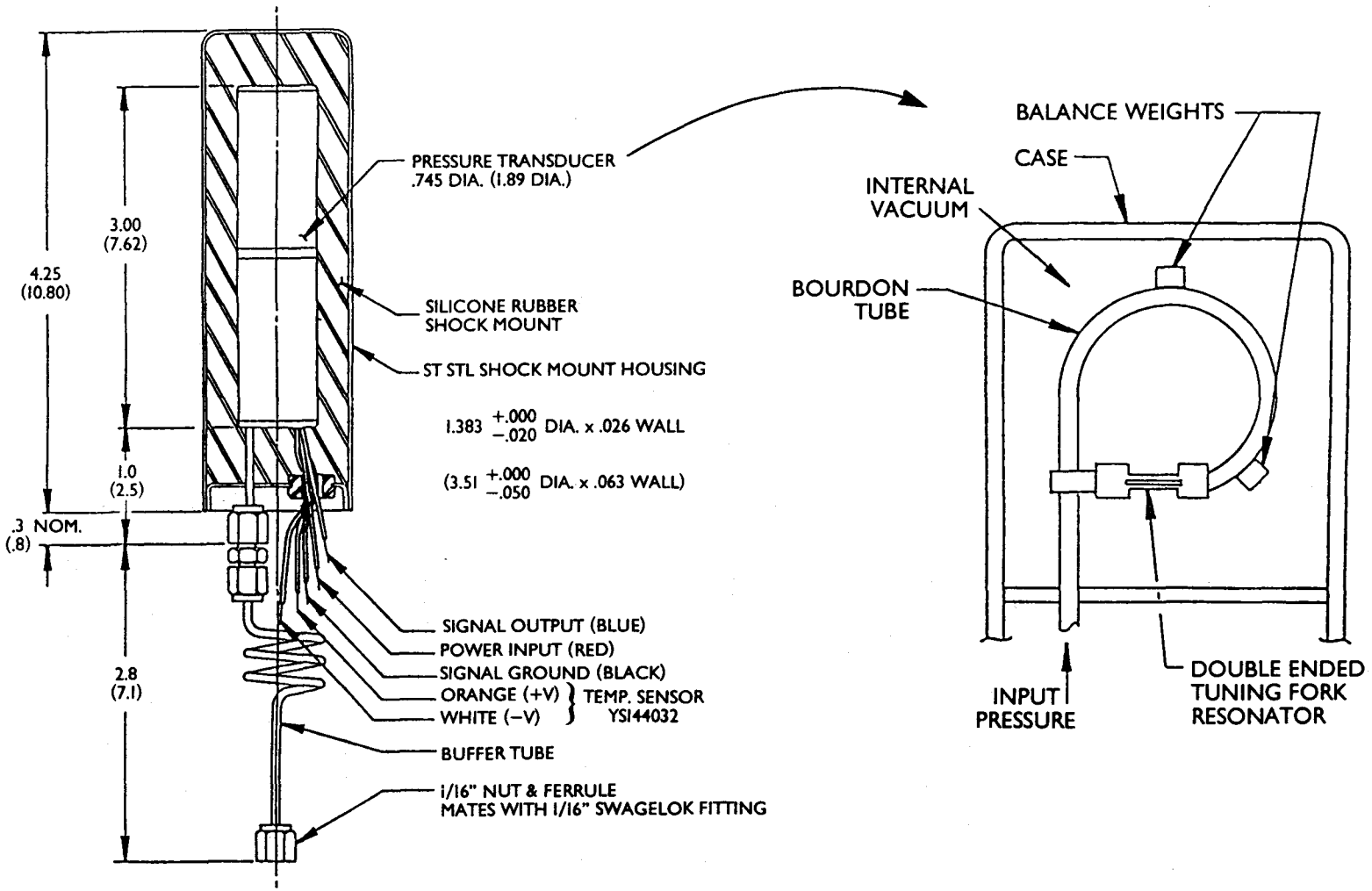

Figure 2. Internal design and housing of the Paroscientific pressure transducer. Dimensions are given in inches, with centimeters in parentheses.

TABLE 2. Paroscientific pressure transducer, temperature sensor, and instrument specifications.

PRESSURE SENSOR		
Type:		Paroscientific Digiquartz Model 410 K
Range:		10,000 PSIA full scale
Resolution:		0.15 ppm
Accuracy:		0.015% of full scale, 0.003% corrected
Overrange:		20% maximum without sensor damage
TEMPERATURE SENSOR		
Type:		Yellow Springs International Model 44032 thermistor
Range:		−4.3°C to +34.0°C
Resolution:		0.001°C
Accuracy:		0.07°C (special versions to 0.01°C)
Stability:		0.005°C (small temperature excursions); 0.02°C (full range)
FM Noise:		0.002°C
TIMEBASE		
Type:		Multi-mode quartz crystal oscillator
Frequency:		2.097152 MHz
Stability:		0.1 ppm/°C, 1 ppm/year
DATA CHARACTERISTICS		
Sampling rate:		Selectable at 4, 8, 16, 32, 64 or 128 measurements per hour
Storage format:		One record consists of one 20-bit time, one 16-bit temperature, one 24-bit pressure, and fifteen 16-bit pressure words.
Storage Media:		Standard 800 bpi, 4-track, digital certified, 450′ cassette tapes
Capacity:		15 megabits, corresponding to 6×10^5 pressure measurements
POWER		
Battery:	(635-7H)	Preibe Electronics BSPC 07006-00U, 180 Amp-hr lithium battery pack (de-rated to 132 useful Amp-hr for sensor and logic), and 10 Amp-hr alkaline battery pack for tape transport
	(1635-7H)	Sea Data SDB-16, 80 Amp-hr alkaline battery pack de-rated to 70 useful Amp-hrs (50 Amp-hrs for sensor, logic, and tape transport; 20 Amp-hrs for acoustic release)
Requirement:	(635-7H)	Average 7 mA data collection drain @ 64 measurements per hour or 13 Amp-hrs per 100,000 measurements
	(1635-7H)	Average 4.5 mA data collection drain @ 64 measurements per hour. Average acoustic release drain 0.85 Amp-hr per month
WEIGHT (BPR unit only)		
	(635-7H)	105 lbs. in air, 41 lbs. in water
	(1635-7H)	105 lbs. in air, −25 lbs (buoyant) in water

2.1 Transducer Conformance Equation

The output of the Paros pressure sensor is a sine wave of frequency f or period τ. To increase the sensitivity of the instrument, f is increased by a factor of 2^n by means of a frequency multiplier circuit with output $F \equiv 2^n f$. An estimate of the final output frequency, F, is obtained by electronically counting the number of cycles, N, completed over one averaging period (or "integration period"), $\bar{\tau}$. If the applied pressure is constant over this time interval, then the "count," or number of cycles counted, is given by:

$$N = F\bar{\tau} = 2^n f\bar{\tau} = 2^n \bar{\tau}/\tau , \tag{1}$$

with n an integer. The relationships between applied pressure and the output frequency of a Paros sensor is given by the conformance equation (Well-Test Instruments, Inc., 1984)

$$P(\tau) = C\left\{1-(\tau_0/\tau)^2-D\left[1-(\tau_0/\tau)^2\right]^2\right\} , \tag{2a}$$

where the three calibration coefficients C, D, and τ_0 are functions of temperature Θ.

$$C = C_1 + C_2\Theta + C_3\Theta^2 , \tag{2b}$$

$$D = D_1 , \tag{2c}$$

$$\tau_0 = \tau_1 + \tau_2\Theta + \tau_3\Theta^2 + \tau_4\Theta^3 . \tag{2d}$$

Using (1) to eliminate τ in (2a) yields

$$P(N) = C\left\{1-(N/N_0)^2-D\left[1-(N/N_0)^2\right]^2\right\} , \tag{3}$$

where N_0 is the number of counts at zero pressure and temperature. Other useful relationships are given by:

$$\tau(P) = \tau_0\left[1-1/(2D) + (1-4DP/C)^{1/2}/(2D)\right]^{-1/2} , \tag{4a}$$

$$F(P) = F_0\left[1-1/(2D) + (1-4DP/C)^{1/2}/(2D)\right]^{1/2} , \tag{4b}$$

and

$$N(P) = N_0\left[1-1/(2D) + (1-4DP/C)^{1/2}/(2D)\right]^{1/2} . \tag{4c}$$

The values of C, D, and τ_0 for selected Paros gauges owned by PMEL are given in Table 3, and the functions $P(\tau)$ for each gauge at 0°C are presented in Figure 3.

TABLE 3. Sensor calibration coefficients C, D, and τ_0 for PMEL Paroscientific pressure gauges, the least-count pressure resolution dH_{ro}, dH_{10K} at 0 and 10 K psia, and the equivalent ocean depth, H_{ro}, at which rollover of the 24-bit register occurs.

Ser. No.	θ (°C)	C (psia)	D (–)	τ_0 (5-sec)	dH_0 (mm)	dH_{10K} (mm)	H_{ro} (m)
21988	0.00	–52194.19	.035749	28.51323	1.108	1.225	4569.9
21988	21.00	–52185.73	.035749	28.51118	1.108	1.225	4563.5
24026	0.00	–41436.90	.034214	30.89031	.953	1.078	9161.6
24026	21.00	–41444.68	.034214	30.88131	.953	1.078	9141.4
24061	0.00	–45366.10	.034682	30.05558	1.015	1.138	7839.1
24061	21.00	–45327.91	.034682	30.06153	1.014	1.137	7847.9
24063	0.00	–44649.60	.033164	29.35602	.976	1.095	5958.1
24063	21.00	–44604.49	.033164	29.36149	.975	1.094	5965.6
24064	0.00	–42237.20	.033131	29.97430	.942	1.064	7100.5
24064	21.00	–42215.17	.033131	29.97696	.942	1.063	7103.1
26704	.00	–52620.61	.033635	28.73163	1.126	1.243	5224.4
26704	21.00	–52584.21	.033635	28.73443	1.125	1.242	5228.7
26706	.00	–61131.14	.029991	28.73928	1.308	1.424	6092.2
26706	21.00	–61103.66	.029991	28.73955	1.307	1.424	6089.5
29103	.00	–41060.88	.033623	29.17046	.892	1.010	5059.1
29103	21.00	–41077.88	.033623	29.15760	.892	1.010	5032.2

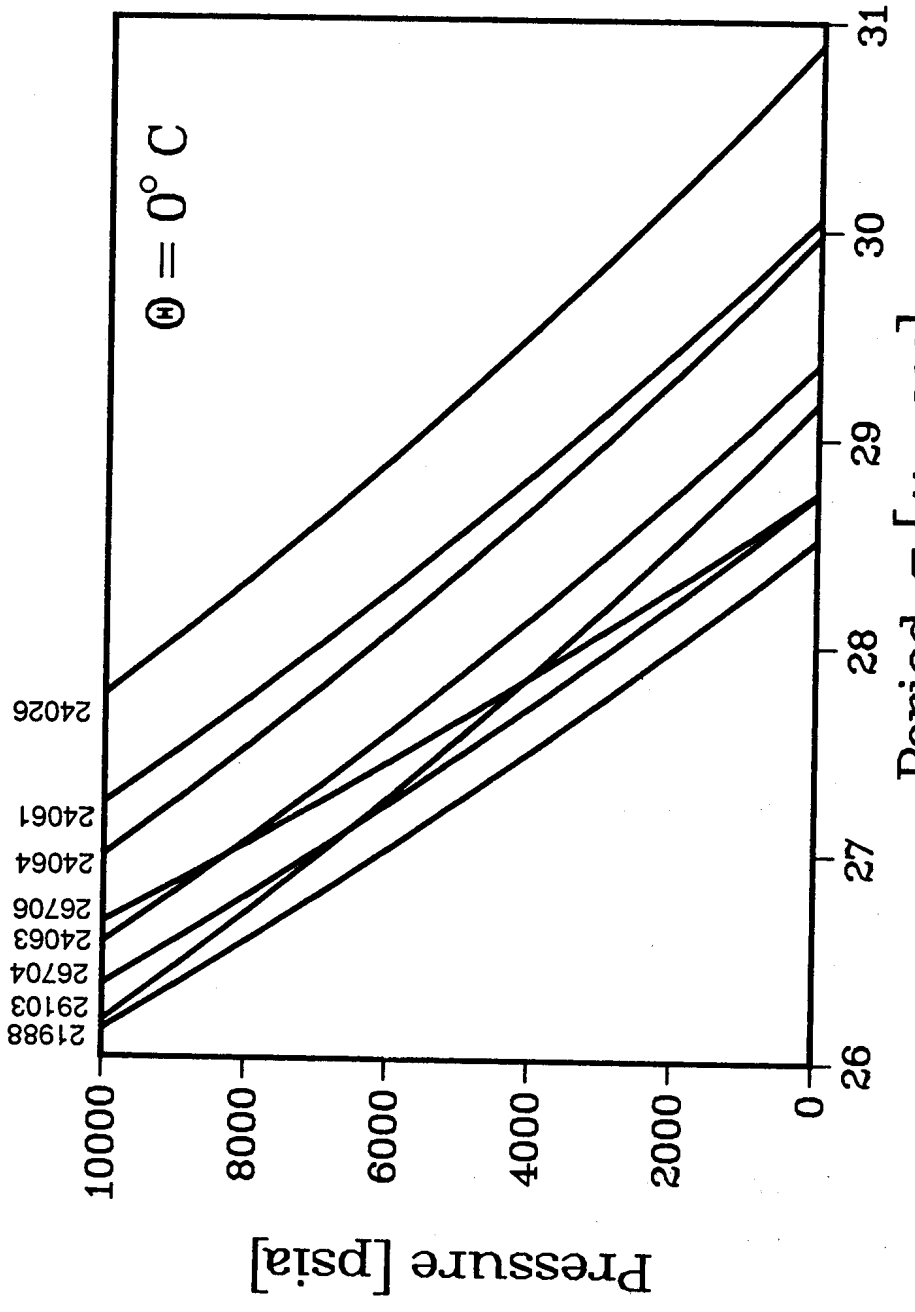

Figure 3. Paroscientific pressure sensor calibration curves for 0°C.

2.2 Static Sensitivity

The static sensitivity of the instrument is given by differentiating and rearranging (4c) to obtain

$$dP = -(2C/N_0)\,[1-1/(2D) + (1-4DP/C)^{1/2}/(2D)]^{1/2}\,(1-4DP/C)^{1/2}\,dN\,. \qquad (5)$$

For each particular instrument, the basic count N_0 is kept constant by varying the integer n in (1) as a function of the integration period, $\bar{\tau}$. The integration period is obtained by partitioning one hour into 2^k equal divisions. Thus, for $\bar{\tau}$ in seconds

$$N_0 = F_0\,\bar{\tau} = 2^n f_0 \bar{\tau} = 2^n f_0\, 3600/2^k = 2^{n-k}\, 3600\, f_0 = 1800\, f_0 = 1800/\tau_0\,,$$

where the relationship

$$n = k - 1$$

has been chosen to give each instrument a sensitivity of approximately 1 mm per count. As an illustrative example, assume

$C \sim -45{,}000$ [psia] ,
$D \sim .03$,
$\tau_0 \sim 30$ [μ–sec] ,
$f_0 = 1/\tau_0 \sim 33$ [KHz] ,

as representative of the values in Table 3. The case in which k = 6 implies

$$\bar{\tau} = 3600/2^6 = 3600/64 = 56.25 \text{ seconds.}$$

Then n = 5, and

$$F_0 = 2^5 f_0 = 32\, f_0 \sim 32 \times 33 \text{ KHz} \sim 1.056 \times 10^6 \text{ cycles/second,}$$

so that

$$N_0 = F_0\bar{\tau} \sim 56.25 \times 1.056 \times 10^6 = 59.4 \times 10^6 \text{ cycles.}$$

Using this value in (5) and setting dN = 1 cycle and P = 0 psia yields

$$dP = -2C/N_0 = 2 \times 45 \times 10^3/59.4 \times 10^6 = 1.5 \times 10^{-3} \text{ psia}$$

for the change in pressure corresponding to 1 instrument count (the "least count" sensitivity). In pure water, 1 psia = .703 m, and in sea water, 1 psia ~.67 m = 670 mm, so that dH, the equivalent least count change of the sea water head, is

$$dH \sim 670\, dP = 1.005 \text{ mm}$$

at P = 0. Note that if representative values for D and C are used, the quantity

$$D/C \cong -6.7 \times 10^{-7} \text{ [psia]}^{-1},$$

so that, even for full scale values of P ~ 10^4 psia

$$4DP/C \sim -2.7 \times 10^{-2},$$

and

$$(4DP/C)^2 \sim 7.3 \times 10^{-4} << 1.$$

Therefore, the approximation

$$(1-4DP/C)^{1/2} = \sim 1-2DP/C,$$

is made, which, when inserted in (5) yields:

$$dP \sim -(2C/N_0)(1-P/C-4DP/C + 4DP^2/C^2)^{1/2}\, dN. \qquad (6)$$

Typically, C is approximately 5 times the value of the full-scale pressure capability of the sensor. Therefore, the factor in parentheses reaches a value of approximately 1.1 at full-scale pressure, and the static sensitivity thus varies by approximately 10% across the entire range of the instrument. Table 3 also includes the static sensitivities for each gauge, dH_0 and dH_{10K}, at zero pressure and full-scale pressure of 10,000 psia, respectively.

2.3 Frequency Response

Consider the case of a time-harmonic signal

$$P(t) = P_{msl} + p\, e^{i\sigma t}\,, \tag{7}$$

where P_{msl} corresponds to the pressure induced at a particular site by mean sea level (and some mean density distribution). Here, $\sigma = 2\pi/T$ is the radial frequency of the signal with period T, and p is the amplitude of the signal. The number of counts induced by the time-varying pressure measured over a period $\bar{\tau}$, centered at time t, is given by

$$N(t) = \int_{t-\bar{\tau}/2}^{t+\bar{\tau}/2} F(s)\, ds = \int_{t-\bar{\tau}/2}^{t+\bar{\tau}/2} F(P(s))\; ds\,, \tag{8}$$

where F(P(t)) is obtained by inserting (7) in (4b). As a consequence of the finite integration time $\bar{\tau}$, the peak value of a time-varying pressure signal will always be underestimated. In practice, N is also an integer; i.e. a fractional cycle of the oscillator is not counted. This error introduced by truncating N to an integer is insignificant and will be ignored here.

To integrate (8), the expression for F given by (4b) could be expanded in a binomial series based on the small parameter (D/C). The function F would then be approximated by a polynomial in P. A better strategy for dealing with pressures given by (7) is to expand F in a polynomial based on the reference pressure P_{msl}, and require the expansion to match the value of the function and all of its derivatives at $P = P_{msl}$. This is a Taylor expansion about P_{msl}, and results in the approximation

$$F(P) \sim \tilde{F}(P) = F(P_{msl}) + F'(P_{msl})\,(P-P_{msl}) + \tfrac{1}{2}F''(P_{msl})\,(P-P_{msl})^2 + \ldots$$

Inserting (7) and truncating the series to a quadratic yields

$$F(P) \sim \tilde{F}(P) = F(P_{msl}) + F'(P_{msl})\, pe^{i\sigma t} + \tfrac{1}{2}F''(P_{msl})\, p^2 e^{i2\sigma t}\,, \tag{9a}$$

where constant temperature is assumed and where primes denote partial derivatives with respect to the pressure P. Here, using (4b), we have also defined:

$$F_{msl} \equiv F(P_{msl}) = F_0 Y\,, \tag{9b}$$

$$F'_{msl} \equiv F'(P_{msl}) = -\varepsilon F_0/(2XY)\,, \tag{9c}$$

$$F''_{msl} \equiv F''(P_{msl}) = -\varepsilon^2 F_0(3X-2+4D)/(4X^3Y^3)\,, \tag{9d}$$

with

$$X \equiv (1-4\varepsilon D P_{msl})^{1/2} , \tag{9e}$$

$$Y \equiv [1-1/(2D)+X/(2D)]^{1/2} , \tag{9f}$$

and $\varepsilon \equiv C^{-1}$.

To compare this Taylor expansion with the exact expression, set $\sigma = 0$ in (9a), so that we are examining a small, constant pressure increment to P_{msl}

$$P = P_{msl} + p . \tag{10a}$$

The difference in counts is then given by

$$\Delta N(P) = N(P) - \tilde{N}(P) = \bar{\tau} F(P) - \bar{\tau} \tilde{F}(P) , \tag{10b}$$

where F is computed using (4b), and $\tilde{F}$ is computed using (9). ΔN represents an upper limit for the error in the number of counts obtained in the integration (8). If this error is less than one count, the approximation is acceptable. Table 4a lists values of the error ΔN for p = 10 psia and the temperatures $\Theta = 0$ and 21°C, over the full range of ambient pressure values, P_{msl}. The approximation is excellent, with typical errors on the order of 10^{-5}. Further, if only the first two terms in (9a) are retained, the error is still less than one, as shown by the results in Table 4b.

Equation (8) then becomes

$$\tilde{N}(t) = F_{msl} \int_{t-\bar{\tau}/2}^{t+\bar{\tau}/2} ds + F'_{msl}\, p \int_{t-\bar{\tau}/2}^{t+\bar{\tau}/2} e^{i\sigma s}\, ds + \tfrac{1}{2} F''_{msl}\, p^2 \int_{t-\bar{\tau}/2}^{t+\bar{\tau}/2} e^{i2\sigma s}\, ds , \tag{11}$$

or, performing the integration,

$$\tilde{N}(t) = N_{msl} + p N'_{msl}\, \phi_1(\sigma)\, e^{i\sigma t} + \tfrac{1}{2} p^2 N''_{msl}\, \phi_2(\sigma)\, e^{i2\sigma t} , \tag{11b}$$

where we have defined

$$N_{msl} \equiv \bar{\tau} F_{msl} = \bar{\tau} F_0 Y = N_0 Y \tag{11c}$$

$$N'_{msl} \equiv \bar{\tau} F'_{msl} = -\varepsilon N_0/(2XY) \tag{11d}$$

TABLE 4a. The error count, ΔN, using three terms of a Taylor's expansion for the sensor frequency F.

P_{msl} [psia]	=	0.	2000.	4000.	6000.	8000.	10000.
Paros SN	Temp (°C)	p (psia)	ΔN (Count error given by Equation 10)				
21988	.0	1.0	−4.5E-08	0.0E-01	−1.0E-07	1.7E-07	1.5E-08	−4.5E-08
21988	.0	10.0	−3.2E-05	−2.9E-05	−2.7E-05	−2.4E-05	−2.2E-05	−2.1E-05
21988	21.0	1.0	1.5E-08	3.7E-08	−1.5E-08	−1.6E-07	−1.0E-07	1.5E-08
21988	21.0	10.0	−3.2E-05	−2.9E-05	−2.7E-05	−2.5E-05	−2.2E-05	−2.1E-05
24026	.0	1.0	−1.5E-08	−8.2E-08	−6.7E-08	−1.5E-08	−5.2E-08	−8.2E-08
24026	.0	10.0	−5.9E-05	−5.2E-05	−4.7E-05	−4.2E-05	−3.8E-05	−3.4E-05
24026	21.0	1.0	−7.5E-09	−8.2E-08	−1.2E-07	−2.2E-08	−1.3E-07	−7.5E-08
24026	21.0	10.0	−5.9E-05	−5.2E-05	−4.7E-05	−4.2E-05	−3.8E-05	−3.4E-05
24061	.0	1.0	−3.7E-08	−1.3E-07	−7.5E-09	−5.2E-08	−8.2E-08	0.0E-01
24061	.0	10.0	−4.6E-05	−4.2E-05	−3.7E-05	−3.4E-05	−3.1E-05	−2.8E-05
24061	21.0	1.0	−4.5E-08	−8.2E-08	2.2E-08	−3.0E-08	5.2E-08	−1.5E-07
24061	21.0	10.0	−4.7E-05	−4.2E-05	−3.7E-05	−3.4E-05	−3.1E-05	−2.8E-05
24063	.0	1.0	0.0E-01	6.7E-08	5.2E-08	−7.5E-08	−4.5E-08	−4.5E-08
24063	.0	10.0	−5.0E-05	−4.4E-05	−4.0E-05	−3.6E-05	−3.2E-05	−3.0E-05
24063	21.0	1.0	−5.2E-08	7.5E-08	−1.0E-07	−8.2E-08	−6.0E-08	1.5E-08
24063	21.0	10.0	−5.0E-05	−4.4E-05	−4.0E-05	−3.6E-05	−3.3E-05	−3.0E-05
24064	.0	1.0	−3.7E-08	−1.5E-08	−1.4E-07	−8.9E-08	−6.7E-08	−5.2E-08
24064	.0	10.0	−5.7E-05	−5.1E-05	−4.5E-05	−4.1E-05	−3.7E-05	−3.3E-05
24064	21.0	1.0	−1.2E-07	−1.5E-08	−1.2E-07	2.2E-08	−1.0E-07	−1.2E-07
24064	21.0	10.0	−5.7E-05	−5.1E-05	−4.5E-05	−4.1E-05	−3.7E-05	−3.3E-05
26704	.0	1.0	−7.5E-08	−5.2E-08	5.2E-08	0.0E-01	−6.0E-08	7.5E-08
26704	.0	10.0	−3.1E-05	−2.8E-05	−2.6E-05	−2.3E-05	−2.2E-05	−2.0E-05
26704	21.0	1.0	3.0E-08	−1.0E-07	1.5E-08	7.5E-08	8.9E-08	0.0E-01
26704	21.0	10.0	−3.1E-05	−2.8E-05	−2.6E-05	−2.4E-05	−2.1E-05	−2.0E-05
26706	.0	1.0	3.0E-08	−2.2E-08	−3.0E-08	0.0E−01	1.5E-08	−1.5E-08
26706	.0	10.0	−1.9E-05	−1.8E-05	−1.7E-05	−1.5E-05	−1.4E-05	−1.3E-05
26706	21.0	1.0	1.2E-07	−3.0E-08	−2.2E-08	−1.0E-07	−1.0E-07	−7.5E-08
26706	21.0	10.0	−1.9E-05	−1.8E-05	−1.7E-05	−1.5E-05	−1.4E-05	−1.3E-05
29103	.0	1.0	−5.2E-08	−1.4E-07	−2.1E-07	−5.2E-08	−4.5E-08	−4.5E-08
29103	.0	10.0	−6.4E-05	−5.7E-05	−5.1E-05	−4.5E-05	−4.1E-05	−3.7E-05
29103	21.0	1.0	−6.7E-08	−1.6E-07	3.0E-08	−6.7E-08	7.5E-08	0.0E-01
29103	21.0	10.0	−6.4E-05	−5.7E-05	−5.1E-05	−4.5E-05	−4.1E-05	−3.7E-05

TABLE 4b. The error count, ΔN, using two terms of a Taylor's expansion for the sensor frequency F.

P_{msl} [psia]	=	0.	2000.	4000.	6000.	8000.	10000.
Paros SN	Temp (°C)	p (psia)	ΔN (Count error given by Equation 10)				
21988	0.0	1.0	3.3E-03	3.1E-03	3.0E-03	2.8E-03	2.7E-03	2.5E-03
21988	0.0	10.0	3.3E-01	3.1E-01	3.0E-01	2.8E-01	2.7E-01	2.5E-01
21988	21.0	1.0	3.3E-03	3.1E-03	3.0E-03	2.8E-03	2.7E-03	2.5E-03
21988	21.0	10.0	3.3E-01	3.1E-01	3.0E-01	2.8E-01	2.7E-01	2.5E-01
24026	0.0	1.0	4.8E-03	4.5E-03	4.2E-03	3.9E-03	3.7E-03	3.5E-03
24026	0.0	10.0	4.8E-01	4.5E-01	4.2E-01	3.9E-01	3.7E-01	3.5E-01
24026	21.0	1.0	4.8E-03	4.5E-03	4.2E-03	3.9E-03	3.7E-03	3.5E-03
24026	21.0	10.0	4.8E-01	4.5E-01	4.2E-01	3.9E-01	3.7E-01	3.5E-01
24061	0.0	1.0	4.1E-03	3.9E-03	3.6E-03	3.4E-03	3.2E-03	3.1E-03
24061	0.0	10.0	4.1E-01	3.9E-01	3.6E-01	3.4E-01	3.2E-01	3.1E-01
24061	21.0	1.0	4.1E-03	3.9E-03	3.6E-03	3.4E-03	3.2E-03	3.1E-03
24061	21.0	10.0	4.1E-01	3.9E-01	3.6E-01	3.4E-01	3.2E-01	3.1E-01
24063	0.0	1.0	4.4E-03	4.1E-03	3.8E-03	3.6E-03	3.4E-03	3.2E-03
24063	0.0	10.0	4.4E-01	4.1E-01	3.8E-01	3.6E-01	3.4E-01	3.2E-01
24063	21.0	1.0	4.4E-03	4.1E-03	3.8E-03	3.6E-03	3.4E-03	3.2E-03
24063	21.0	10.0	4.4E-01	4.1E-01	3.8E-01	3.6E-01	3.4E-01	3.2E-01
24064	0.0	1.0	4.8E-03	4.4E-03	4.2E-03	3.9E-03	3.7E-03	3.5E-03
24064	0.0	10.0	4.8E-01	4.4E-01	4.2E-01	3.9E-01	3.7E-01	3.5E-01
24064	21.0	1.0	4.8E-03	4.4E-03	4.2E-03	3.9E-03	3.7E-03	3.5E-03
24064	21.0	10.0	4.8E-01	4.4E-01	4.2E-01	3.9E-01	3.7E-01	3.5E-01
26704	0.0	1.0	3.2E-03	3.0E-03	2.9E-03	2.7E-03	2.6E-03	2.5E-03
26704	0.0	10.0	3.2E-01	3.0E-01	2.9E-01	2.7E-01	2.6E-01	2.5E-01
26704	21.0	1.0	3.2E-03	3.0E-03	2.9E-03	2.7E-03	2.6E-03	2.5E-03
26704	21.0	10.0	3.2E-01	3.0E-01	2.9E-01	2.7E-01	2.6E-01	2.5E-01
26706	0.0	1.0	2.3E-03	2.2E-03	2.1E-03	2.0E-03	1.9E-03	1.9E-03
26706	0.0	10.0	2.3E-01	2.2E-01	2.1E-01	2.0E-01	1.9E-01	1.9E-01
26706	21.0	1.0	2.3E-03	2.2E-03	2.1E-03	2.0E-03	1.9E-03	1.9E-03
26706	21.0	10.0	2.3E-01	2.2E-01	2.1E-01	2.0E-01	1.9E-01	1.9E-01
29103	0.0	1.0	5.2E-03	4.8E-03	4.5E-03	4.2E-03	4.0E-03	3.7E-03
29103	0.0	10.0	5.2E-01	4.8E-01	4.5E-01	4.2E-01	4.0E-01	3.7E-01
29103	21.0	1.0	5.2E-03	4.8E-03	4.5E-03	4.2E-03	4.0E-03	3.7E-03
29103	21.0	10.0	5.2E-01	4.8E-01	4.5E-01	4.2E-01	4.0E-01	3.7E-01

$$N''_{msl} \equiv \bar{\tau}F''_{msl} = -\varepsilon^2 N_0(3X-2+4D)/(4X^3Y^3) \tag{11e}$$

$$\phi_k(\sigma) \equiv \sin(k\sigma\bar{\tau}/2)/(k\sigma\bar{\tau}/2)\ ;\ k = 1,2. \tag{11f}$$

Returning to equation (3),

$$\tilde{P}(t) = C(1-D) + C(2D-1)\left(\tilde{N}/N_0\right)^2 - CD\left(\tilde{N}/N_0\right)^4 ,$$

or, inserting (11), performing the indicated algebra, and collecting terms,

$$\tilde{P}(t) = P_{msl} + p\left[\phi_1 e^{i\sigma\tau} + \sum_{k=1}^{7} \varepsilon^k p^k A_k e^{ik\sigma\tau}\right]$$

so that the ratio of detected signal to applied signal amplitude is

$$\tilde{p}(t)/p \equiv \left[\tilde{P}(t) - P_{msl}\right]/p = \phi_1 e^{i\sigma\tau} + \sum_{k=1}^{7} \varepsilon^k p^k A_k e^{ik\sigma\tau} \tag{12a}$$

where the coefficients A_k are given by

$$A_1 = u\left(\phi_2 - \phi_1^2\right)/4X^2Y^2 \tag{12b}$$

$$A_2 = \left(2vx\phi_1^2 - u^2\phi_2\right)/8X^4Y^4 \tag{12c}$$

$$A_3 = \left(12uvx\phi_1^2\phi_2 - 2vx^2\phi_1^4 - u^3\phi_2^2\right)/64X^6Y^6 \tag{12d}$$

$$A_4 = Du\left(3u\phi_2 - 2x\phi_1^2\right)\phi_1\phi_2/32X^7Y^6 \tag{12e}$$

$$A_5 = Du^2\left(u\phi_2 - 3x\phi_1^2\right)\phi_2^2/128X^9Y^8 \tag{12f}$$

$$A_6 = -Du^3\phi_1\phi_2^3/256X^{10}Y^{10} \tag{12g}$$

$$A_7 = -Du^4\phi_2^4/4096X^{12}Y^{12} \tag{12h}$$

and where we have defined

$$u \equiv 3X-2+4D \tag{12i}$$

$$v \equiv X-1+2D\ . \tag{12j}$$

The coefficients A_k are thus functions of σ and the five parameters $(\bar{\tau}, P_{msl}, C, D, \tau_0)$; that is

$$A_k = A_k(\sigma; \bar{\tau}, P_{msl}, C, D, \tau_0) .$$

The Fourier transform of (12a) yields the frequency response function

$$\psi(\omega) = \int_{-\infty}^{\infty} [\tilde{p}(t)/p]\, e^{-i\omega t}\, dt = \phi_1 \int_{-\infty}^{\infty} e^{i(\sigma-\omega)t}\, dt + \sum_{k=1}^{7} \varepsilon^k p^k A_k \int_{-\infty}^{\infty} e^{i(k\sigma-\omega)t}\, dt ,$$

or

$$\psi(\omega) = \phi_1\, \delta(\sigma-\omega) + \sum_{k=1}^{7} \varepsilon^k p^k A_k\, \delta(k\sigma-\omega)$$

where δ is Kronecker's delta function, so that

$$\psi(\omega) = \phi_1(\omega) + \sum_{k=1}^{7} \varepsilon^k p^k A_k(\sigma=\omega/k) . \qquad (13)$$

Since the coefficients A_k are proportional to ε^k, their magnitude falls off very rapidly and, to a very good approximation, we have

$$\psi(\omega) \approx \phi_1(\omega) = \sin(\omega\bar{\tau}/2)/(\omega\bar{\tau}/2) .$$

Tables 5a-d present ψ, computed using (13), for a pressure signal of p = 10 psia and an ambient temperature of $\theta = 0°C$, for integration times $\bar{\tau} = 28.125$ and 56.25 secs, and ambient pressure values of $P_{msl} = 0$ and 10K psia. There is essentially no difference between gauges, and the 95% response level is achieved for periods of 3 and 6 minutes in the case of 28.125 and 56.25 second averaging times, respectively. This holds for ambient pressures of both 0 and 10K psia.

2.4 Temperature Sensitivity

Rewriting (2a) as

$$P = Cs(1-Ds), \qquad (14a)$$

and defining the quantities

$$s \equiv 1-r^2 \qquad (14b)$$

TABLE 5a. The frequency response function, ψ.

$\bar{\tau}$	P_{msl}	θ	p
56.25 secs	0 psia	0°C	10 psia

T (min)	Paros Serial Number							
	21988	24026	24061	24063	24064	26704	26706	29103
1.00	.066	.066	.066	.066	.066	.066	.066	.066
2.00	.676	.676	.676	.676	.676	.676	.676	.676
3.00	.847	.847	.847	.847	.847	.847	.847	.847
4.00	.912	.912	.912	.912	.912	.912	.912	.912
5.00	.943	.943	.943	.943	.943	.943	.943	.943
6.00	.960	.960	.960	.960	.960	.960	.960	.960
7.00	.971	.971	.971	.971	.971	.971	.971	.971
8.00	.978	.978	.978	.978	.978	.978	.978	.978
9.00	.982	.982	.982	.982	.982	.982	.982	.982
10.00	.986	.986	.986	.986	.986	.986	.986	.986
11.00	.988	.988	.988	.988	.988	.988	.988	.988
12.00	.990	.990	.990	.990	.990	.990	.990	.990
13.00	.991	.991	.991	.991	.991	.991	.991	.991
14.00	.993	.993	.993	.993	.993	.993	.993	.993
15.00	.994	.994	.994	.994	.994	.994	.994	.994

TABLE 5b. The frequency response function, ψ.

$\bar{\tau}$	$P_{msl.}$	θ	p
56.25 secs	10K psia	0°C	10 psia

T (min)	Paros Serial Number							
	21988	24026	24061	24063	24064	26704	26706	29103
1.00	.066	.066	.066	.066	.066	.066	.066	.066
2.00	.676	.676	.676	.676	.676	.676	.676	.676
3.00	.847	.847	.847	.847	.847	.847	.847	.847
4.00	.912	.912	.912	.912	.912	.912	.912	.912
5.00	.943	.943	.943	.943	.943	.943	.943	.943
6.00	.960	.960	.960	.960	.960	.960	.960	.960
7.00	.971	.971	.971	.971	.971	.971	.971	.971
8.00	.978	.978	.978	.978	.978	.978	.978	.978
9.00	.982	.982	.982	.982	.982	.982	.982	.982
10.00	.986	.986	.986	.986	.986	.986	.986	.986
11.00	.988	.988	.988	.988	.988	.988	.988	.988
12.00	.990	.990	.990	.990	.990	.990	.990	.990
13.00	.991	.991	.991	.991	.991	.991	.991	.991
14.00	.993	.993	.993	.993	.993	.993	.993	.993
15.00	.994	.994	.994	.994	.994	.994	.994	.994

TABLE 5c. The frequency response function, ψ.

$\bar{\tau}$	P_{msl}	θ	p
28.125 secs	0 psia	0°C	10 psia

T (min)	Paros Serial Number							
	21988	24026	24061	24063	24064	26704	26706	29103
1.00	.676	.676	.676	.676	.676	.676	.676	.676
2.00	.912	.912	.912	.912	.912	.912	.912	.912
3.00	.960	.960	.960	.960	.960	.960	.960	.960
4.00	.978	.978	.978	.978	.978	.978	.978	.978
5.00	.986	.986	.986	.986	.986	.986	.986	.986
6.00	.990	.990	.990	.990	.990	.990	.990	.990
7.00	.993	.993	.993	.993	.993	.993	.993	.993
8.00	.994	.994	.994	.994	.994	.994	.994	.994
9.00	.996	.996	.996	.996	.996	.996	.996	.996
10.00	.996	.996	.996	.996	.996	.996	.996	.996
11.00	.997	.997	.997	.997	.997	.997	.997	.997
12.00	.997	.998	.997	.997	.997	.997	.997	.998
13.00	.998	.998	.998	.998	.998	.998	.998	.998
14.00	.998	.998	.998	.998	.998	.998	.998	.998
15.00	.998	.998	.998	.998	.998	.998	.998	.998

TABLE 5d. The frequency response function, ψ.

$\bar{\tau}$	$P_{msl.}$	θ	p
28.125 secs	10K psia	0°C	10 psia

T (min)	Paros Serial Number							
	21988	24026	24061	24063	24064	26704	26706	29103
1.00	.676	.676	.676	.676	.676	.676	.676	.676
2.00	.912	.912	.912	.912	.912	.912	.912	.912
3.00	.960	.960	.960	.960	.960	.960	.960	.960
4.00	.978	.978	.978	.978	.978	.978	.978	.978
5.00	.986	.986	.986	.986	.986	.986	.986	.986
6.00	.990	.990	.990	.990	.990	.990	.990	.990
7.00	.993	.993	.993	.993	.993	.993	.993	.993
8.00	.994	.994	.994	.994	.994	.994	.994	.994
9.00	.996	.996	.996	.996	.996	.996	.996	.996
10.00	.996	.996	.996	.996	.996	.996	.996	.996
11.00	.997	.997	.997	.997	.997	.997	.997	.997
12.00	.997	.998	.997	.997	.997	.997	.997	.998
13.00	.998	.998	.998	.998	.998	.998	.998	.998
14.00	.998	.998	.998	.998	.998	.998	.998	.998
15.00	.998	.998	.998	.998	.998	.998	.998	.998

$$r \equiv \tau_0/\tau \, . \tag{14c}$$

For a constant pressure P

$$\dot{P} = \dot{C}s(1-Ds) + C\dot{s}(1-2Ds) \, , \tag{15a}$$

or

$$\dot{P} = [\dot{C}/C + \dot{s}/s - D\dot{s}/(1-Ds)]\, P \, , \tag{15b}$$

where the dot indicates differentiation with respect to the temperature θ, and where (using (2b), (2d), and (4a))

$$\dot{C} = C_2 + 2C_3\Theta \, , \tag{15c}$$

$$\dot{s} = -2r\dot{r} = -2r^2\dot{\tau}_0/\tau_0 \, , \tag{15d}$$

$$\dot{r} = \dot{\tau}_0/\tau_0 \, , \tag{15e}$$

$$\dot{\tau}_0/\tau_0 = (\tau_2 + 2\tau_3\Theta + 3\tau_4\Theta^2)/(\tau_1 + \tau_2\Theta + \tau_3\Theta^2 + \tau_4\Theta^3) \, , \tag{15f}$$

$$r = \tau_0/\tau = [1-1/(2D) + (1-4DP/C)^{1/2}/(2D)]^{1/2} \, . \tag{15g}$$

To convert units from [psia/°C] to [cm/°C],

$$\dot{H} \sim 67\,\dot{P} \, . \tag{15h}$$

This is approximately true in sea water. Tables 6a and 6b present $\dot{H}$ as a function of the ambient pressure P, for $\theta = 0$ and 21°C, respectively. There is considerable variation of temperature sensitivity between gauges, but the sensitivity can be on the order of 1 m/°C. This is not a problem in a stable temperature environment, since relative pressure is the usual parameter of interest. However, in shallow nearshore environments where the temperature regime is not constant, accurate tracking of the temperature of the quartz crystal sensor can be an important concern, especially if small signals on the order of centimeters are of interest.

3. FIELD OPERATIONS

Two BPR models are presently in use at PMEL, Models 635-7H and 1635-7H. Both use the Paroscientific pressure transducer and Sea Data recording devices. However, the physical

TABLE 6a. The temperature sensitivity, $\dot{H}$, as a function of ambient pressure at 0°C. Units are (cm/°C).

P (psia)	Paros Serial Number							
	21988	24026	24061	24063	24064	26704	26706	29103
0.0	39.6	93.4	−41.3	−34.0	−7.9	−13.6	18.6	132.5
2000.0	38.4	87.0	−34.9	−27.1	−5.0	−9.5	20.0	122.7
4000.0	37.2	81.2	−29.1	−20.8	−2.4	−5.6	21.4	113.8
6000.0	36.2	75.9	−23.7	−15.1	0.0	−2.1	22.6	105.8
8000.0	35.2	71.0	−18.8	−9.7	2.1	1.2	23.8	98.4
10000.0	34.3	66.6	−14.2	−4.9	4.1	4.2	24.9	91.7

TABLE 6b. The temperature sensitivity, $\dot{H}$, as a function of ambient pressure at 21°C. Units are (cm/°C).

P (psia)	Paros Serial Number							
	21988	24026	24061	24063	24064	26704	26706	29103
.0	8.1	60.8	−73.3	−72.0	−39.9	−51.7	−25.8	98.6
2000.0	9.5	57.4	−64.2	−61.7	−34.1	−44.8	−21.4	92.0
4000.0	10.7	54.3	−56.0	−52.4	−28.9	−38.4	−17.4	86.0
6000.0	11.8	51.5	−48.4	−43.8	−24.1	−32.5	−13.6	80.6
8000.0	12.9	49.0	−41.5	−36.0	−19.7	−27.0	−10.0	75.6
10000.0	13.9	46.6	−35.1	−28.7	−15.7	−21.8	−6.6	71.1

configuration of each is significantly different. A sketch of the units and a typical mooring configuration for each model is presented in Fig. 4.

Model 635-7H is the earliest BPR version in which the electronics are housed in a cylindrical anodized aluminum pressure case. Design and fabrication was a collaborative PMEL/ SeaData effort. The BPR unit and separate acoustic release are mounted on a flat circular platform with an aluminum tripod. Below the platform is an expendable anchor which is held in place by the acoustic release mechanism. The top of the tripod is tethered to a cluster of five Benthos glass spheres by approximately 30 feet of 1/2-inch nylon line; the five spheres are the principal mooring flotation, and are arranged in either series, pairs, or a combination of both. Another 30 feet of either 3/8-inch Samson Super Strong or 1/2-inch three-strand polypropelene is used to tether the sphere cluster to a marker buoy, which is designed to aid in mooring recovery.

Model 1635-7H is an adaptation of the Sea Data Inverted Echo Sounder (IES), and was designed and fabricated by Sea Data to PMEL specifications in 1987. The configuration of this

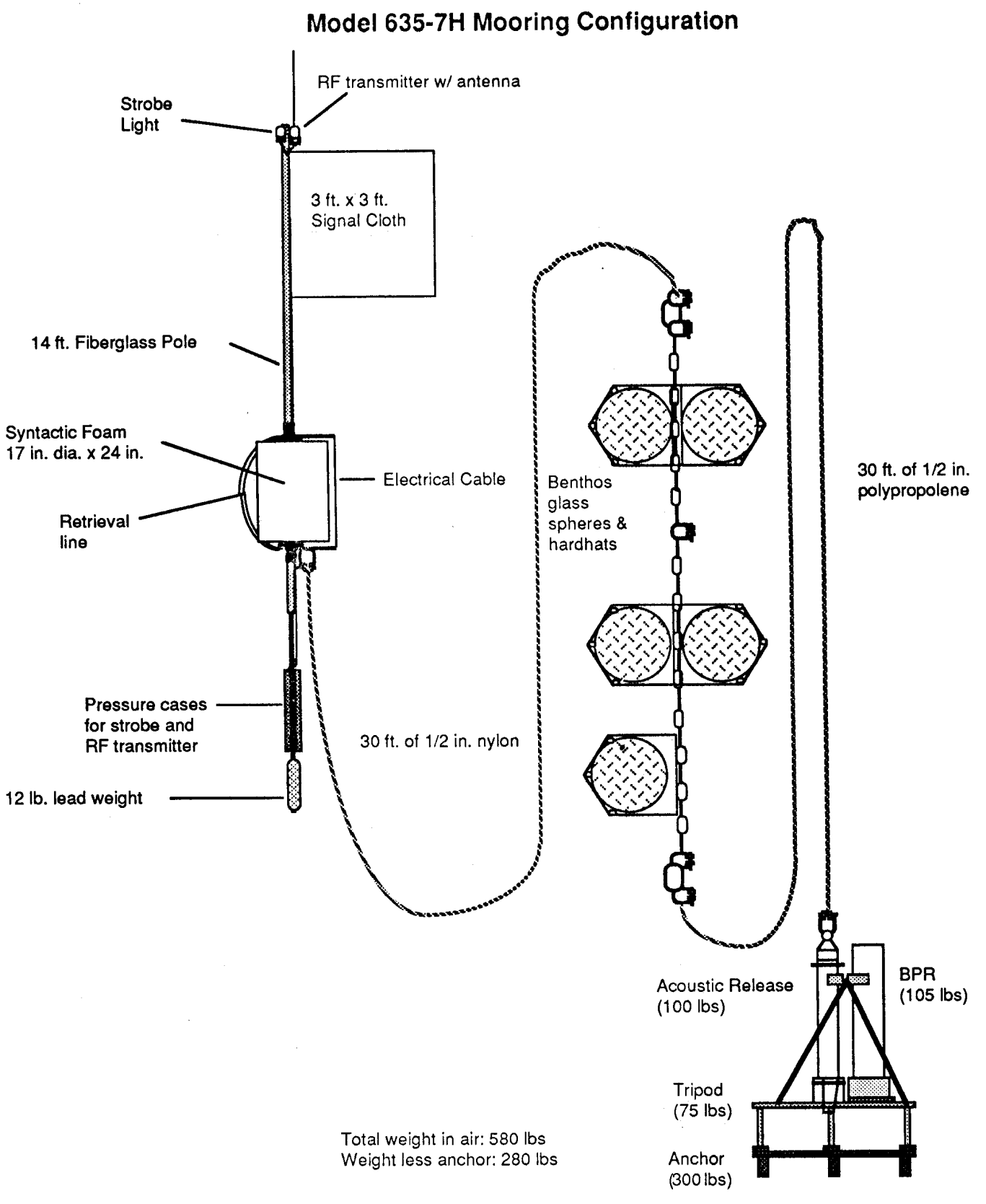

Figure 4a. Model 635-7H BPR mooring configuration.

Model 1635-7H Mooring Configuration

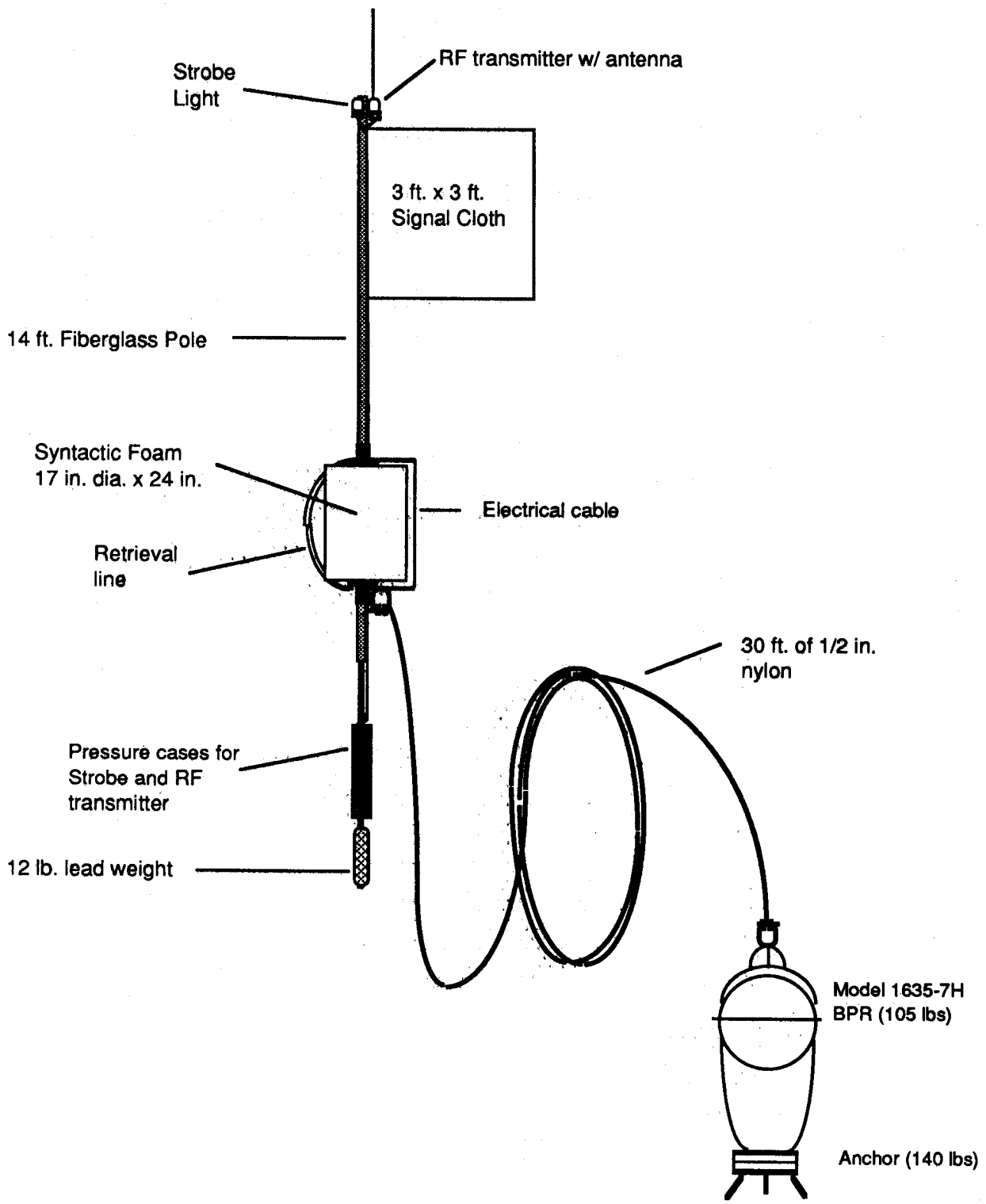

Figure 4b. Model 1635-7H BPR mooring configuration.

model includes a Benthos 17-inch glass sphere housing all of the electronics, and a syntactic foam flotation package staged inside a protective composite shroud (see Fig. 4b). Two additional systems are mounted externally; at the top of the shroud is the acoustic transponder for communicating with the unit from the deck of a ship, and at the bottom is the anchor and burn-wire release mechanism. Although this unit is self-contained in the sense that it can be deployed without additional flotation, it is nonetheless always tethered to a marker buoy to aid recovery due to its low surface profile.

The marker buoy is spar-like in design to improve stability, and utilizes cylindrical syntactic foam for flotation. The upper mast of the buoy incorporates three separate recovery aids: a VHF transmitter, a strobe light, and an international orange flag approximately 3 by 3 feet square. A fourth recovery aid system is represented by the acoustic release unit associated with each BPR, since they can be tracked by either a portable acoustic deck unit or the ship's precision depth recorder (PDR) (see Section 3.2, below).

3.1 Pre-Deployment

Before deployment, all BPR units are refurbished with battery packs and other single use deployment parts and then subjected to a series of in-house laboratory tests. A pre-deployment checksheet (Fig. 5) has been developed to aid in making the instrument preparations as uniform, complete, and error-free as possible. All recorded times are accurate to within one second or less, and are referenced to the U.S. Naval Observatory time checks which are broadcast over radio station WWV by the National Bureau of Standards.

The time base clock frequency is measured at ambient temperature and at 3-5°C for the purpose of estimating any time base drift which might occur during deployment. (These clock frequency measurements were first incorporated into the procedures on deployment number 15.) Data cassette tapes are degaussed and the type, batch, and part number of each tape are recorded. The cassette tape itself is annotated with the location and identification number of the intended station, and the date of the instrument preparation. The tape heads are cleaned, after which the tape is manually advanced past the leader, loaded into the recorder, and checked to insure proper fit. The sampling rate is set for the desired number of measurements per hour, the unit is switched on, and the exact time is recorded.

An LED indicator light flashes each time a data record (consisting of temperature, time, and sixteen pressure values) is written to tape. If the unit is set to acquire 64 samples per hour, this data recording cycle occurs every fifteen minutes. The exact time of at least two of these LED flashes are logged as a check on the proper operation of the unit. Several independent measurements of atmospheric pressure are recorded and time tags which consist of carefully timed pressure pulses of 10 to 100 psia are applied to the BPR record in the laboratory or aboard ship using a portable Sinco Pressure unit, part number 51491, as a time reference. Typically, the

BPR Worksheet Deployment #_____

MODEL NO. _____ Date: _____
RECORDER SERIAL NO. _____ Initials: _____

PURPOSE: (test, pre-deployment, post-deployment)
DESCRIPTION: _____

Preliminary Steps

___ Perform and record frequency measurements before tape insertion.
___ Set watch to WWV (circle one) GMT PST (+8) PDST (+7)
___ Degauss tape.
___ Tape: (new, used) Type _____, Batch No. _____, Part No. _____
___ Attach label to Side A. Label with Station No. and time (GMT) of first and last LED blink.
___ Label Side B with project name and general deployment location.
___ Advance tape past leader and/or hole.
___ Clean tape heads.
___ Load tape into recorder & check for proper fit (capstans, etc.).
___ Set measurements for (64, 128) per hour. (See back for recording 1635-7H computer set-up)

M / D / Y - h : m : s	EVENT / COMMENTS	LED Flashes min : sec
/ / - : :	Power on	:
/ / - : :	Run "tape advance" to take up slack	:
/ / - : :	Create 4 sec. file gap	:
/ / - : :	Reset	:
/ / - : :	Operate (635-7H only)	:
/ / - : :	LED flash	
/ / - : :	LED flash	
/ / - : :	Record atmospheric pressure measurements. Include Model No., Serial No.,calib. offset.	
/ / - : :		
/ / - : :		
/ / - : :		
/ / - : :		
/ / - : :		
/ / - : :		
/ / - : :		
/ / - : :		
/ / - : :		
/ / - : :		
/ / - : :		
/ / - : :		
/ / - : :		
/ / - : :		
/ / - : :		
/ / - : :		
/ / - : :	Record atmospheric pressure measurements. Include Model No., Serial No.,calib. offset.	

___ Perform frequency measurements after tape removal.

Figure 5. Pre-deployment checksheets.

Atmospheric Pressure Readings Deployment # _____

Date: ______________________

Instrument: ______________________

Type No.: ______________________

Range: ______________________

Serial No.: ______________________

Offset Corr.: ______________________

Manufacturer: ______________________

Time (GMT)	Reading (mb)

Figure 5 (continued). Pre-deployment checksheets.

duration of the pressure pulse is 15 to 20 minutes and is initiated just prior to the beginning of a data recording cycle; this avoids rollover problems (discussed in Section 4.2), during the data processing by ensuring that a full 24-bit pressure word is recorded during the application of the time tag.

3.2 Deployment

Both BPR models have been successfully deployed by either the float-first or anchor-first method. The method used depends upon the weather, sea state, A-frame configuration and winch type available. As each unit descends, it is tracked to the ocean bottom by either a portable acoustic deck unit or the ship's depth recorder (PDR).

Upon deployment of a Model 635-7H BPR, the acoustic transducer of an EG&G Model 8011 deck unit is lowered into the water at the end of a cable. The acoustic release is then interrogated for range information as the BPR falls to the ocean bottom. Since range estimates are relative to the ship's position, any drift away from the station is undesirable. However, some drift is usually unavoidable, since safety requires that the ship's propeller be stopped to avoid entanglement with over-the-side cable.

The Model 1635-7H transmits at 12 kHz and is tracked with the ship's PDR upon deployment. Since the ship's PDR transponder is mounted on the hull and there is no need for a cable over the side, there is no danger of fouling the propellers and the ship can attempt to maintain station. The acoustic transponder is disabled when the mooring is judged to be on the bottom.

3.3 Recovery

Once the ship is on site, the BPR is interrogated and the transponder is enabled and the release activated with the acoustic release deck unit. As the unit ascends, it is tracked either by the deck unit or the ship's PDR, depending on the BPR model. The VHF transmitter has proven most useful in locating the unit on the sea surface, especially at night, in fog, or inclement weather. Actual recovery is accomplished either with the help of a small boat, or by using a grappling hook to snag the mooring or recovery line alongside ship. Either method is satisfactory, although in inclement weather the use of a small boat is avoided.

3.4 Post-Recovery

After recovery, the unit is returned to PMEL's laboratory where one or two pressure pulse time tags are applied, as described in Section 3.1. Battery voltage is checked, the time base frequency is measured, and several independent measurements of barometric pressure are made. The data cassette tape is then removed, and the data are processed as discussed in Section 4.

4. DATA PROCESSING

All pressure and temperature data obtained using Paroscientific pressure transducers coupled with Sea Data recorders are presently processed on a VAX 11/785 computer operating under VMS in a VAXcluster. All hardware is located and maintained at PMEL. Much of the software used has been developed specifically for BPR data and is continuously evolving. A flowchart of the present processing procedures is given in Fig. 6. The basic procedural steps are discussed below.

4.1 Data Ingestion

Raw data on each cassette tape consists of a sequence of binary numbers forming 18 binary words: one 16-bit temperature word, one 20-bit clock word, one 24-bit pressure word, and fifteen 16 least significant bit pressure words. The 16-bit pressure words are combined with the 8 high bits of the 24-bit pressure word to obtain 24-bit or "full" pressure values. The binary data cassettes are read by a Sea Data Model 12B Cassette Tape Reader, which transcribes the data to computer compatible binary words. If data quality is poor, as indicated by the cassette tape reader as short records or parity errors, data ingestion is repeated one or more times to maximize the recovery of any non-repeatable errors associated with data transfer. The decoded raw data are then translated into their hexadecimal equivalent and transferred to online storage of the VAX for further processing.

4.2 Frequency to Pressure Conversion

Raw temperature counts (M) and pressure counts (N) are converted into scientific units by using standard calibration coefficients provided by the manufacturer for each instrument. Temperature data in degrees C are computed as:

$$\Theta = 10^4 \, (9.07 + 2.253 \ln R + 1.136 \, (\ln R)^3)^{-1} - 273.16 \, , \tag{16}$$

where

$$R = 169050 \, / \, (1 + 1.3995 \, M/57600) - 50000 \, .$$

Pressure is computed using the conformance equation (3), repeated here for convenience,

$$P(N) = C\left\{ 1-(N/N_0)^2 - D\left[1-(N/N_0)^2\right]^2 \right\} \, , \tag{3}$$

where (see section 2.2)

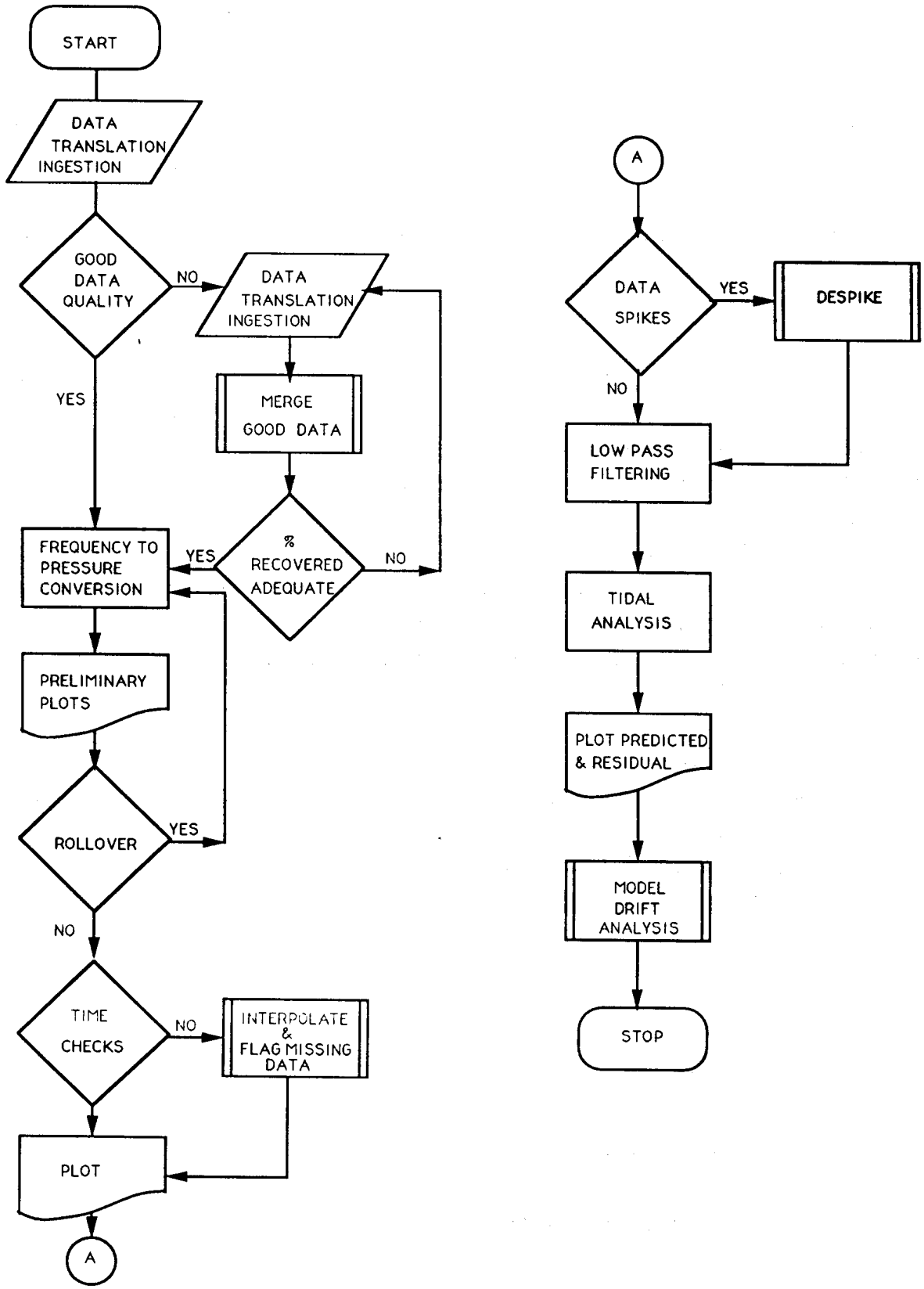

Figure 6. Flowchart of data processing procedures.

$$N_0 = 1800 \times 10^6/\tau_0$$

with τ_0 in micro-seconds. The three calibration coefficients C, D, and τ_0 are functions of temperature Θ,

$$C = C_1 + C_2\Theta + C_3\Theta^2 , \tag{2b}$$

$$D = D_1 , \tag{2c}$$

$$\tau_0 = \tau_1 + \tau_2\Theta + \tau_3\Theta^2 + \tau_4\Theta^3 . \tag{2d}$$

All coefficients are determined simultaneously by a non-linear least squares fit to calibration data (Well-Test Instruments, Inc., 1984).

In processing the data to arrive at a final value for N in equation (3), it is necessary to account for the fact that the number of cycles completed during each individual integration period $\bar{\tau}$ will exceed the limited capacity of the 16- and 24-bit registers, due to the relatively high base frequency of the oscillator. The number of cycles completed, as a function of pressure, is given by equation (4c) of section 2.2,

$$N(P) = N_0 [1 - 1/(2D) + (1 - 4DP/C)^{1/2}/(2D)]^{1/2} . \tag{4c}$$

Since C is negative and is typically of order 5 times the value of the full scale pressure for a given transducer, and a typical value for D is 0.03, then the factor in brackets varies from a value of 1 at P = 0 to a value of 1.09 at $P = 10^4$ psia = full scale. For the typical case discussed in section 2.2, N_0, the number of cycles completed during an integration period at pressure P = 0, is

$$N_0 = F_0\bar{\tau} \sim 1.056 \times 10^6 \times 56.25 = 59.4 \times 10^6 \text{ cycles} .$$

Therefore,

$$59 \times 10^6 \leq N(P) \leq 65 \times 10^6 \text{ cycles} .$$

This large number of completed cycles (counts) will exceed the capacity of a 24-bit register resulting in register rollover of this large base count for each transducer. The number of times the 24-bit register rolls over n_{ro} is given by:

$$n_{ro} = \text{Integer } (N/2^{24}) .$$

For typical deep water deployment depths of approximately 4500 meters, n_{ro} is 3 or 4 since $3.5 \leq N/2^{24} \leq 4$. Thus, if n is the observed value of the 24-bit register at the end of an integration period, then the *total* number of completed cycles is

$$N = n + n_{ro} \times 2^{24} .$$

A 24-bit register spans an *equivalent* ocean depth of approximately 2^{24} mm or 16,777 meters, since the least count sensitivity of the transducer is approximately 1 mm/count (see section 2.2). Because of this very large *equivalent* depth span there is only one physically reasonable depth at which the 24-bit register would be expected to roll over. In general, the rollover pressures are given by equation (3) with N set to a multiple of the maximum register value; i.e., by:

$$P_{ro} = C\left\{ 1-(kM/N_0)^2 - D\left[1-(kM/N_0)^2\right]^2 \right\} ,$$

where

$$k = 0,1,2,\ldots ,$$

and

$$M = 2^{24} .$$

The 24-bit rollover depths H_{ro}, calculated from equation (3), are listed in Table 3 for each PMEL sensor. Any rollover of a 24-bit register occurs primarily as the result of the large base oscillation frequency of each transducer, and, therefore, rollover between successive 24-bit measurements is unlikely. A 16-bit register, however, spans an *equivalent* ocean depth of only 2^{16} mm or 65.5 meters; rollover of this register between successive measurements is likely to be encountered during data processing. Careful tracking of N is therefore required as P oscillates around these "rollover pressures", which may be identified by setting $M = 2^{16}$ in equation (3).

4.3 Time Tag Checks, Editing, and Filtering

Time tags applied as part of pre-deployment preparation (Section 3.1) and post-recovery procedures (Section 3.4) are examined for identification of missing data, as a preliminary data quality check, and as a quantitative determination of clock drift. (Note, however, that unambiguous determination of clock drift requires actual measurements of the time base frequency.) The rollover-corrected calibrated data are next machine-edited to remove pre- and post-deployment data including pressure data contaminated as a result of slow thermistor response to the ambient environment, due primarily to the insulation quality of the potting material within

which the thermistor resides. Temperature equilibrium periods of up to 15 hours have been observed in data from instruments deployed at a depth of approximately 4500 m. After the working series is generated and preliminary time and data quality checks completed, values exceeding reasonable bounds on each variable ("spikes") are identified by a successive point differencing routine in which statistics from first differences are used as the limiting criteria. Each outlier is replaced with values interpolated from the nearest acceptable data points.

Filtering techniques based on the FESTSA (Fast and EaSy Time Series Analysis) package (Brooks, 1976) are appropriate to separate the frequency domain of each data set. A 2-hour low pass (2 HRLP) filter is applied to reduce sampling noise and possible aliasing due to discrete sampling (Bendat and Piersol, 1971). A 40-hour low pass (40 HRLP) filter is then applied to separate the daily and semidaily tidal and inertial motions from those lower frequency motions having periods of several days or longer. For all filters, the specified cutoff period is the period at which the filter energy is 0.25 times its long period response (−6 db point). A Lanczos taper is used in each case, and the response function of the 40 HRLP filter is shown in Fig. 7. After filtering, all data are decimated to 1-hour intervals.

4.4 Tidal Analysis and Removal

The 2 HRLP data are used as input for the tidal analyses. Three independent procedures are used to obtain estimates of the tidal constituents: fast Fourier transform (FFT) analysis, harmonic least squares analysis, and response analysis.

Fast Fourier Transform (FFT) analyses of sequential 29-day segments are used for a preliminary examination of the amplitude and phase of each dominant tidal constituent. Significant changes in the sequential results, other than those attributable to seasonal fluctuations, are indicative of poor data quality and possible instrument unreliability.

Harmonic least squares analysis is a commonly employed method, in which a least squares fit of the amplitude A_j and phase ϕ_j of each tidal constituent is performed in order to minimize the residual

$$r \equiv \sum_{i-1}^{N} (Y_i - \overline{Y}_i)^2 \ ,$$

where Y_i represent the N observations at times t_i, and the assumed model function Y_i is given by

$$\overline{Y}_i = C_0 + \sum_{j=1}^{M} A_j \cos[2\pi(\sigma_j t_i - \phi_j)] \ , \qquad (17)$$

where the σ_j are known tidal frequencies. Equation (17) may also be expressed as:

$$\overline{Y}_i = C_0 + \sum_{j=1}^{M} [C_j \cos(2\pi \sigma_j t_i) + S_j \sin(2\pi \sigma_j t_i)] \qquad (18)$$

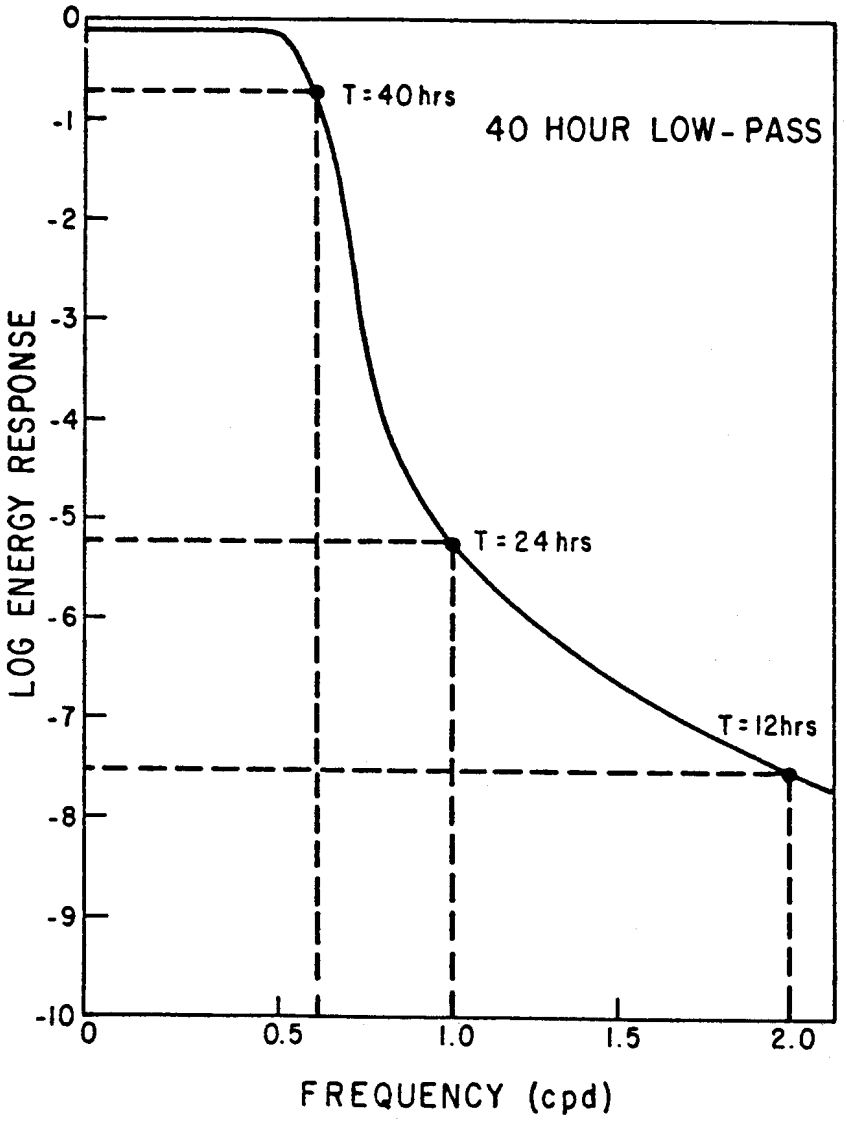

Figure 7. Frequency response function of 40 HRLP filter.

where

$$A_j = (C_j^2 + S_j^2)^{1/2}$$

and

$$\phi_j = (2\pi)^{-1} \tan^{-1} (S_j/C_j) .$$

Equation 18 is more easily solved, since it is linear in the parameters S_j and C_j.

Numerous numerical packages to implement harmonic analyses exist, varying, primarily, in the method of determinant solution and in the number and type of corrections applied to the results (such as corrections for astronomical phase and amplitude). Software developed by the

Canadian Government for which Foreman (1977) has provided a rigorous examination has been adapted for use.

Response analysis involves a spherical-harmonic expansion rather than a time-harmonic expansion as representation of the tides. The weighted sum of a reference series is fitted to the observed series by means of least squares. The input function, x(t), and output function, $\zeta(t)$, are related by Munk and Cartwright (1966):

$$\zeta(t) = \int_{-\infty}^{\infty} x(t-\tau)\, W(t)\, d\tau \tag{19}$$

where $W(\tau)$ is the impulse response. The Fourier transform of the impulse response is the admittance and is given by:

$$\zeta(f) = \int_{-\infty}^{\infty} W(\tau)\, e^{-2\pi i f \tau}\, d\tau\,. \tag{20}$$

Therefore, if input and output are alike, $W(\tau) = \zeta(\tau)$, and $Z(f) = 1$.

The SCOR working group (1975) has provided a comparison between the response method and that of harmonic least squares. Investigators were given a two-month data record and instructed to perform a tidal analysis. Results indicated that the response method performed significantly better than harmonic analysis, having the advantage of separating astronomic forcing from ocean response. However, an appropriate choice of input functions is critical in maximizing response analysis results.

Both the harmonic analysis and response analysis have been applied to each BPR data set, with little difference in the results of each. This is probably because of significant improvement in harmonic analysis results when performed on longer records (typically year-long) than on those of duration similar to that used for the SCOR study. Because of greater agreement between results of the response and harmonic analysis performed on the long duration BPR time series, less stringent input considerations, and larger number of constituent results, the harmonic analyses is used to remove the tidal signal from each BPR record.

4.5 Drift Modeling and Removal

Hysteresis and drift are characteristic of each Paroscientific pressure transducer, but the magnitude of these properties is unique to each instrument. Hysteresis is the inability of a transducer to return to an exact initial pressure when cycled through its full pressure range. The maximum excursion occurs in the high range transducers when cycling is rapidly induced (Wearn and Larson, 1982). Error introduced as the result of hysteresis is insignificant for applications in which the pressure transducer remains within some finite pressure window, and therefore, effects due to hysteresis are not addressed in the processing of PMEL BPR data. The

residual, i.e., de-tided pressure records, typically exhibit a long-term instrumental drift as shown in the BPR data records presented in Appendix B. There are many possible causes of long-term drift, including slow sinking of the BPR into soft ocean bottom material, time base drift, transducer crystal aging, degradation of the vacuum in the crystal chamber, and creep of either the metal of the Bourdon tube itself or the joint material used to connect the crystal to the tube (R. Wearn, personal communication). The last of these mechanisms, i.e. creep of materials, was shown to be reversible and repeatable (Wearn and Larson, 1982) for an older Paroscientific transducer design which utilized metal bellows.

If a similar mechanism is responsible for the creep in the Bourdon tube transducers, the component of drift due to materials creep could be determined experimentally in the laboratory for each individual transducer. Once this drift component was removed from a record, it would be easier to identify and compensate for other sources of drift. In practice, however, these laboratory measurements are very difficult to perform. The primary obstacle is the long-term maintenance of a stable high pressure and low temperature environment characteristic of the deep ocean bottom. Therefore, the laboratory measurement of drift is impractical at this time. Instead, the usual approach of choosing an analytic function as a model for the total observed drift and then fitting this function to the data by means of least square techniques has been adopted.

A number of studies have found that pressure sensor drift is most accurately described by one or a linear combination of four basic models: linear, logarithmic, exponential, and power law functions (Orowan, 1951; Marin, 1962; Filloux, 1971; Wearn and Baker, 1980; Wearn and Larsen, 1982; Banaszek and MacDonald, 1985; Watts and Kontoyiannis, 1986). It is important to note that errors associated with this approach are greatest in the low frequency end of the spectrum.

Initial attempts to model the drift, p, present in PMEL BPR data records have utilized a (linear + exponential) function, written in the form

$$p = A_1 + A_2(t-A_5) + A_3 \exp[A_4(t-A_5) - 1] \ . \tag{21}$$

In this expression, t is time and all five coefficients, A_n, are determined simultaneously. The IMSL subroutine DRNLIN, which implements the Lavenberg-Marquardt algorithm for the solution of a system of nonlinear equations has been used (IMSL, 1987). In those cases for which it seems questionable to assume an exponential component to the drift, the parameters A_3 and A_4 are forced to zero. The fit and subsequent removal of this function from each BPR record is presented in Appendix B. The (linear + exponential) model works reasonably well, although it does have difficulty tracking the initial rapid rise which characterizes records such as those shown in Appendix B (B1, B2, B7, B8, B15, B16). The (linear + exponential) function used thus far is an initial attempt at modeling the drift present in each BPR record. (Linear + power law)

and (linear + logarithmic) models are currently under formulation so as to incorporate all modeling functions into the standard processing procedure to optimize the fit to each BPR data record.

5. ACKNOWLEDGMENTS

We thank Ryan Whitney for manuscript preparation and Gini Curl for figure drafting. This report is Contribution No. 1000 from NOAA/Pacific Marine Environmental Laboratory. All work was conducted as part of the Marine Services Research Division Tsunami Project.

6. REFERENCES

Banaszek, A.D. and D.C.C. MacDonald, 1985. UK Continental Slope Experiment (CONSLEX) 1982/1983. Offshore bottom pressure records: Rockall Trough, Hebrides Shelf, West Shetland Shelf and Faeroe-Shetland Shelf. Institute of Oceanographic Sciences Report No. 216, Patricia Bay, Victoria, B.C., 71 pp.

Beardsley, R.C., H. Mofjeld, M. Wimbush, C.N. Flagg, and J.A.Vermersch, Jr., 1977. Ocean tides and weather-induced bottom pressure fluctuations in the Middle Atlantic Bight. *J. Geophys. Res., 82*(21), 3175-3182.

Bendat, J.S., and A.G Piersol, 1971. Random Data: Analysis and Measurement Procedures. John Wiley and Sons, Inc., 407 pp.

Bernard, E.N., and H.B. Milburn, 1985. Long-wave observations near the Galápagos Islands. *J. Geophys. Res., 90*(C2), 3361-3366.

Bernard, E.N., and R. Goulet, 1981. Tsunami research opportunities, an assessment and comprehensive guide. National Science Foundation and National Oceanic and Atmospheric Administration, Washington, DC., 50 pp.

Brooks, D.A., 1976. Fast and easy time series analysis at NCSU. Technical Report Center for Marine and Coastal Studies, North Carolina State University, Raleigh, NC.

Collar, P.G., and D.E. Cartwright, 1972. Open sea tidal measurements near the edge of the northwest European continental shelf. *Deep-Sea Res., 19*, 673-689.

Eyries, M., 1968. Maregraphes de grandes profondeurs. *Cahiers Oceanogr., 20*(5), 355-368.

Filloux, J.H., 1969. Bourdon tube deep-sea tide gauges. Proceedings of the International Symposium on Tsunamis and Tsunamis Research, East-West Center Press, 223-238.

Filloux, J.H., 1970. Deep-sea tide gauge with optical readout of bourdon tube rotations. *Nature, 226*, 936-937.

Filloux, J.H., 1971. Deep-sea tide observations from the northeastern Pacific. *Deep-Sea Res., 18*, 275-284.

Filloux, J.H., 1982. Tsunami recorded on the open ocean floor. *Geophys. Res. Lett., 9*, 25-28.

Filloux, J.H., 1983. Pressure fluctuations on the open-ocean floor off the Gulf of California: Tides, earthquakes, tsunamis. *J. Phys. Oceanogr., 13*, 783-796.

Foreman, M.G.G., 1977. Manual for tidal heights analysis and prediction. Pacific Marine Science Report 77-10, Institute of Ocean Sciences, Patricia Bay, Victoria, B.C., 70 pp.

Gonzalez, F.I., E.N. Bernard, and H.B. Milburn, 1987. A program to acquire deep ocean tsunami measurements in the north Pacific. In: Proceedings of Coastal Zone '87, 26-29 May, Seattle, WA, 3373-3381.

Gwilliam, T.J.P., and P.G. Collar, 1974. A strain gauge pressure sensor for measuring tides on the continental shelf. Institute of Ocean Sciences Report No. 14, Patricia Bay, Victoria, B.C., 27 pp.

Harris, M.J., and M.J. Tucker, 1963. A pressure recorder for measuring sea waves. *Instrument Practice*, 1055-1059.

IMSL, Inc., 1987. Stat/library FORTRAN subroutines for statistical analysis. Version 1.0 Users Manual, 1232 pp.

Jacob, K.H., 1984. Estimates of long-term probabilities for future great earthquakes in the Aleutians. *Geophys. Res. Lett., 11*, 295-298.

Lefcort, M.D., 1968. Vibrating wire pressure transducer technology. *J. Ocean Tech., 2*(2), 37-44.

Marin, J., 1962. Mechanical Behavior of Engineering Materials. Prentice-Hall, NJ, Chapter 7.

Mofjeld, H.O., and M. Wimbush, 1977. Bottom pressure observations in the Gulf of Mexico and Caribbean Sea. *Deep-Sea Res., 24*, 987-1004.

Munk, W.H., and D.E. Cartwright, 1966. Tidal spectroscopy and prediction. *Phil. Trans. Roy. Soc. London A, 259*, 533-581.

Orowan, E., 1951. Creep in metallic and mon-metallic materials. Proceeding of the 1st U.S. National Congress on Applied Mechanics, 453-472.

Raichlen, F. (Chairman), 1985. Report of tsunami research planning group. National Science Foundation, Washington, DC.

SCOR Working Group. No 27, 1975. An intercomparison of open sea tidal pressure sensors. UNESCO Technical Paper in Marine Science No. 21, 67 pp.

Snodgrass, F.E., 1968. Deep-sea instrument capsule. *Science, 162*, 78-87.

Spaeth, M.G., and S.C. Berkman, 1967. The tsunami of March 28, 1964, as recorded at tide stations. U.S. Department of Commerce, ESSA Technical Report C&GS 33, 86 pp.

Warren, B.A., and C. Wunsch, editors, 1981. *Evolution of Physical Oceanography*. The MIT Press, Cambridge, Mass. Chapter 14. 623 pp.

Watts, D.R., and H. Kontoyiannis, 1986. Deep-ocean bottom pressure and temperature sensors report: methods and data. University of Rhode Island Graduate School of Oceanography Technical Report No. 86-8, 111 pp.

Wearn, R.B., Jr., 1985a. Year-long stability measurements on Paroscientific atmospheric pressure transducers. Paroscientific, Inc., Redmond, WA, 6 pp.

Wearn, R.B., Jr., 1985b. 15 July 1985 Technical Update. Well Test Instruments, Inc., Redmond, WA, 15 pp.

Wearn, R.B., Jr. and D.J. Baker, Jr., 1980. Bottom pressure measurements across the Antarctic circumpolar current and their relation to the wind. *Deep-Sea Res., 27*(11A), 875-888.

Wearn, R.B., Jr., and N.G. Larson, 1982. Measurements of the sensitivities of Digiquartz pressure sensors. *Deep-Sea Res., 29*(1A), 111-134.

Well-Test Instruments, Inc., 1984. Calibration, test, and characterization of Well Test Instruments quartz crystal transducers. Document #8062-001.

Wimbush, M., 1976. An inexpensive sea-floor precision pressure recorder. *Deep-Sea Res., 24*, 493-497.

Wunsch, C., and M. Wimbush, 1977. Simultaneous pressure, velocity and temperature measurements in the Florida Straits. *J. Mar. Res., 35*(1), 75-104.

Wyrtki, K. 1979. Sea level variations: Monitoring the breath of the Pacific. *Eos, 60*, 25-27.

APPENDIX A

2-hour low-pass filtered hourly values of pressure and temperature data.

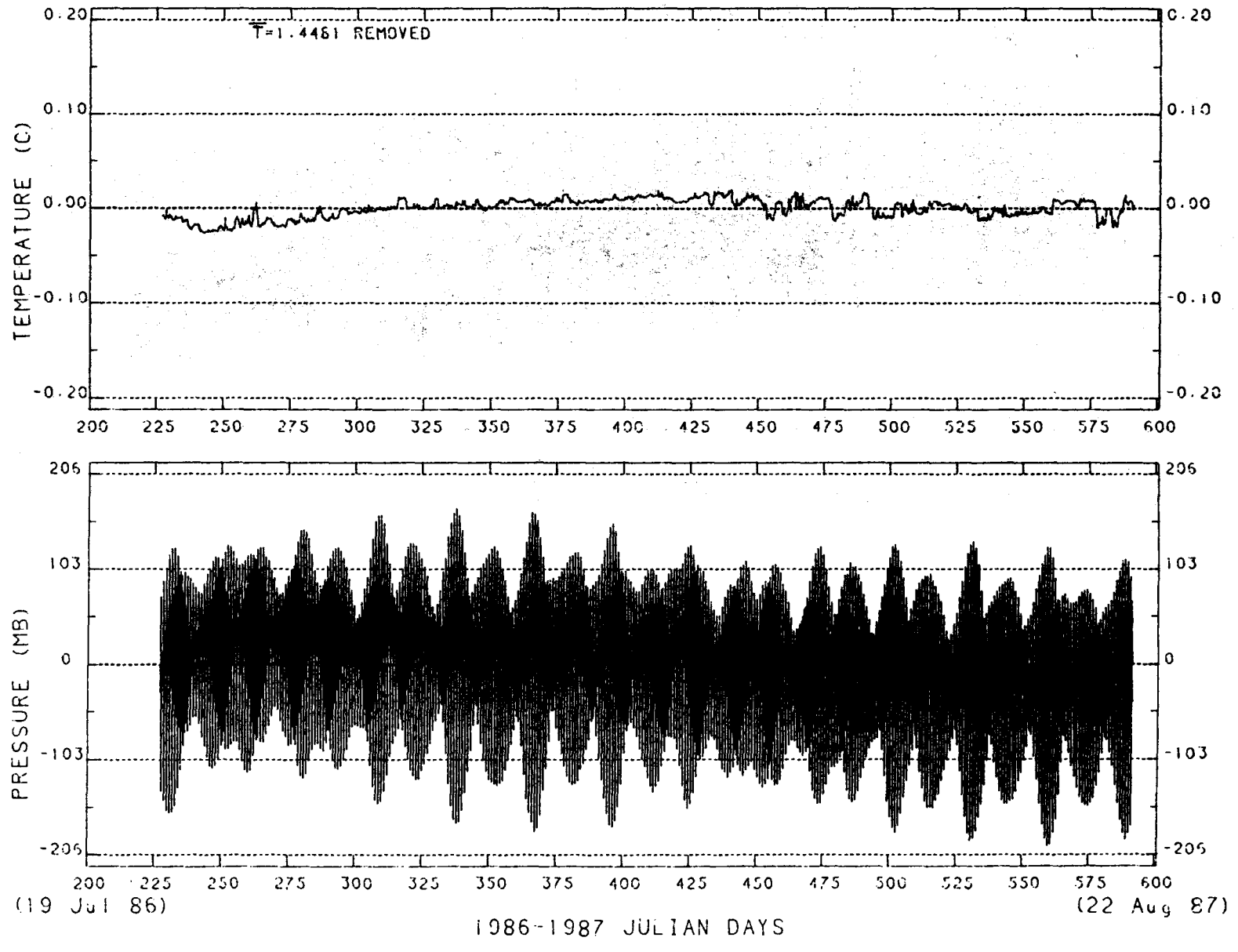
2 HRLP AK1 (24063) AT 4523 M
T=1.4461 REMOVED
TEMPERATURE (C)
0.20
0.10
0.00
-0.10
-0.20
PRESSURE (MB)
206
103
0
-103
-206
200 225 250 275 300 325 350 375 400 425 450 475 500 525 550 575 600
(19 Jul 86)
(22 Aug 87)
1986-1987 JULIAN DAYS

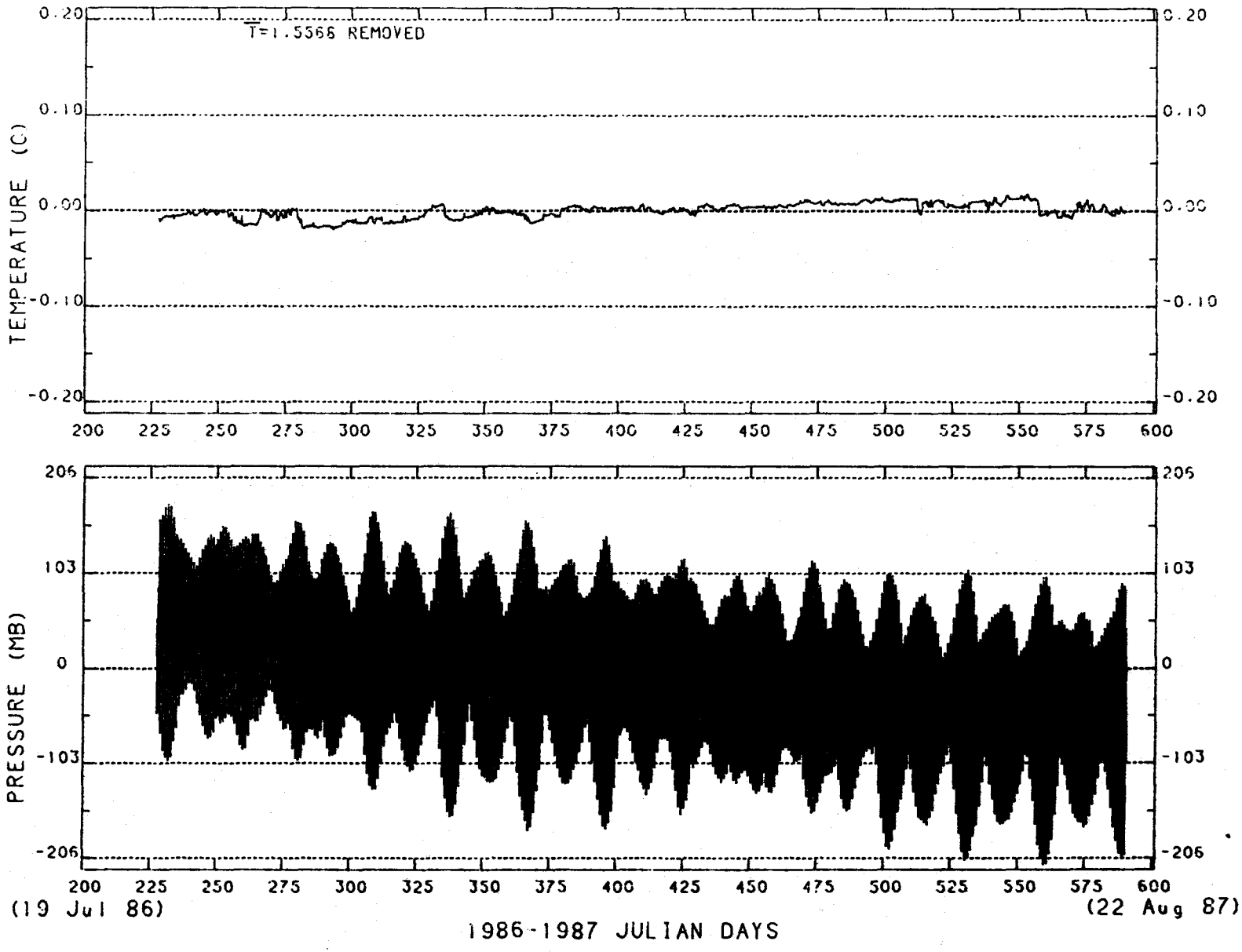
2 HRLP AK3 (24061) AT 4692 M
T=1.5566 REMOVED
TEMPERATURE (C)
0.20
0.10
0.00
-0.10
-0.20
PRESSURE (MB)
206
103
0
-103
-206
200 225 250 275 300 325 350 375 400 425 450 475 500 525 550 575 600
(19 Jul 86)
(22 Aug 87)
1986-1987 JULIAN DAYS

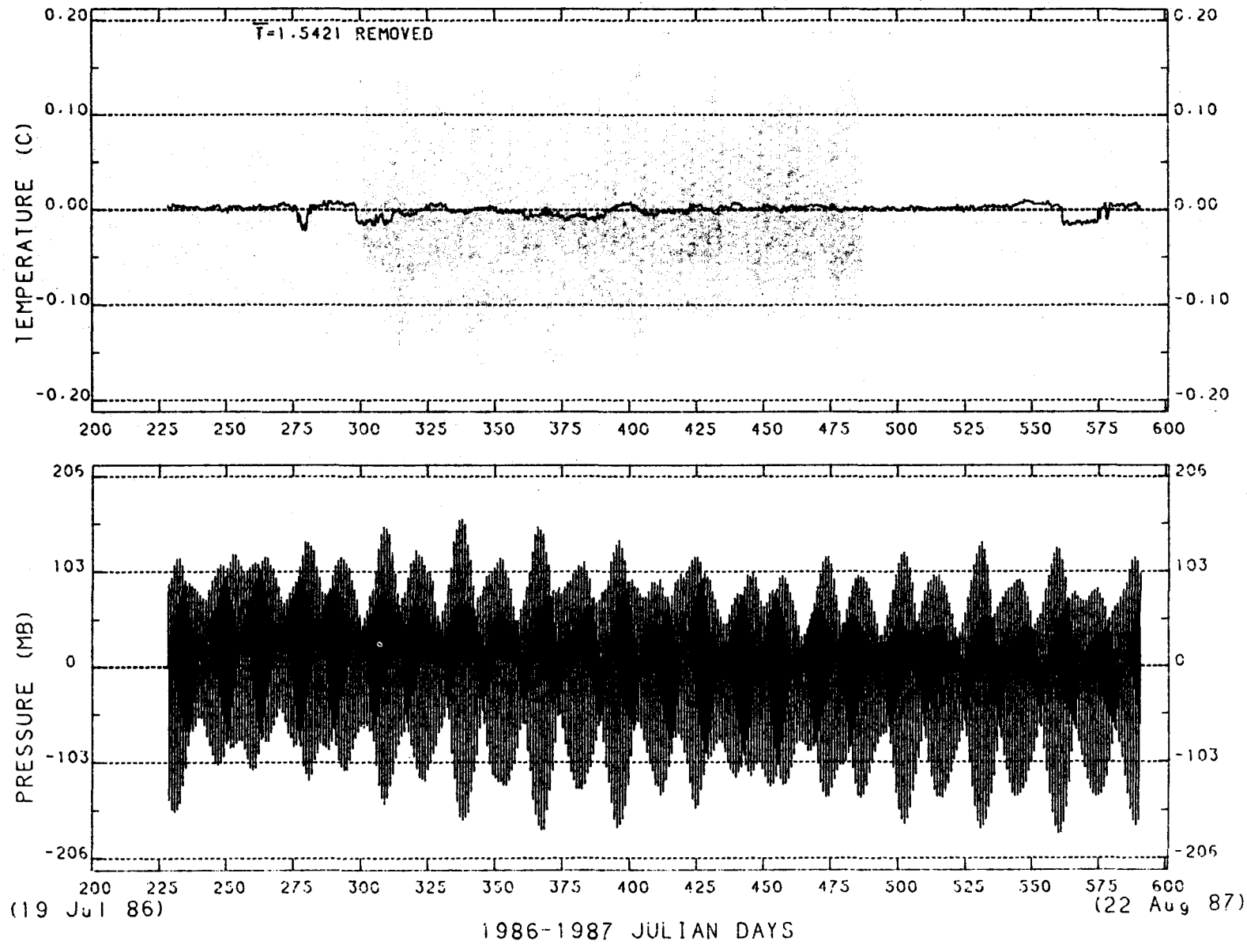
2 HRLP AK4 (24026) AT 4600 M
T=1.5421 REMOVED
TEMPERATURE (C)
0.20
0.10
0.00
-0.10
-0.20
PRESSURE (MB)
206
103
0
-103
-206
200 225 250 275 300 325 350 375 400 425 450 475 500 525 550 575 600
(19 Jul 86)
(22 Aug 87)
1986-1987 JULIAN DAYS

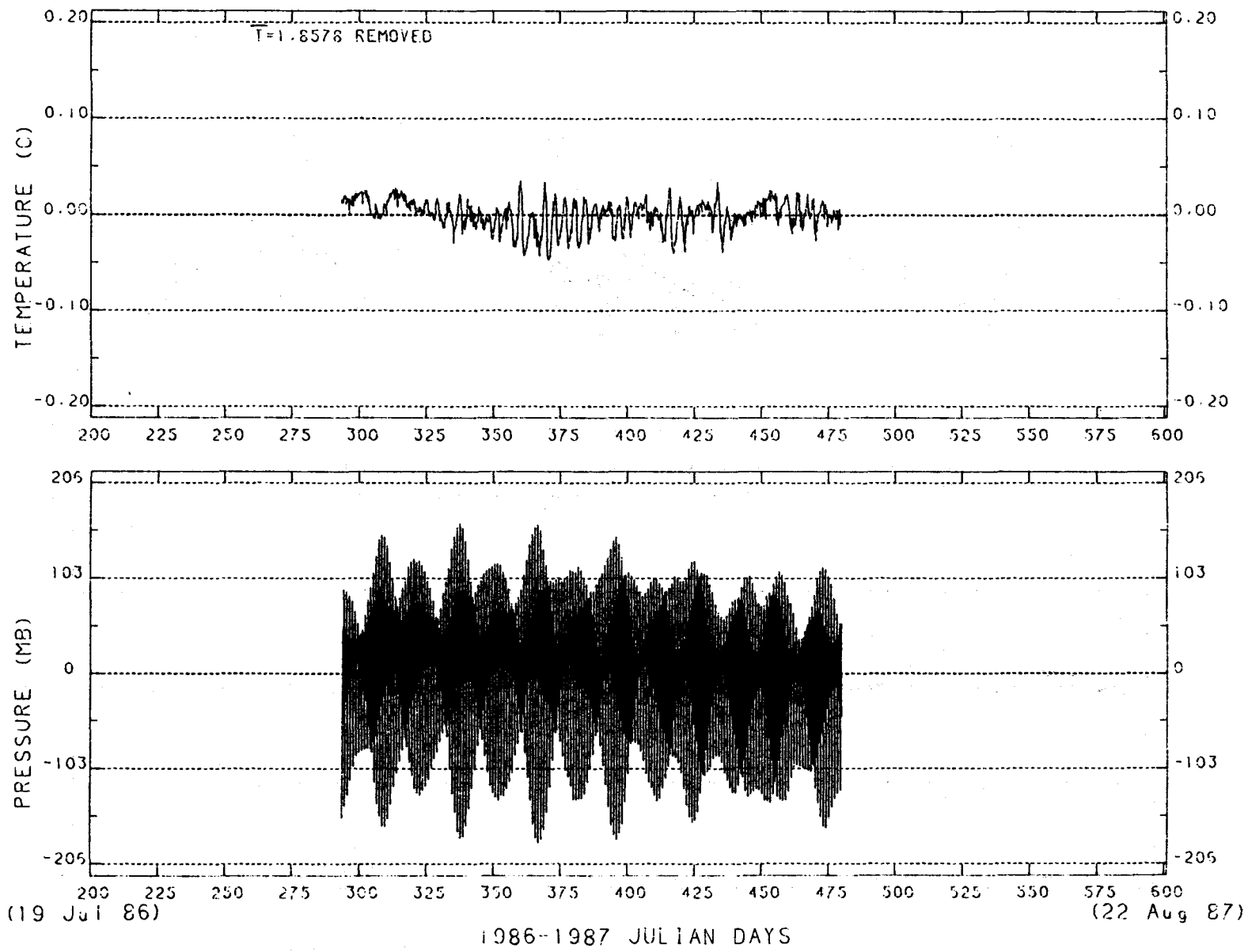
2 HRLP WC5 (21988) AT 2402 M
T=1.8578 REMOVED
TEMPERATURE (C)
0.20
0.10
0.00
-0.10
-0.20
PRESSURE (MB)
206
103
0
-103
-206
200 225 250 275 300 325 350 375 400 425 450 475 500 525 550 575 600
(19 Jul 86)
(22 Aug 87)
1986-1987 JULIAN DAYS

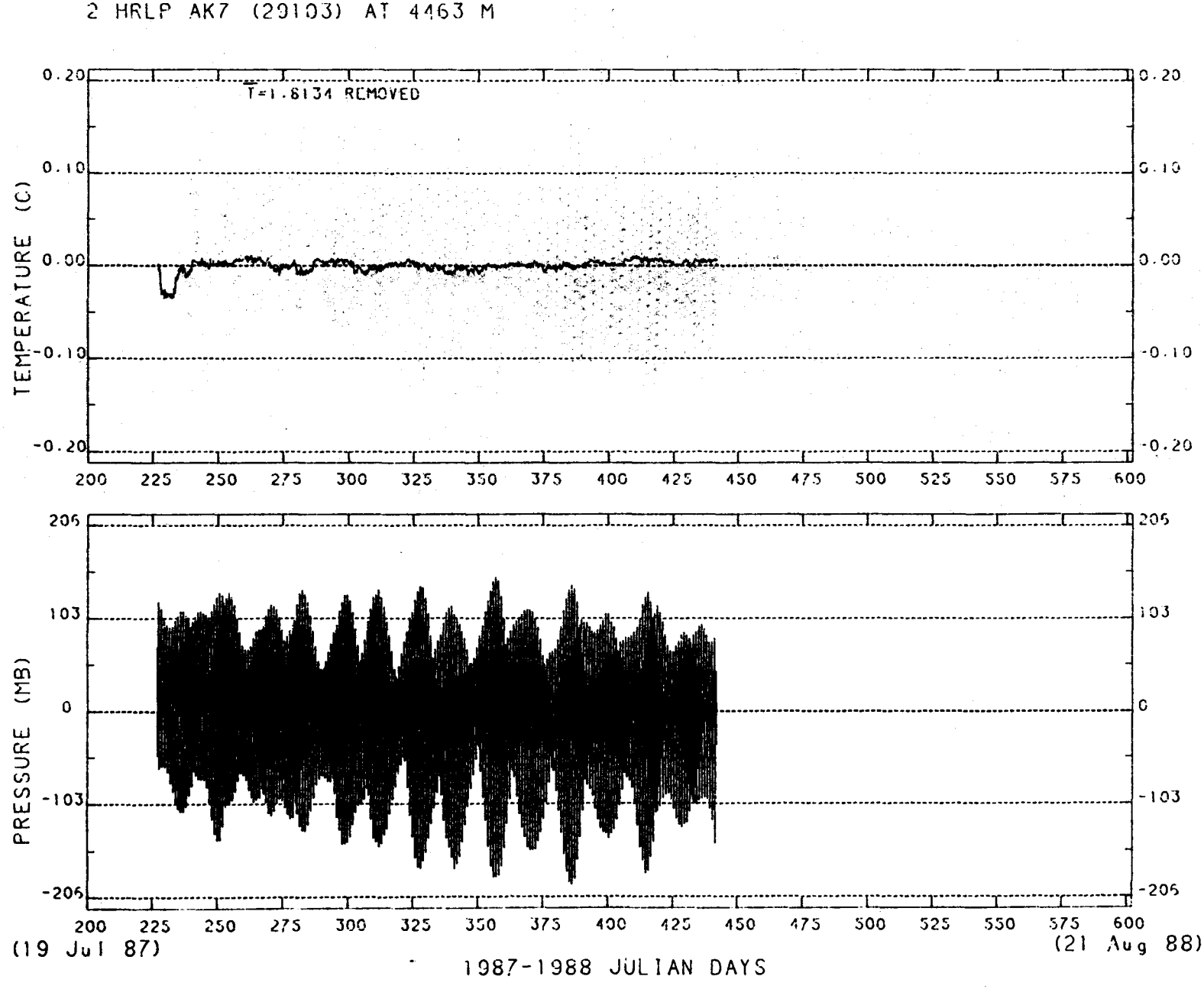
2 HRLP AK7 (29103) AT 4463 M
T=1.8134 REMOVED
TEMPERATURE (C)
0.20
0.10
0.00
-0.10
-0.20
PRESSURE (MB)
206
103
0
-103
-206
200 225 250 275 300 325 350 375 400 425 450 475 500 525 550 575 600
(19 Jul 87)
(21 Aug 88)
1987-1988 JULIAN DAYS

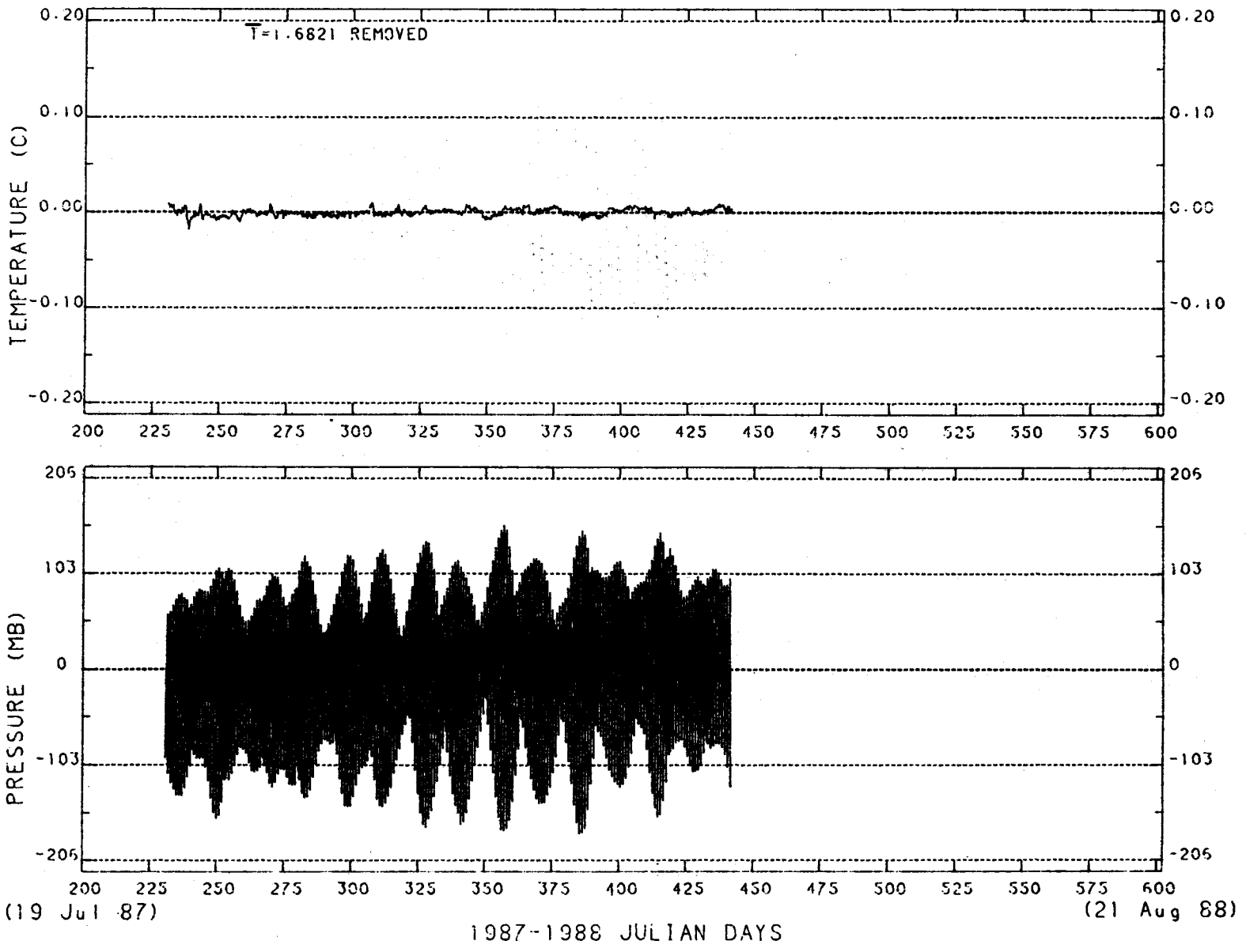
2 HRLP AK8 (26706) AT 4535 M
T=1.6821 REMOVED
TEMPERATURE (C)
0.20
0.10
0.00
-0.10
-0.20
PRESSURE (MB)
206
103
0
-103
-206
200 225 250 275 300 325 350 375 400 425 450 475 500 525 550 575 600
(19 Jul 87)
(21 Aug 88)
1987-1988 JULIAN DAYS

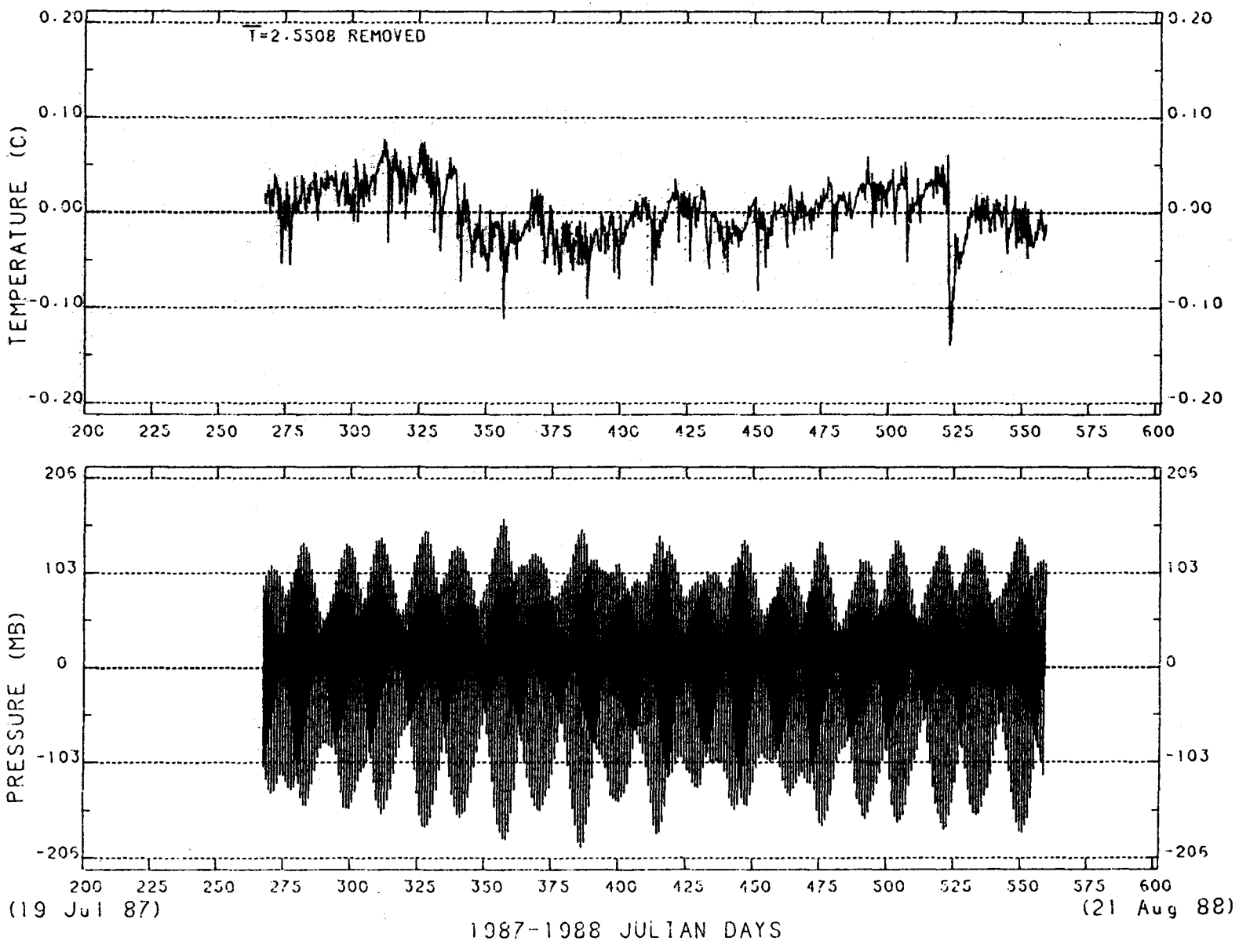
2 HRLP WC9 (24061) AT 1527 M
T=2.5508 REMOVED
TEMPERATURE (C)
0.20
0.10
0.00
-0.10
-0.20
PRESSURE (MB)
206
103
0
-103
-206
200 225 250 275 300 325 350 375 400 425 450 475 500 525 550 575 600
(19 Jul 87)
(21 Aug 88)
1987-1988 JULIAN DAYS

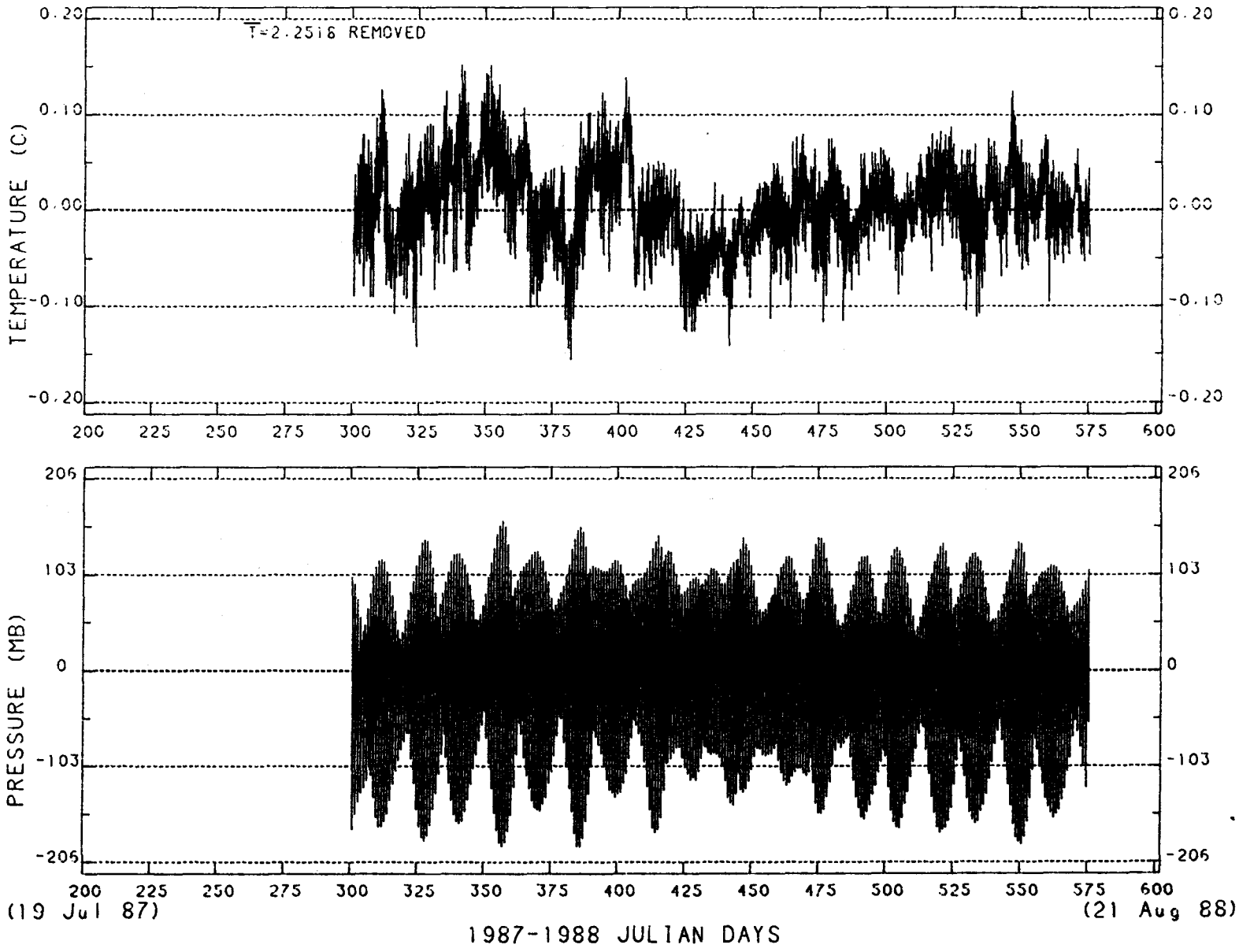
2 HRLP AK10 (24026) AT 1656 M
T=2.2516 REMOVED
TEMPERATURE (C)
0.20
0.10
0.00
-0.10
-0.20
PRESSURE (MB)
206
103
0
-103
-206
200 225 250 275 300 325 350 375 400 425 450 475 500 525 550 575 600
(19 Jul 87)
(21 Aug 88)
1987-1988 JULIAN DAYS

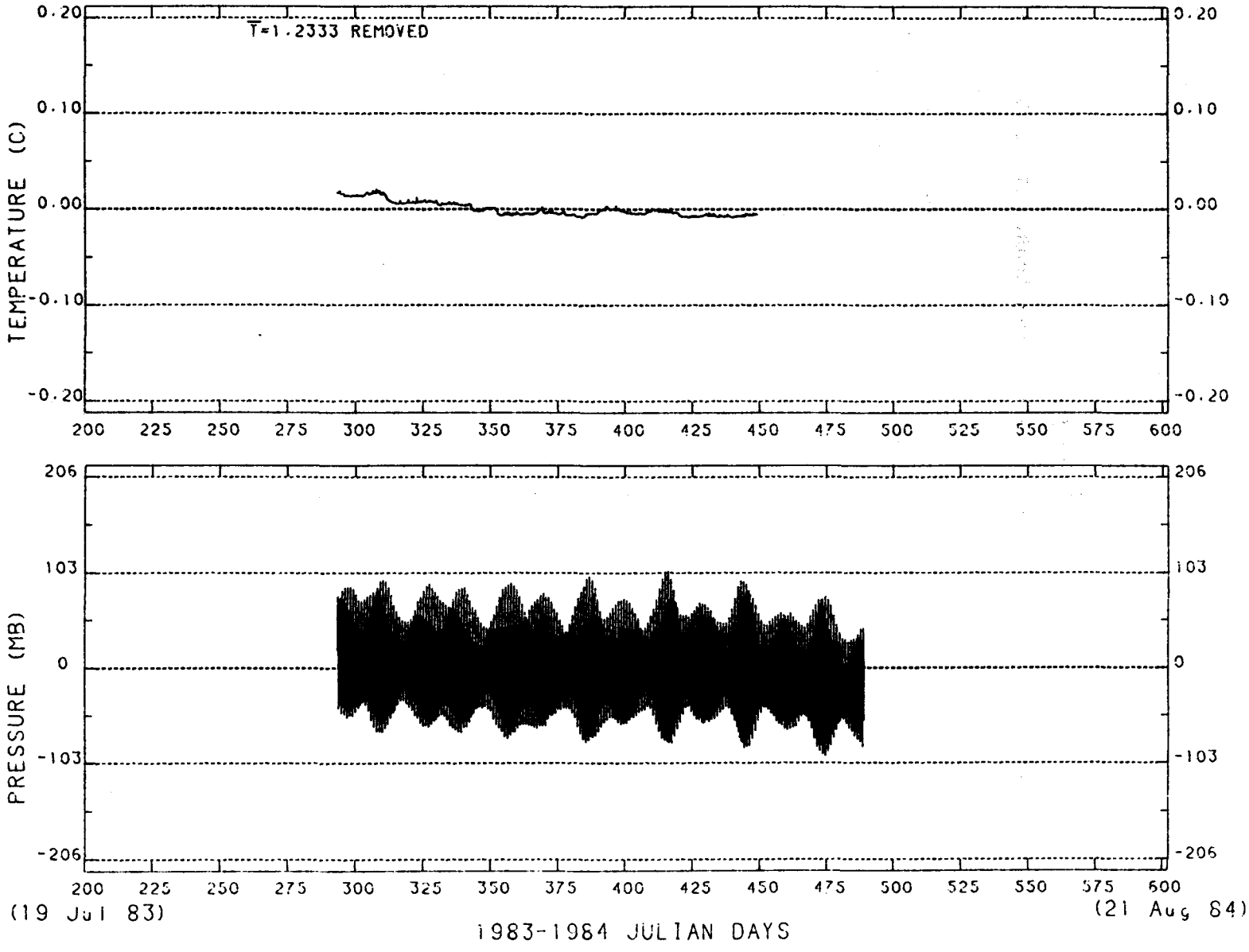
2 HRLP BPR5 (15022) AT 4320 M
T=1.2333 REMOVED
TEMPERATURE (C)
0.20
0.10
0.00
-0.10
-0.20
PRESSURE (MB)
206
103
0
-103
-206
200 225 250 275 300 325 350 375 400 425 450 475 500 525 550 575 600
(19 Jul 83)
(21 Aug 84)
1983-1984 JULIAN DAYS

APPENDIX B

2-hour low-pass filtered and de-tided hourly values of pressure, before and after drift removal.

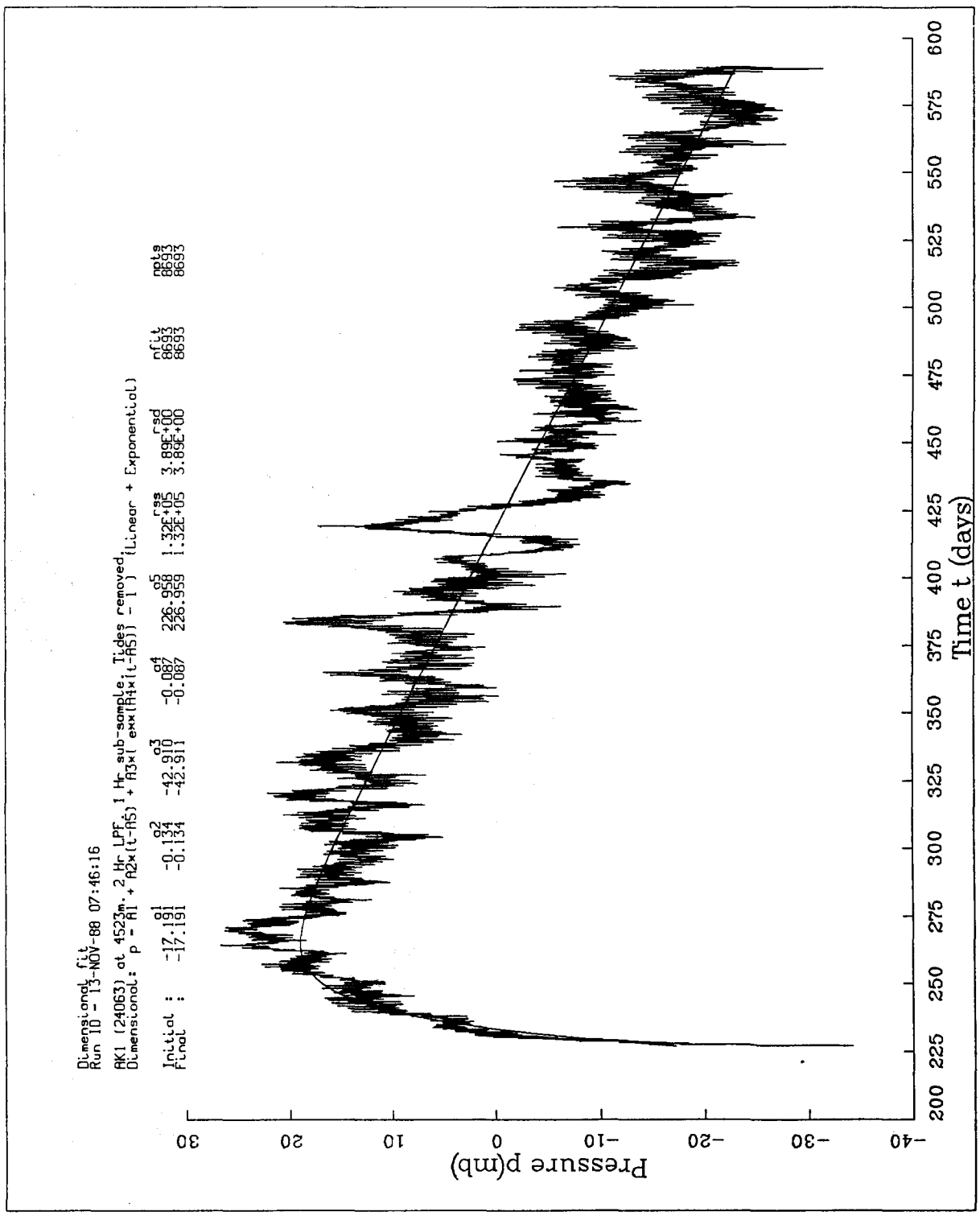
Dimensional fit
Run 10 - 13-NOV-88 07:46:16
AK1 (24063) at 4523m. 2 Hr LPF, 1 Hr sub-sample, Tides removed.
Dimensional: p = A1 + A2x(t-A5) + A3x(exp(A4x(t-A5)) - 1) (Linear + Exponential)
Initial : -17.191 -0.134 -42.911 -0.087 226.959 1.32E-05 3.89E+00 8693
Final : -17.191 -0.134 -42.911 -0.087 226.959 1.32E-05 3.89E+00 8693
Pressure p(mb)
Time t (days)

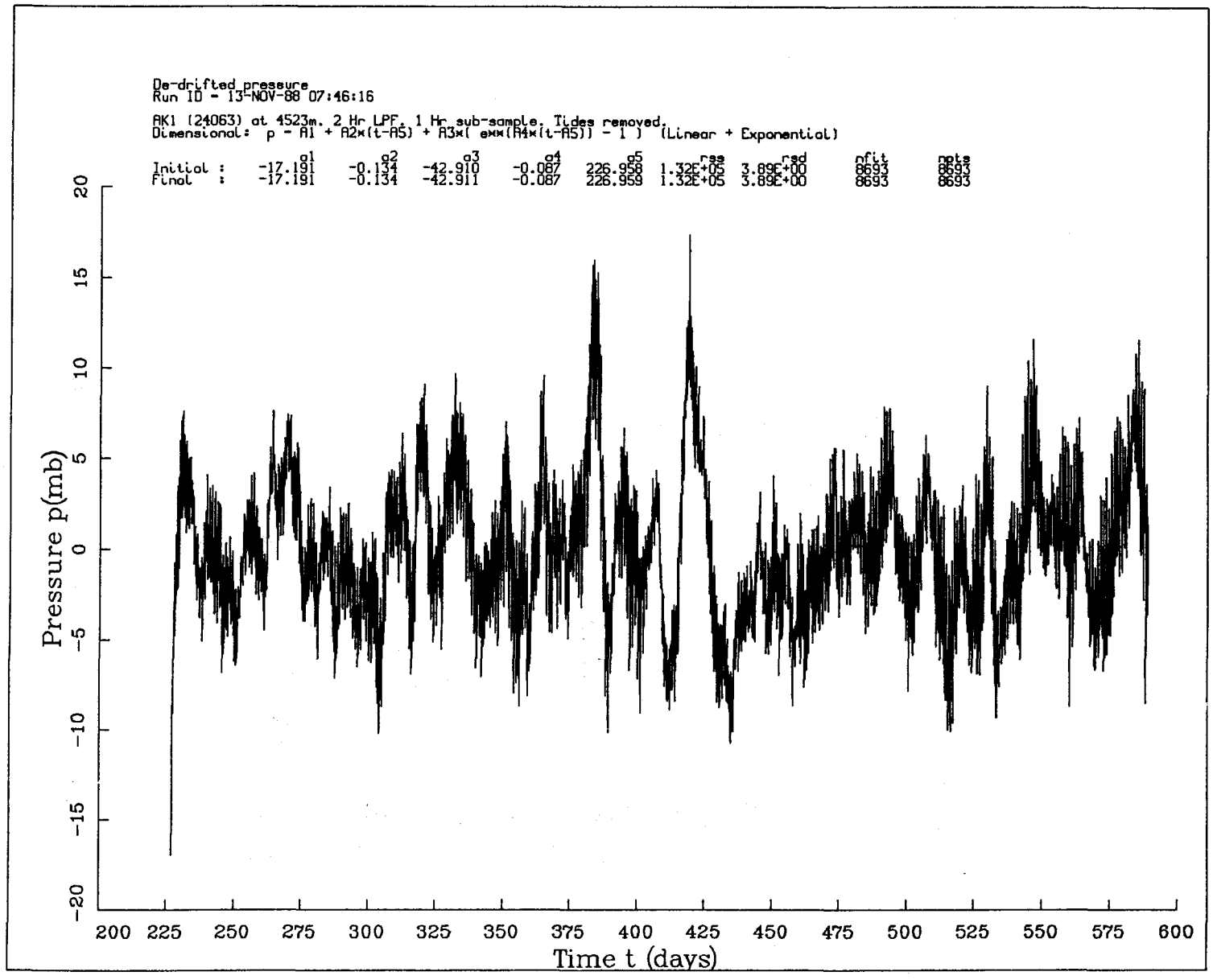
De-drifted pressure
Run ID - 13-NOV-88 07:46:16
AK1 (24063) at 4523m. 2 Hr LPF, 1 Hr sub-sample. Tides removed.
Dimensional: p = A1 + A2*(t-A5) + A3*(exp(A4*(t-A5)) - 1) (Linear + Exponential)
a1 a2 a3 a4 a5 rss rsd nfit npts
Initial : -17.191 -0.134 -42.910 -0.087 226.958 1.32E+05 3.89E+00 8693 8693
Final : -17.191 -0.134 -42.911 -0.087 226.959 1.32E+05 3.89E+00 8693 8693
Pressure p(mb)
20
15
10
5
0
-5
-10
-15
-20
200 225 250 275 300 325 350 375 400 425 450 475 500 525 550 575 600
Time t (days)

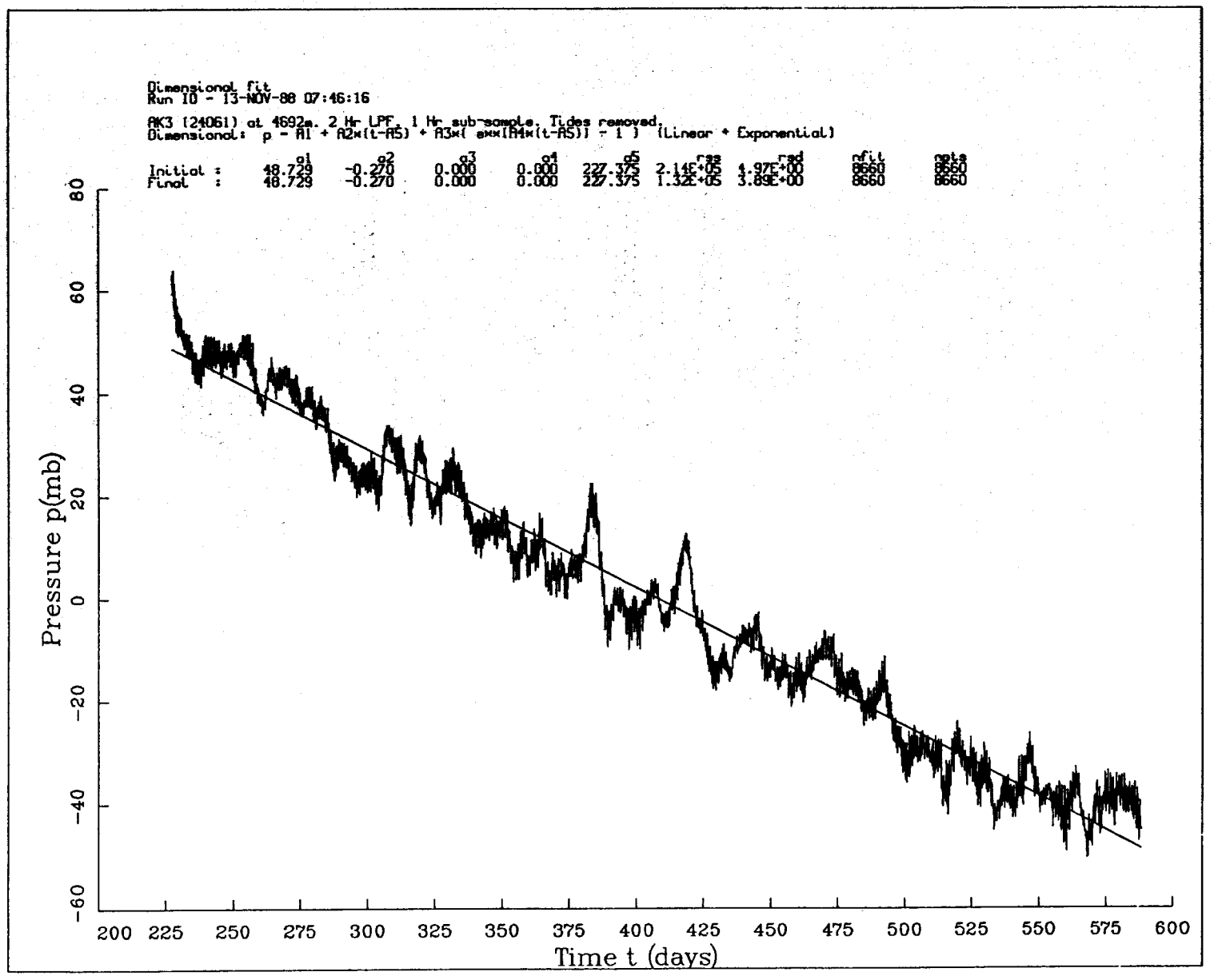
Dimensional fit
Run 10 - 13-NOV-88 07:46:16
AK3 (24061) at 4692m. 2 Hr LPF, 1 Hr sub-sample, Tides removed.
Dimensional: p = A1 + A2*(t-A5) + A3*(exp[A4*(t-A5)] - 1) (Linear + Exponential)
a1 a2 a3 a4 a5 rms rad nfit npts
Initial : 48.729 -0.270 0.000 0.000 227.375 2.14E+05 4.97E+00 8660 8660
Final : 48.729 -0.270 0.000 0.000 227.375 1.32E+05 3.89E+00 8660 8660
Pressure p(mb)
80
60
40
20
0
-20
-40
-60
200 225 250 275 300 325 350 375 400 425 450 475 500 525 550 575 600
Time t (days)

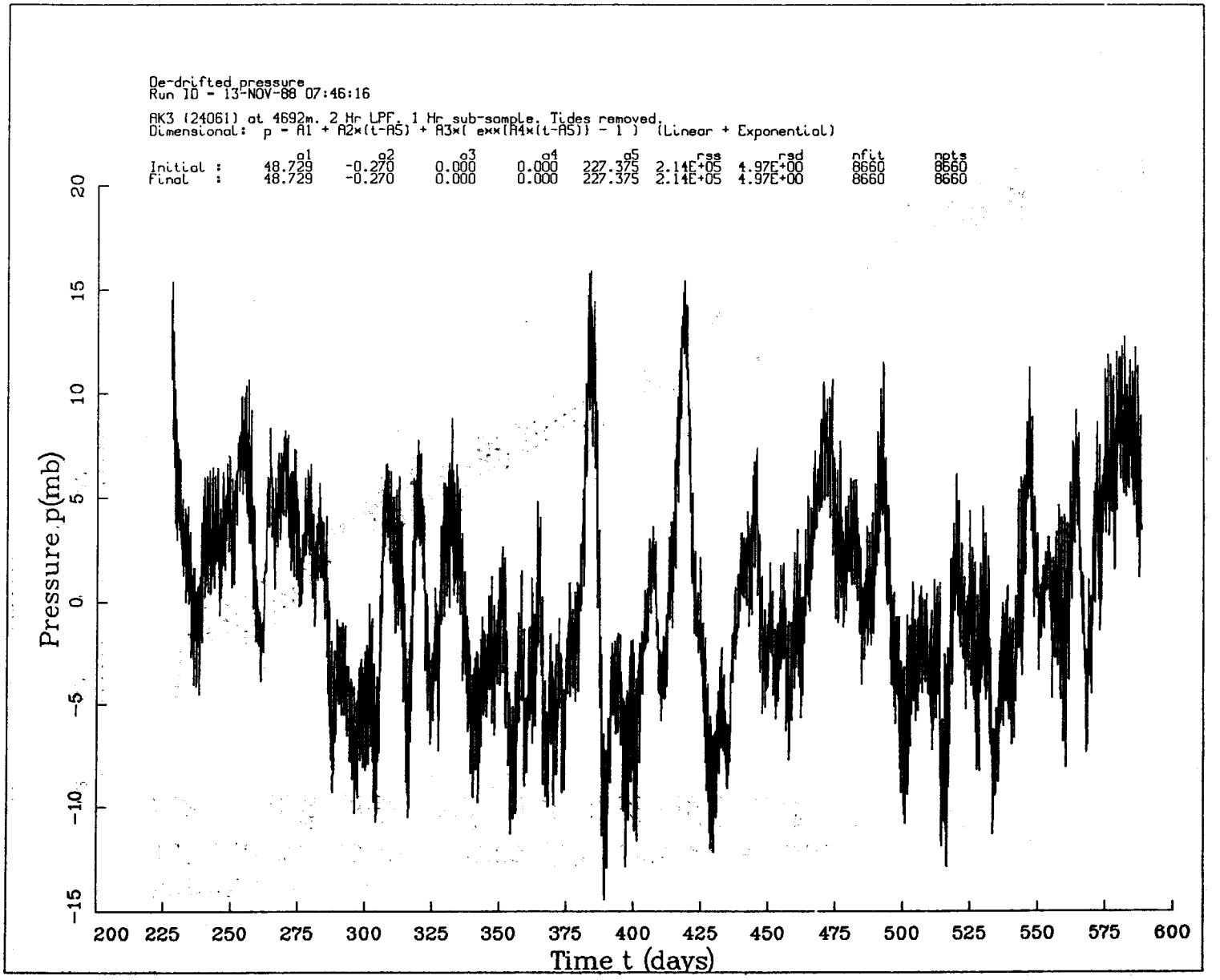
De-drifted pressure
Run ID - 13-NOV-88 07:46:16
AK3 (24061) at 4692m. 2 Hr LPF, 1 Hr sub-sample. Tides removed.
Dimensional: p = A1 + A2×(t-A5) + A3×(ex×(A4×(t-A5)) - 1) (Linear + Exponential)
a1 a2 a3 a4 a5 rss rsd nfit npts
Initial : 48.729 -0.270 0.000 0.000 227.375 2.14E+05 4.97E+00 8660 8660
Final : 48.729 -0.270 0.000 0.000 227.375 2.14E+05 4.97E+00 8660 8660
Pressure p(mb)
20
15
10
5
0
-5
-10
-15
200 225 250 275 300 325 350 375 400 425 450 475 500 525 550 575 600
Time t (days)

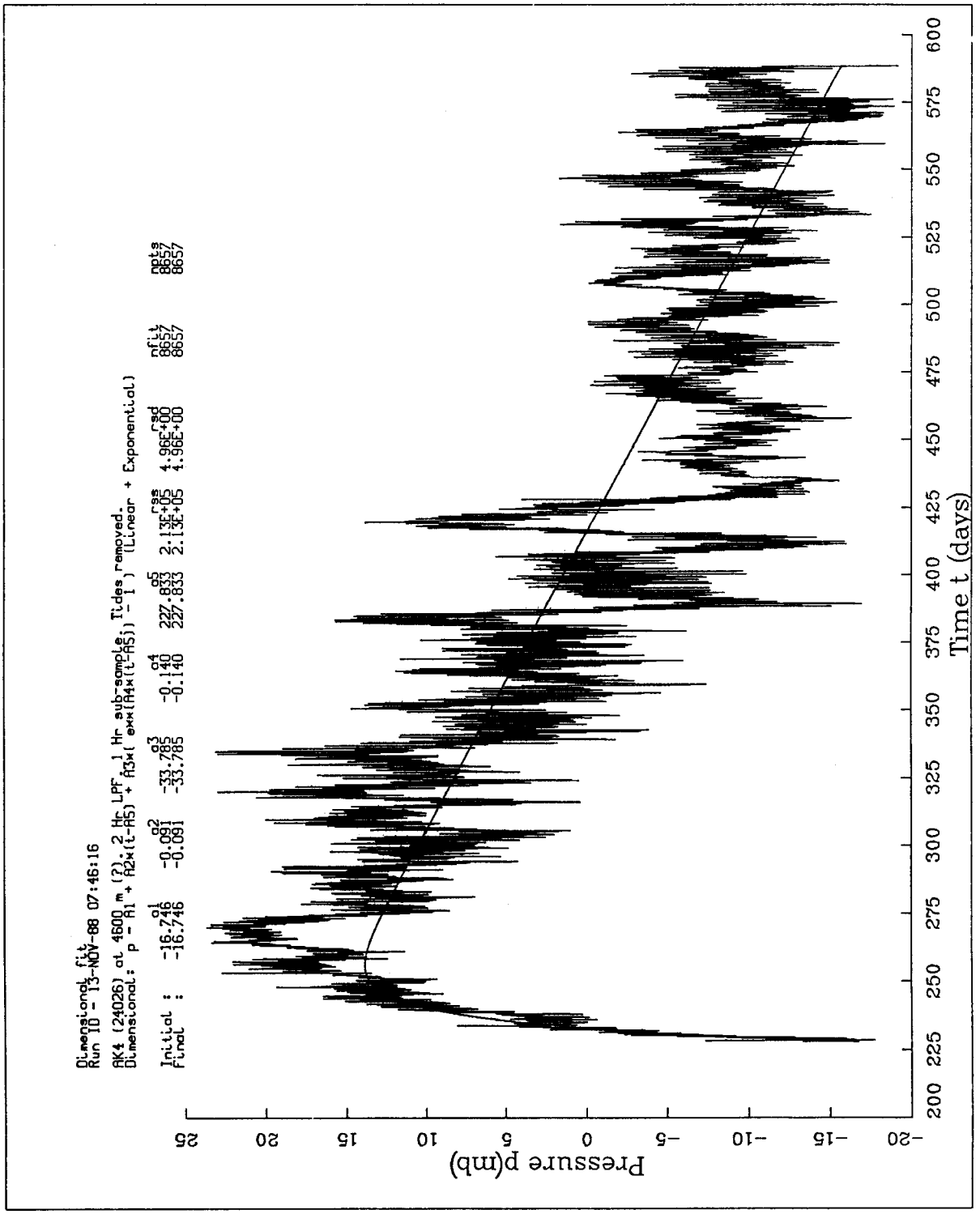
Dimensional fit
Run ID - 13-NOV-88 07:46:16
AK4 (24026) at 4600 m (2), 2 Hr LPF, 1 Hr sub-sample, Tides removed.
Dimensional: p = A1 + A2*(t-A5) + A3*(exp(A4*(t-A5)) - 1) (Linear + Exponential)
Initial : -16.746 -0.091 -33.785 -0.140 227.833 2.13E+05 4.96E+00 8657
Final : -16.746 -0.091 -33.785 -0.140 227.833 2.13E+05 4.96E+00 8657
a1 a2 a3 a4 a5 rms rad nfit npts
Pressure p(mb)
Time t (days)
25
20
15
10
5
0
-5
-10
-15
-20
200
225
250
275
300
325
350
375
400
425
450
475
500
525
550
575
600

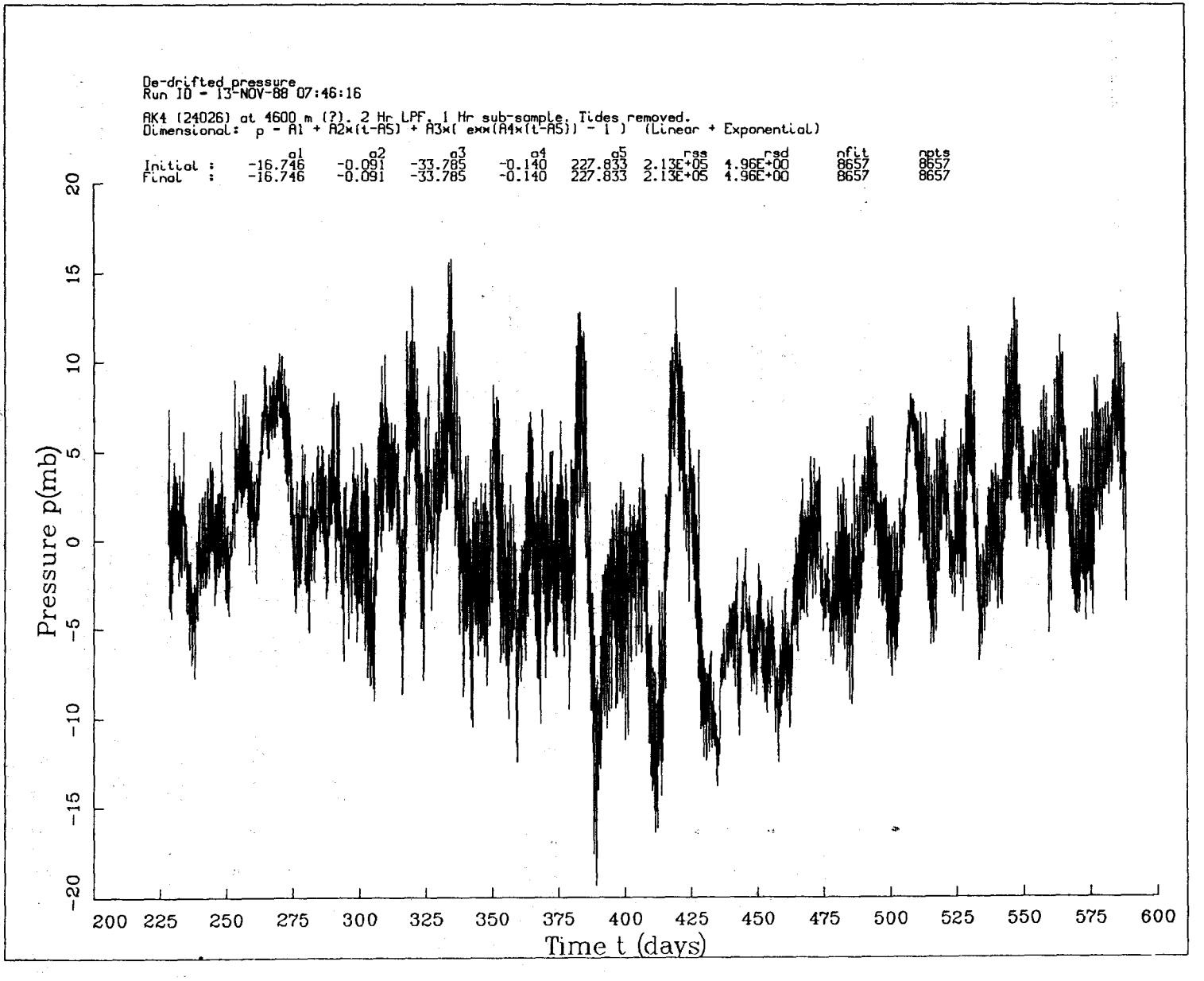
De-drifted pressure
Run ID - 13-NOV-88 07:46:16
AK4 (24026) at 4600 m (?). 2 Hr LPF, 1 Hr sub-sample, Tides removed.
Dimensional: p = A1 + A2*(t-A5) + A3*(exp(A4*(t-A5)) - 1) (Linear + Exponential)
a1 a2 a3 a4 a5 rms rsd nfit npts
Initial : -16.746 -0.091 -33.785 -0.140 227.833 2.13E+05 4.96E+00 8657 8657
Final : -16.746 -0.091 -33.785 -0.140 227.833 2.13E+05 4.96E+00 8657 8657
Pressure p(mb)
20
15
10
5
0
-5
-10
-15
-20
200 225 250 275 300 325 350 375 400 425 450 475 500 525 550 575 600
Time t (days)

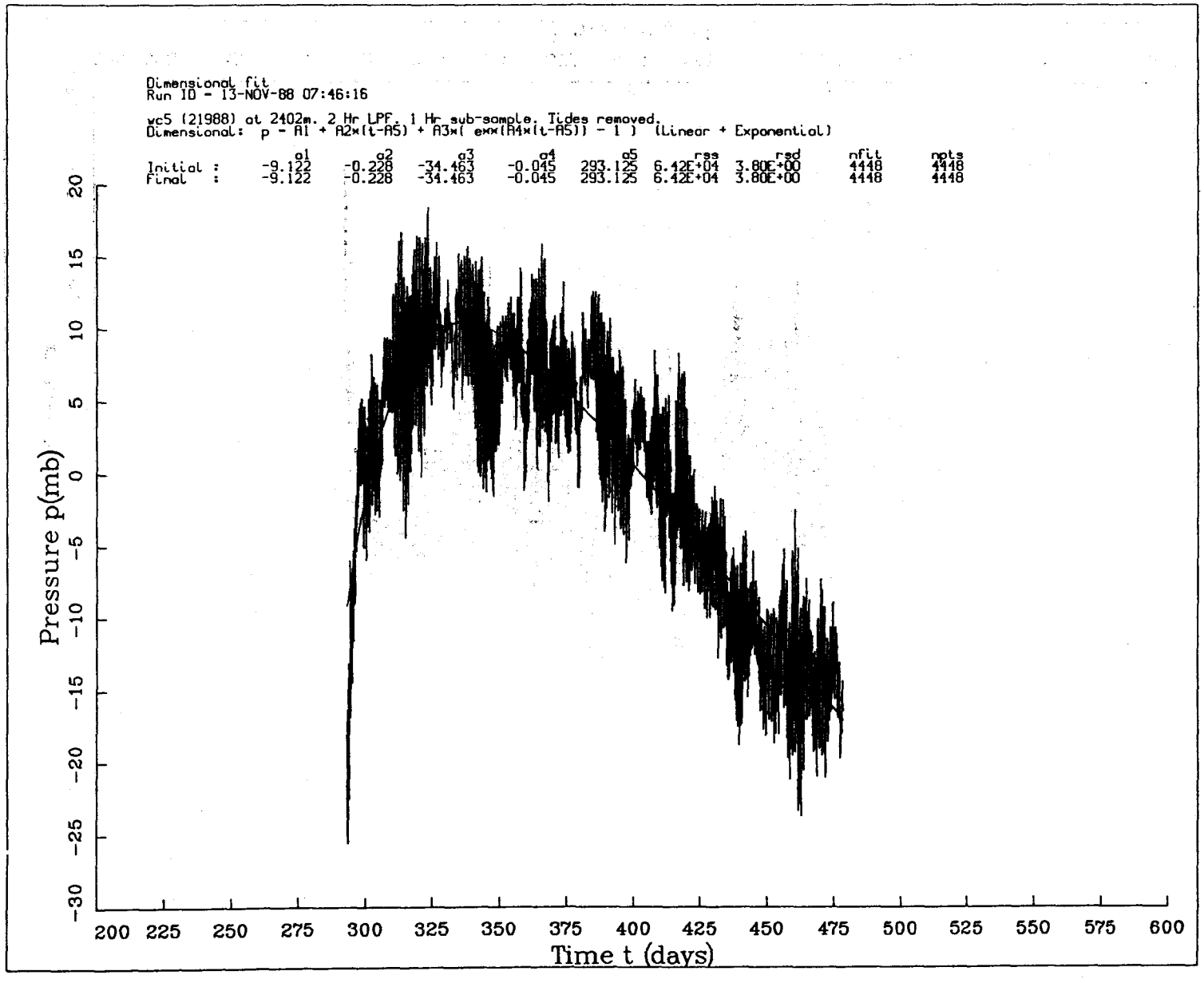
Dimensional fit
Run ID - 13-NOV-88 07:46:16
wc5 (21988) at 2402m. 2 Hr LPF, 1 Hr sub-sample. Tides removed.
Dimensional: p = A1 + A2*(t-A5) + A3*(exp(A4*(t-A5)) - 1) (Linear + Exponential)
a1 a2 a3 a4 a5 rss rsd nfit npts
Initial : -9.122 -0.228 -34.463 -0.045 293.125 6.42E+04 3.80E+00 4448 4448
Final : -9.122 -0.228 -34.463 -0.045 293.125 6.42E+04 3.80E+00 4448 4448
Pressure p(mb)
20
15
10
5
0
-5
-10
-15
-20
-25
-30
200 225 250 275 300 325 350 375 400 425 450 475 500 525 550 575 600
Time t (days)

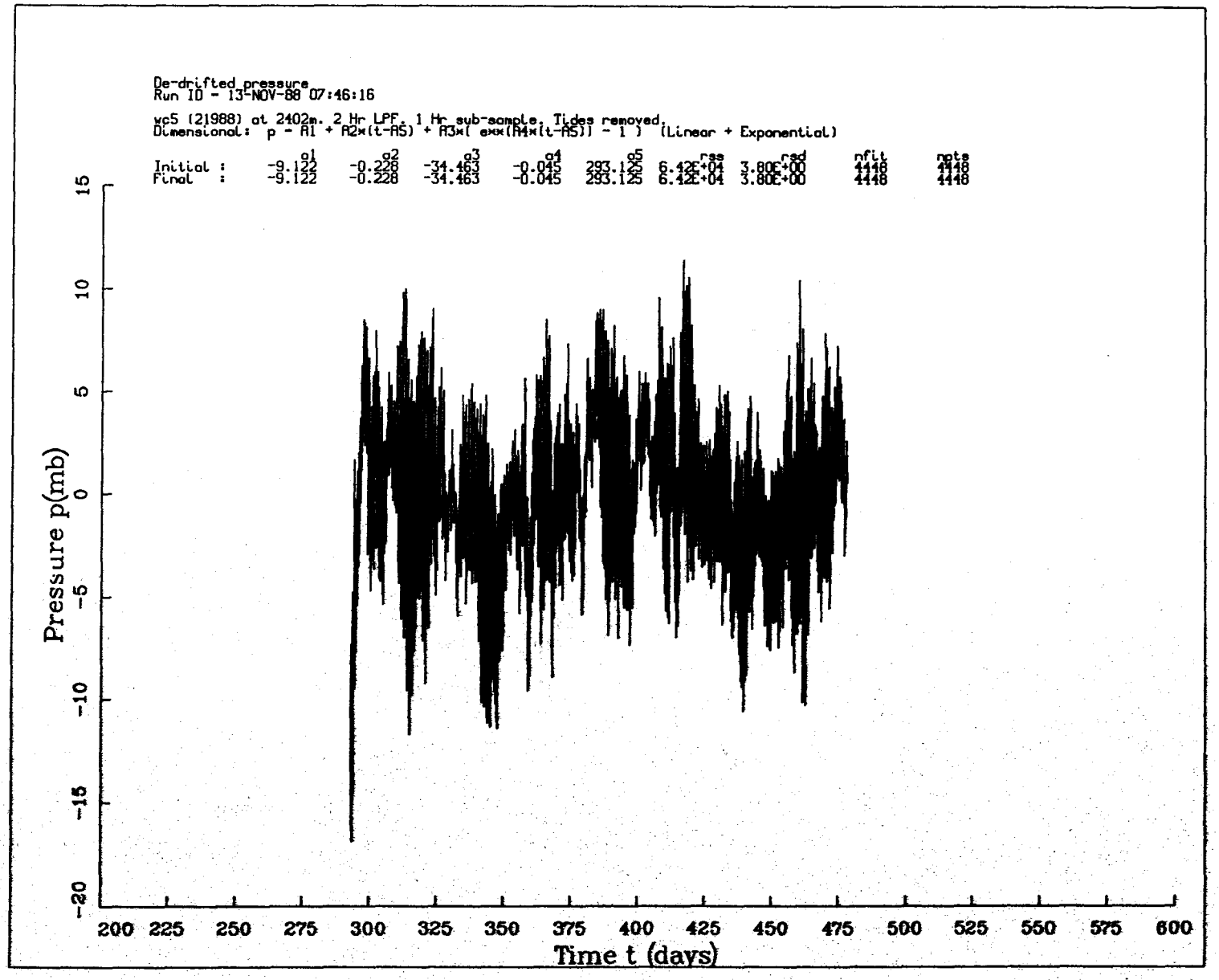
De-drifted pressure
Run ID - 13-NOV-88 07:46:16
wc5 (2)1988) at 2402m. 2 Hr LPF. 1 Hr sub-sample. Tides removed.
Dimensional: p = A1 + A2×(t-A5) + A3×(ex×(A4×(t-A5)] - 1) (Linear + Exponential)
a1 a2 a3 a4 a5 rss rsd nfit npts
Initial : -9.122 -0.228 -34.463 -0.045 293.125 6.42E+04 3.80E+00 4448 4448
Final : -9.122 -0.228 -34.463 -0.045 293.125 6.42E+04 3.80E+00 4448 4448
Pressure p(mb)
15
10
5
0
-5
-10
-15
-20
200 225 250 275 300 325 350 375 400 425 450 475 500 525 550 575 600
Time t (days)

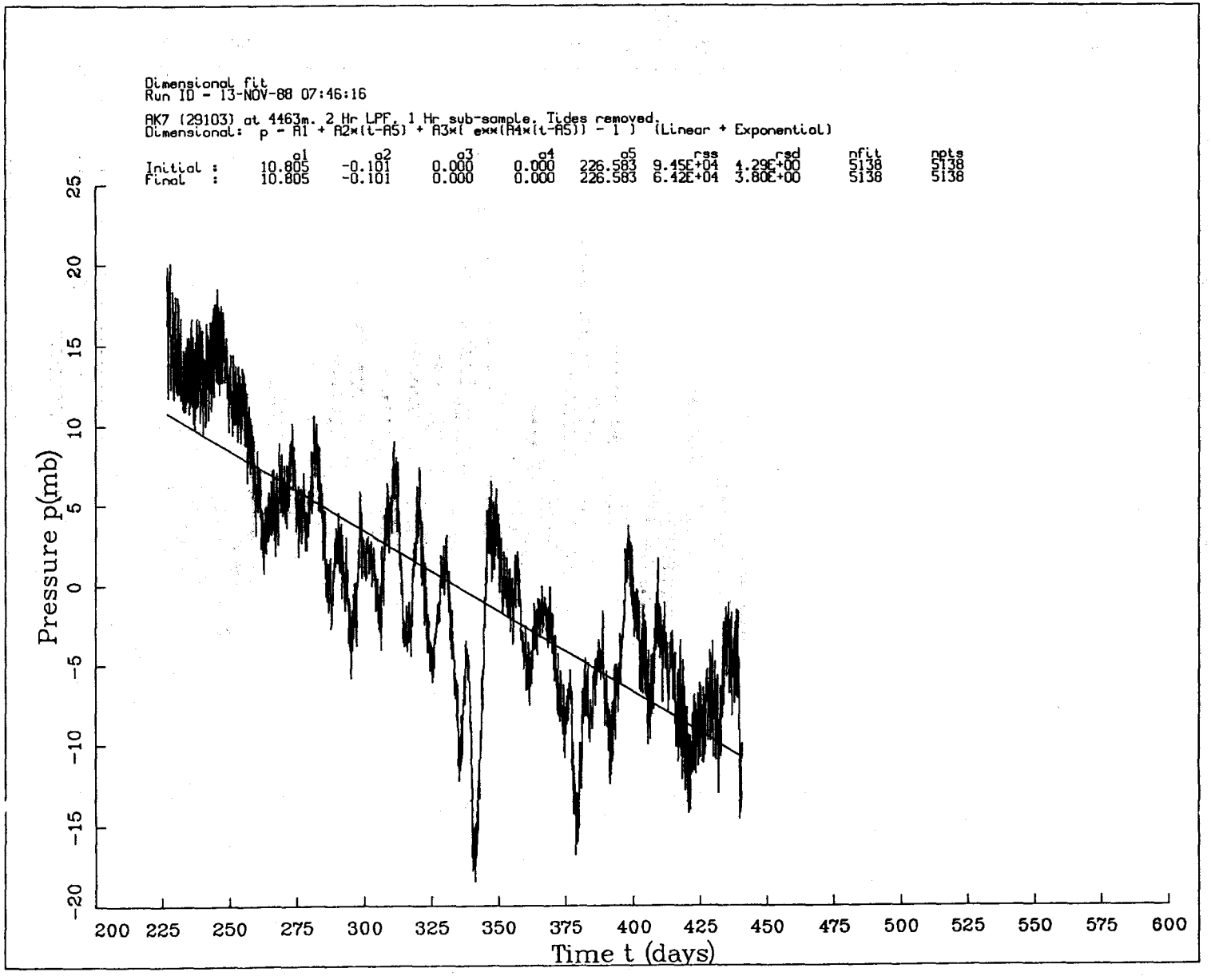
Dimensional fit
Run ID - 13-NOV-88 07:46:16
AK7 (29103) at 4463m. 2 Hr LPF, 1 Hr sub-sample. Tides removed.
Dimensional: p = A1 + A2*(t-A5) + A3*(exp(A4*(t-A5)) - 1) (Linear + Exponential)
a1 a2 a3 a4 a5 rss rsd nfit npts
Initial : 10.805 -0.101 0.000 0.000 226.583 9.45E+04 4.29E+00 5138 5138
Final : 10.805 -0.101 0.000 0.000 226.583 6.42E+04 3.80E+00 5138 5138
Pressure p(mb)
25
20
15
10
5
0
-5
-10
-15
-20
200 225 250 275 300 325 350 375 400 425 450 475 500 525 550 575 600
Time t (days)

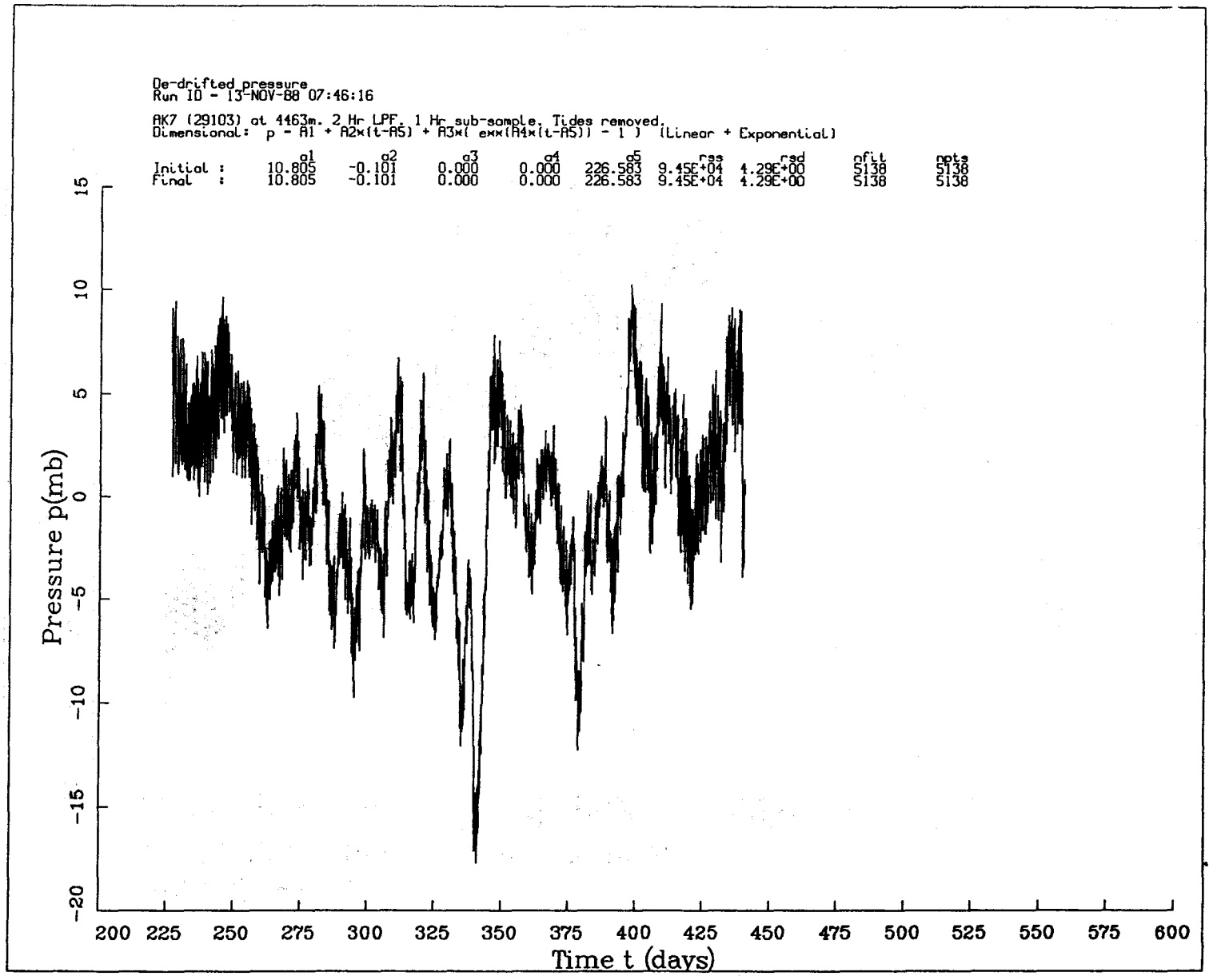
De-drifted pressure
Run ID - 13-NOV-88 07:46:16
AK7 (29103) at 4463m. 2 Hr LPF, 1 Hr sub-sample, Tides removed.
Dimensional: p = A1 + A2x(t-A5) + A3x(exx(A4x(t-A5)) - 1) (Linear + Exponential)
a1 a2 a3 a4 a5 rss rsd nfit npts
Initial : 10.805 -0.101 0.000 0.000 226.583 9.45E+04 4.29E+00 5138 5138
Final : 10.805 -0.101 0.000 0.000 226.583 9.45E+04 4.29E+00 5138 5138
Pressure p(mb)
15
10
5
0
-5
-10
-15
-20
200 225 250 275 300 325 350 375 400 425 450 475 500 525 550 575 600
Time t (days)

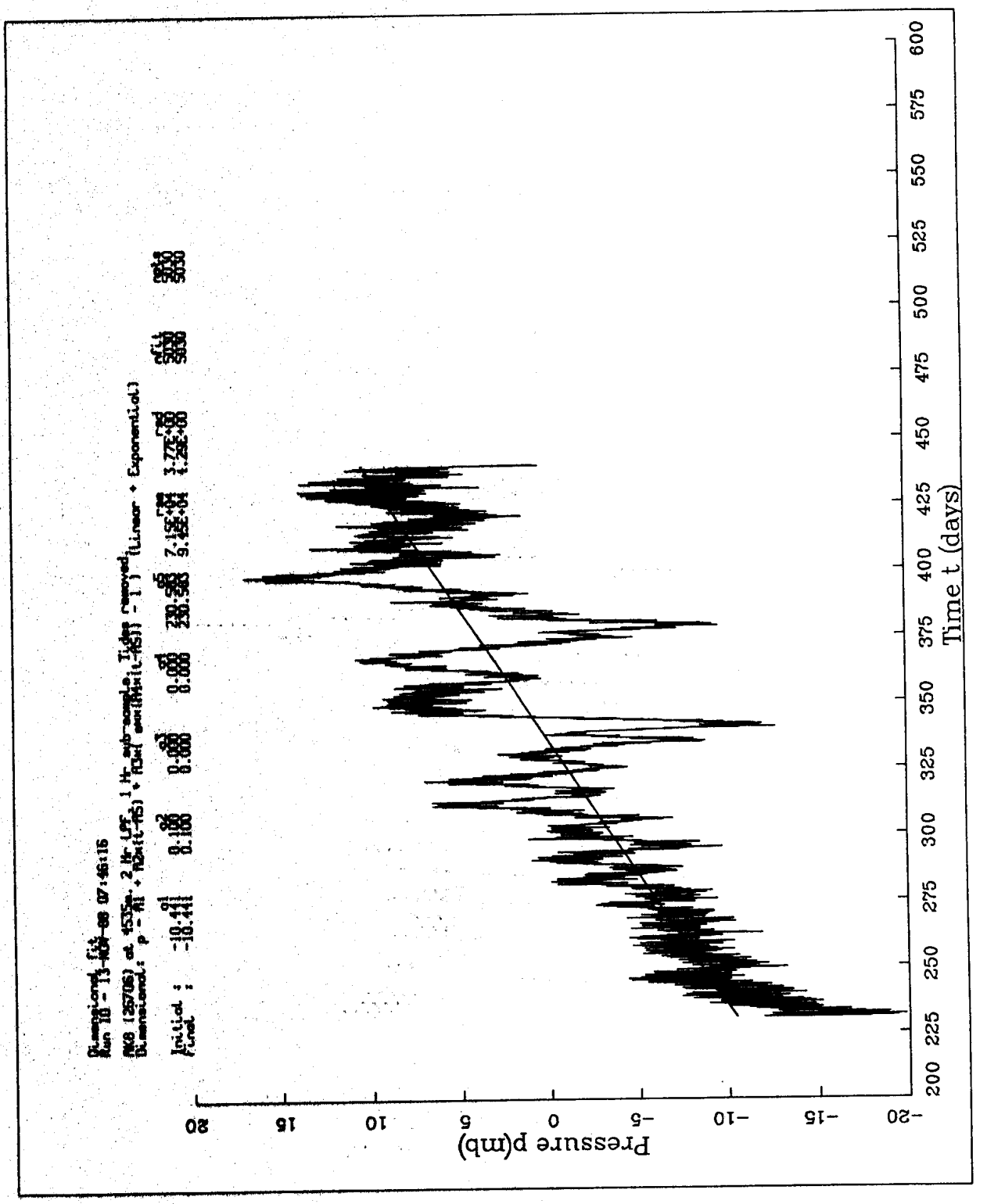
Pressure p(mb)
Time t (days)
20
15
10
5
0
-5
-10
-15
-20
200
225
250
275
300
325
350
375
400
425
450
475
500
525
550
575
600

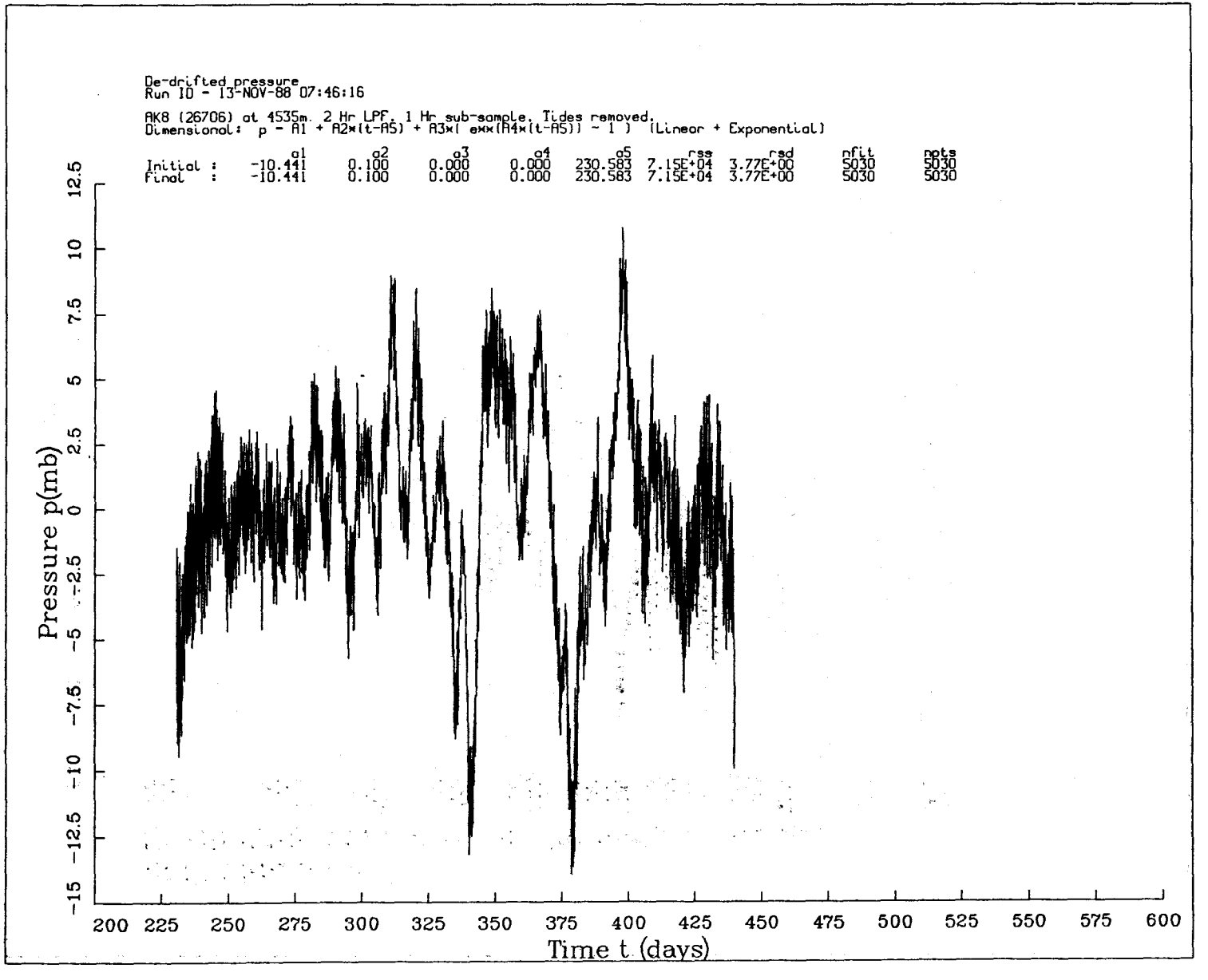
De-drifted pressure
Run ID - 13-NOV-88 07:46:16
AK8 (26706) at 4535m. 2 Hr LPF, 1 Hr sub-sample, Tides removed.
Dimensional: p = A1 + A2*(t-A5) + A3*(exp(A4*(t-A5)) - 1) (Linear + Exponential)
a1 a2 a3 a4 a5 rss rsd nfit npts
Initial : -10.441 0.100 0.000 0.000 230.583 7.15E+04 3.77E+00 5030 5030
Final : -10.441 0.100 0.000 0.000 230.583 7.15E+04 3.77E+00 5030 5030
Pressure p(mb)
12.5
10
7.5
5
2.5
0
-2.5
-5
-7.5
-10
-12.5
-15
200 225 250 275 300 325 350 375 400 425 450 475 500 525 550 575 600
Time t (days)

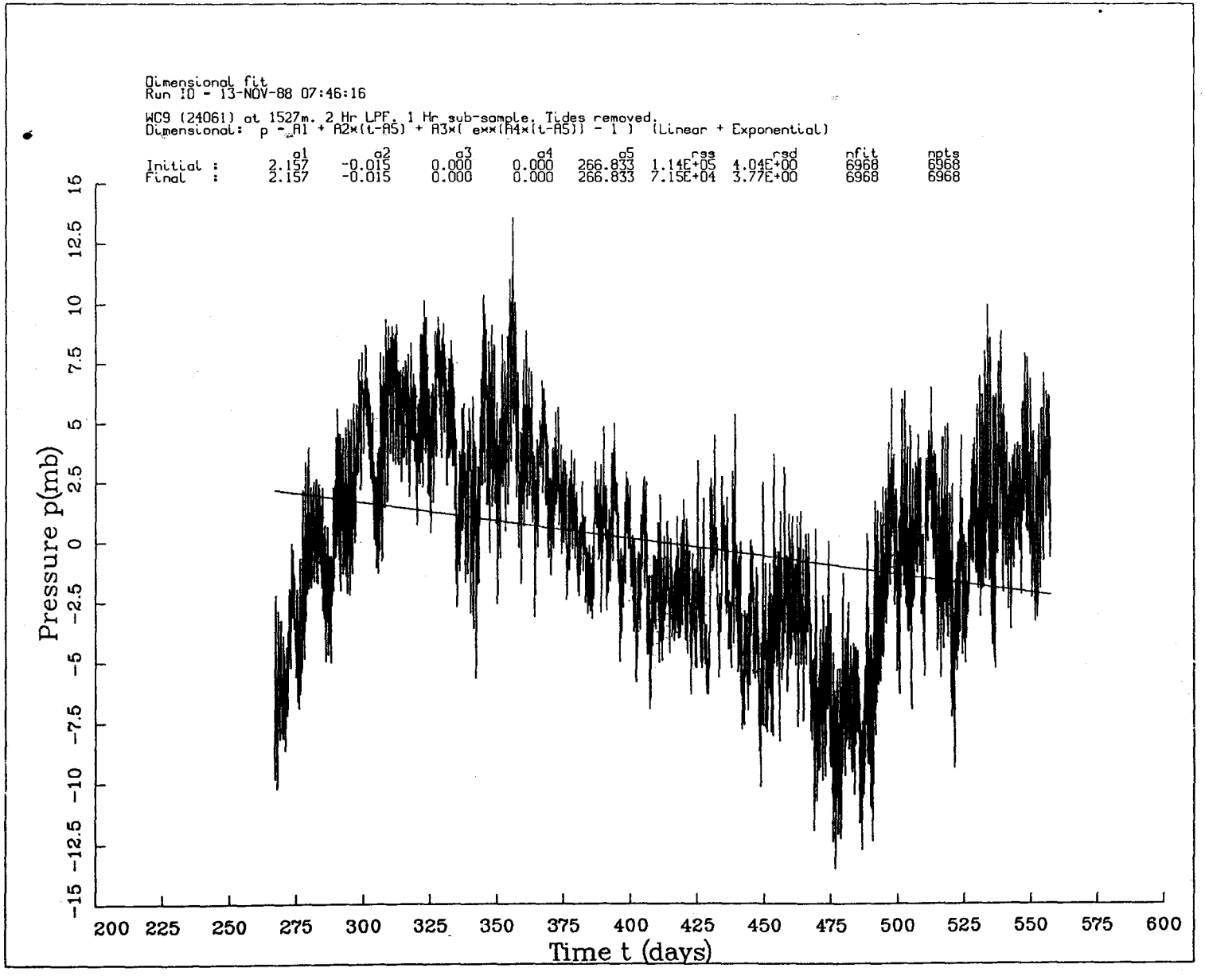
Dimensional fit
Run ID - 13-NOV-88 07:46:16
WC9 (24061) at 1527m. 2 Hr LPF, 1 Hr sub-sample, Tides removed.
Dimensional: p = A1 + A2×(t-A5) + A3×(exp(A4×(t-A5)) - 1) (Linear + Exponential)
a1 a2 a3 a4 a5 rss rsd nfit npts
Initial : 2.157 -0.015 0.000 0.000 266.833 1.14E+05 4.04E+00 6968 6968
Final : 2.157 -0.015 0.000 0.000 266.833 7.15E+04 3.77E+00 6968 6968
Pressure p(mb)
15 12.5 10 7.5 5 2.5 0 -2.5 -5 -7.5 -10 -12.5 -15
200 225 250 275 300 325 350 375 400 425 450 475 500 525 550 575 600
Time t (days)

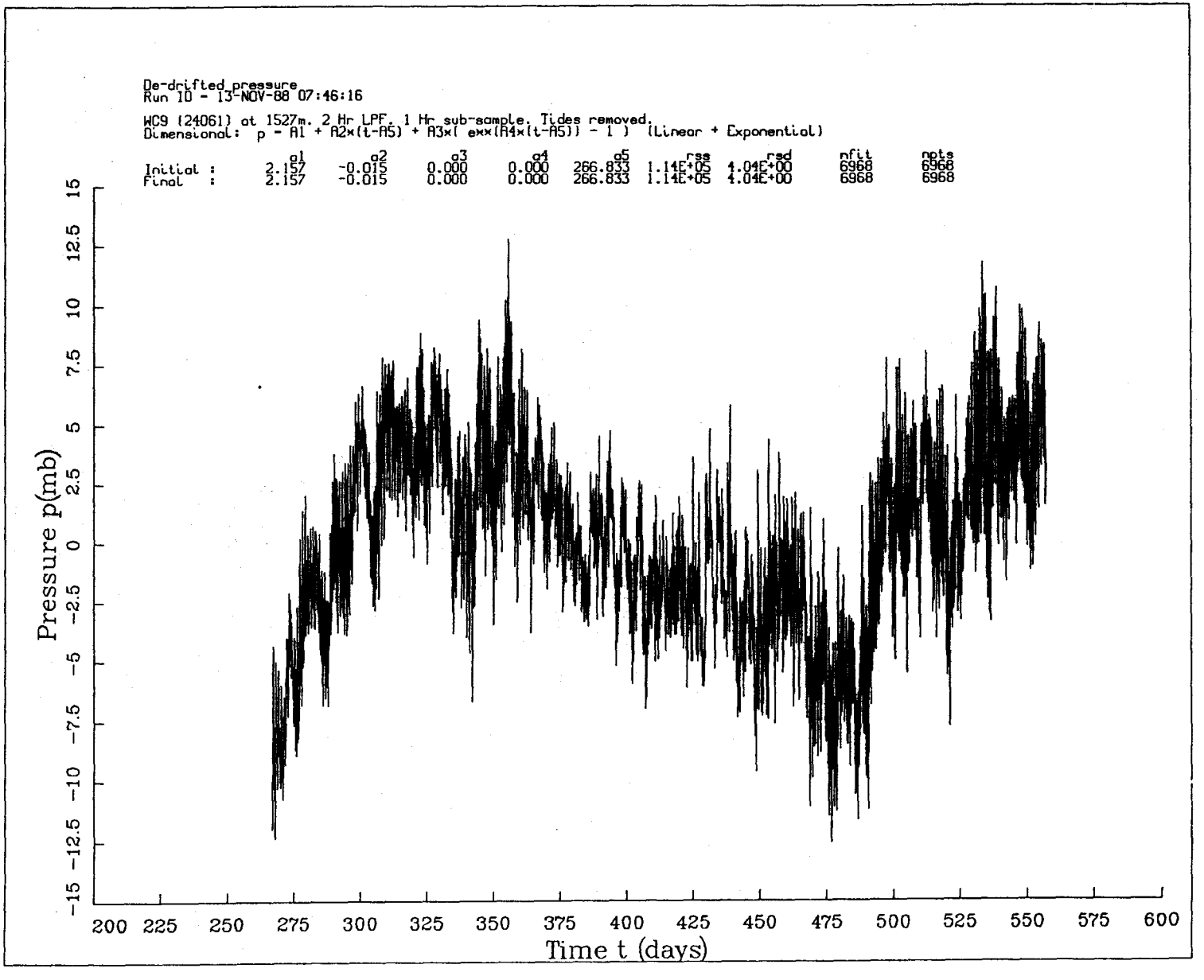
De-drifted pressure
Run 10 - 13-NOV-88 07:46:16
WC9 (24061) at 1527m. 2 Hr LPF. 1 Hr sub-sample. Tides removed.
Dimensional: p = A1 + A2x(t-A5) + A3x(exx(A4x(t-A5)) - 1) (Linear + Exponential)
a1 a2 a3 a4 a5 rss rsd nfit npts
Initial : 2.157 -0.015 0.000 0.000 266.833 1.14E+05 4.04E+00 6968 6968
Final : 2.157 -0.015 0.000 0.000 266.833 1.14E+05 4.04E+00 6968 6968
Pressure p(mb)
15
12.5
10
7.5
5
2.5
0
-2.5
-5
-7.5
-10
-12.5
-15
200 225 250 275 300 325 350 375 400 425 450 475 500 525 550 575 600
Time t (days)

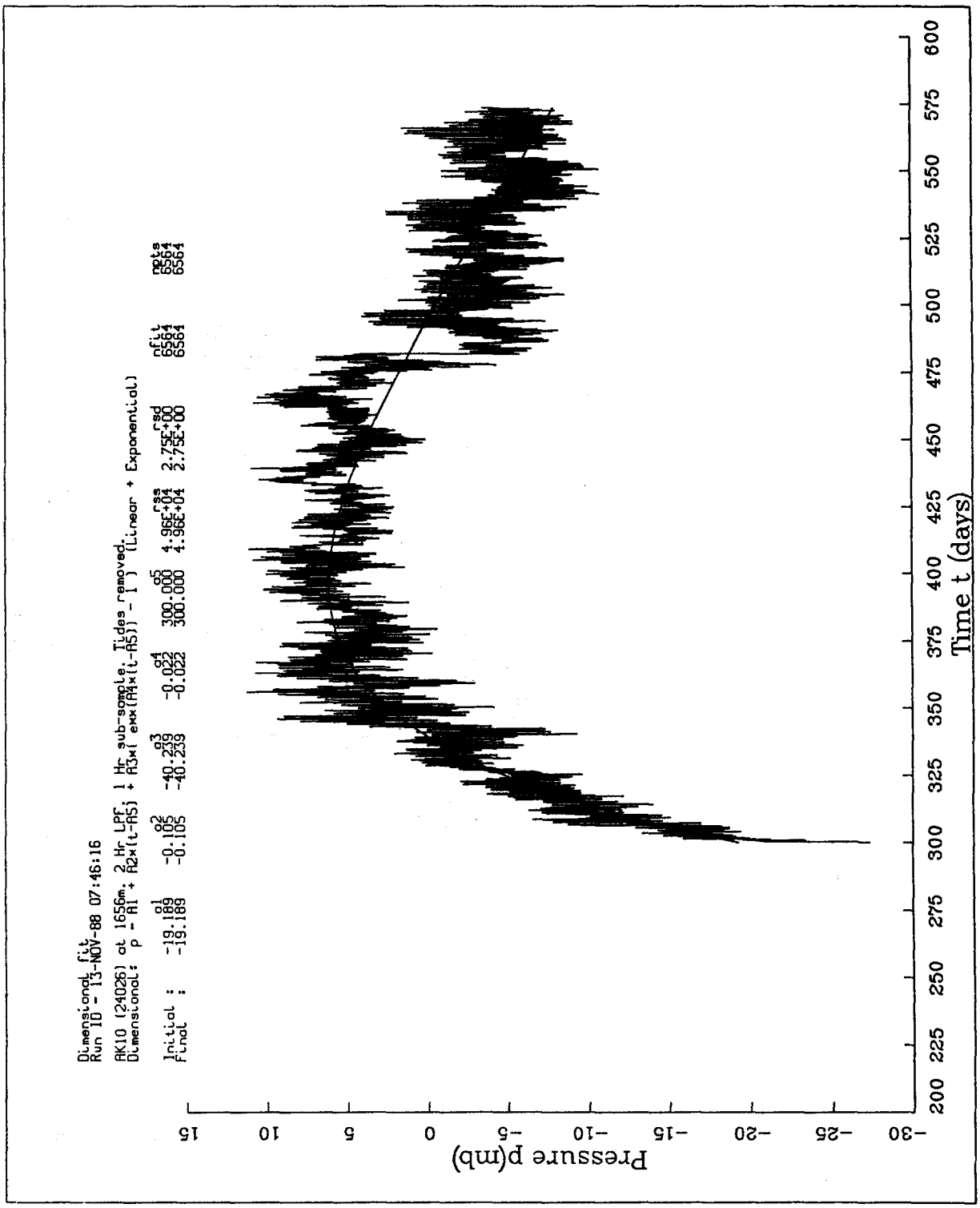
Dimensional fit
Run ID - 13-NOV-88 07:46:16
AK10 (24026) at 1656m. 2 Hr LPF, 1 Hr sub-sample, Tides removed.
Dimensional: p - A1 + A2x(t-A5) + A3x(exp(A4x(t-A5)) - 1) (Linear + Exponential)
a1 a2 a3 a4 a5 rss rsd nfit npts
Initial : -19.189 -0.105 -40.239 -0.022 300.000 4.96E+04 2.75E+00 6564 6564
Final : -19.189 -0.105 -40.239 -0.022 300.000 4.96E+04 2.75E+00 6564 6564
Pressure p(mb)
15
10
5
0
-5
-10
-15
-20
-25
-30
200
225
250
275
300
325
350
375
400
425
450
475
500
525
550
575
600
Time t (days)

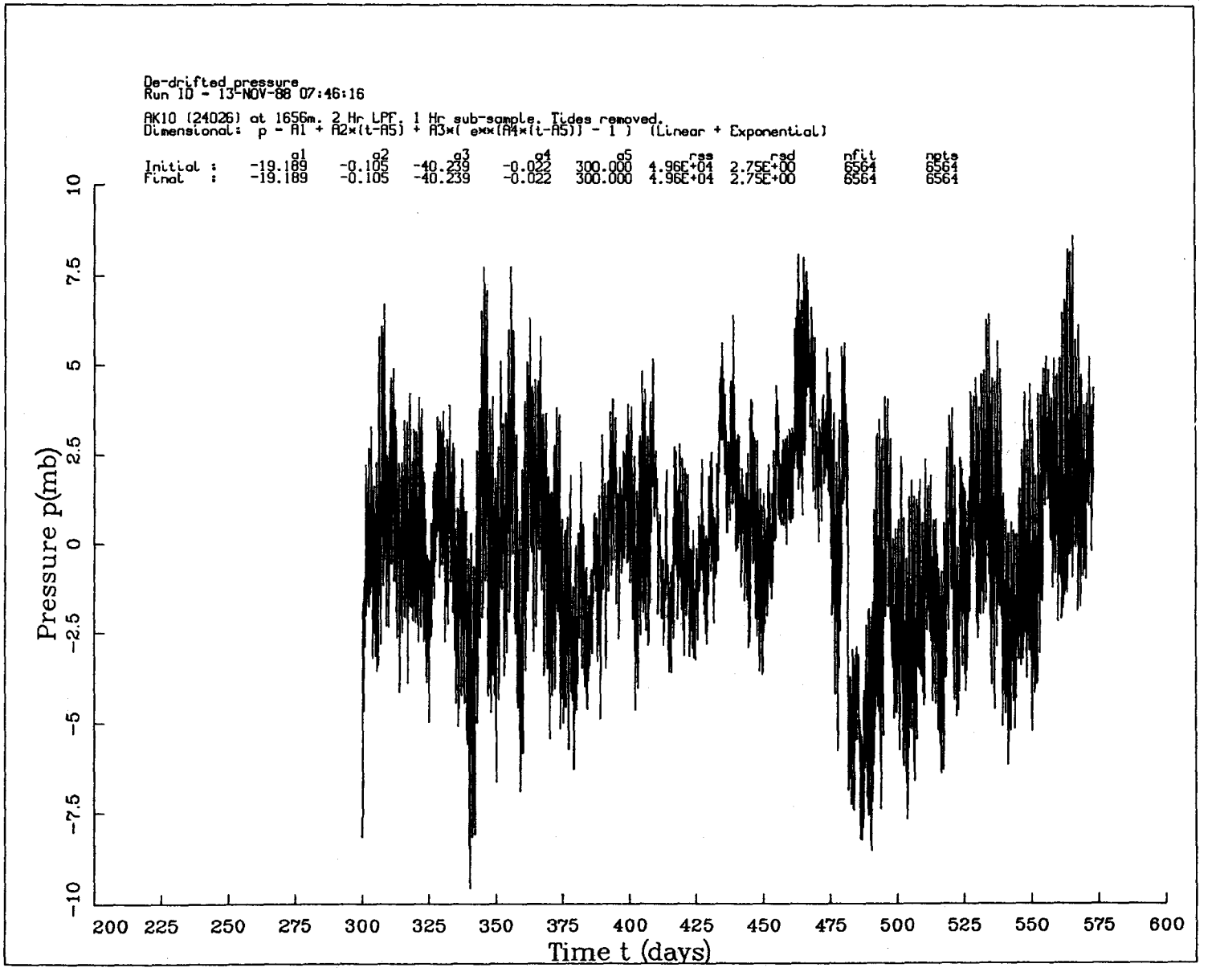
De-drifted pressure
Run ID - 13-NOV-88 07:46:16
AK10 (24026) at 1656m. 2 Hr LPF, 1 Hr sub-sample. Tides removed.
Dimensional: p = A1 + A2×(t-A5) + A3×(exx(A4×(t-A5)) - 1) (Linear + Exponential)
a1 a2 a3 a4 a5 rss rsd nfit npts
Initial : -19.189 -0.105 -40.239 -0.022 300.000 4.96E+04 2.75E+00 6564 6564
Final : -19.189 -0.105 -40.239 -0.022 300.000 4.96E+04 2.75E+00 6564 6564
Pressure p(mb)
10
7.5
5
2.5
0
-2.5
-5
-7.5
-10
200 225 250 275 300 325 350 375 400 425 450 475 500 525 550 575 600
Time t (days)

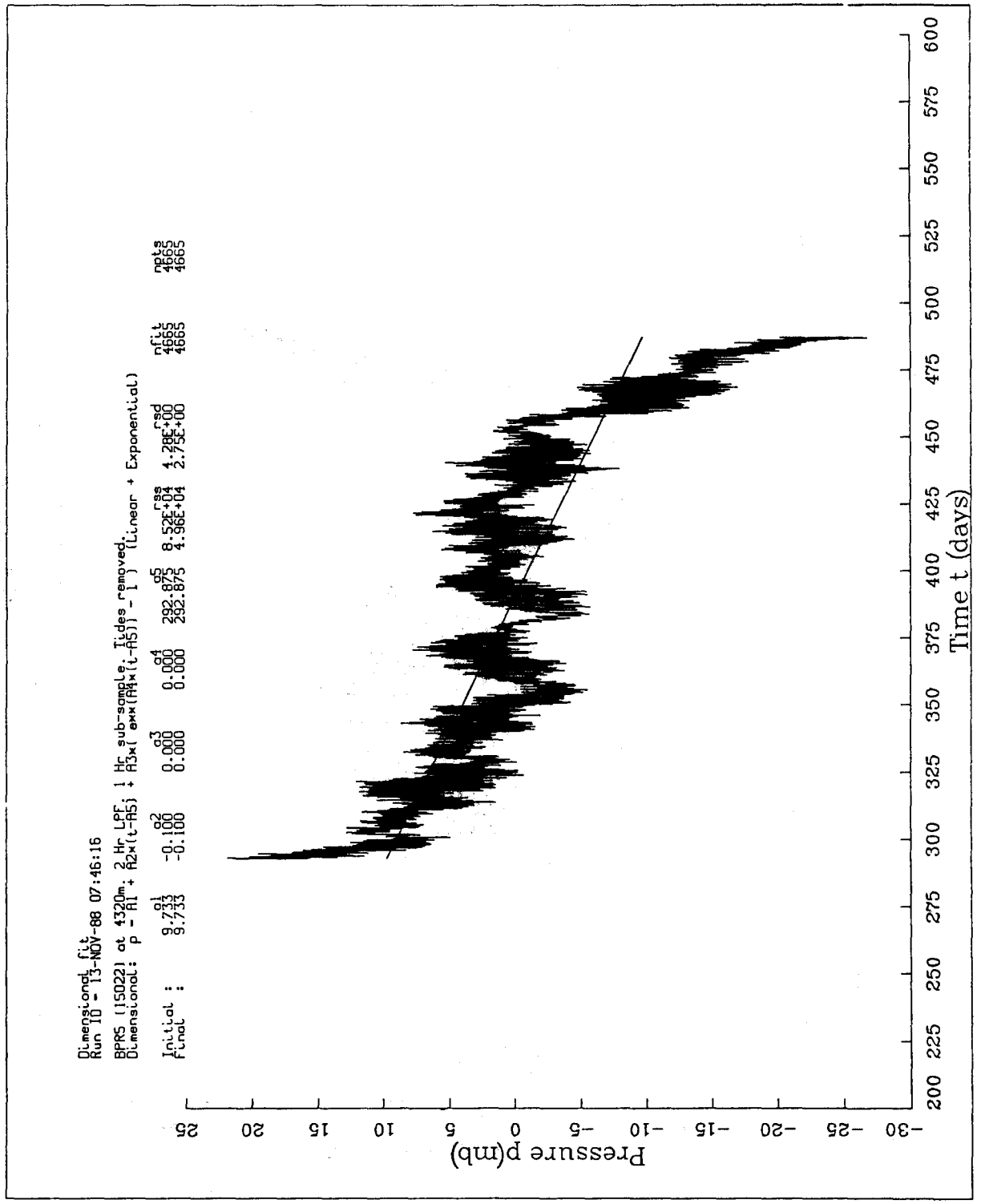
Dimensional fit
Run 10 - 13-NOV-88 07:46:16
BPRS (150221 at 4320m. 2 Hr LPF. 1 Hr sub-sample. Tides removed.
Dimensional: p = A1 + A2x(t-A5) + A3x(exx(A4x(t-A5)) - 1) (Linear + Exponential)
Initial : 9.733 -0.100 0.000 0.000 282.875 8.52E+04 4.28E+00 4665
Final : 9.733 -0.100 0.000 0.000 282.875 4.96E+04 2.75E+00 4665
a1 a2 a3 a4 a5 rss rsd nfit npts
Pressure p(mb)
Time t (days)
25 20 15 10 5 0 -5 -10 -15 -20 -25 -30
200 225 250 275 300 325 350 375 400 425 450 475 500 525 550 575 600

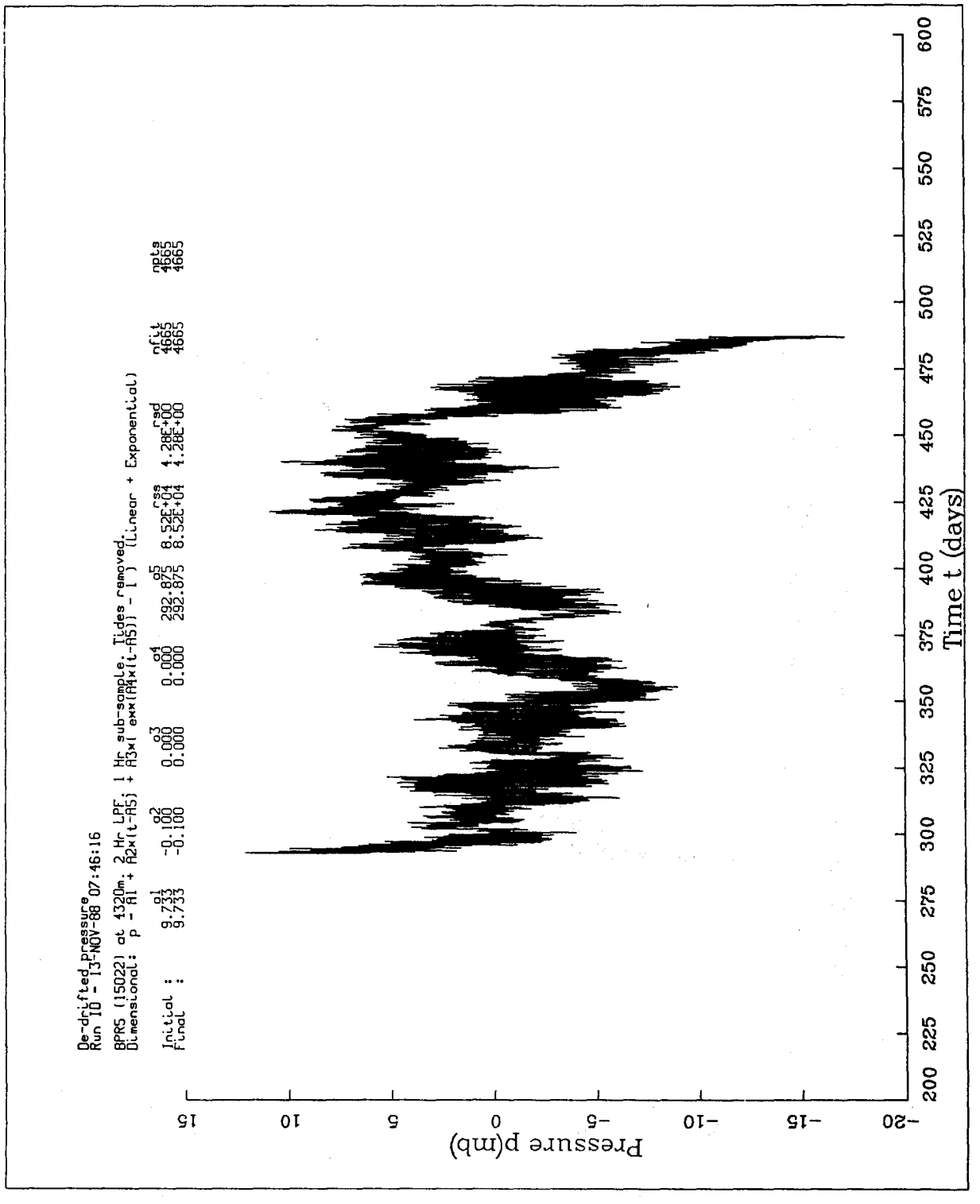

☆ U.S. GOVERNMENT PRINTING OFFICE: 1989-Jacket 673-002/11004 Region 8